
Electronic Thesis and Dissertation Repository

8-18-2015 12:00 AM

Development of a Wearable Mechatronic Elbow Brace for Postoperative Motion Rehabilitation

Anastasiia Kyrylova
The University of Western Ontario

Supervisor
Dr. Ana Luisa Trejos
The University of Western Ontario

Graduate Program in Biomedical Engineering
A thesis submitted in partial fulfillment of the requirements for the degree in Master of Engineering Science
© Anastasia Kyrylova 2015

Follow this and additional works at: <https://ir.lib.uwo.ca/etd>

 Part of the Biomechanical Engineering Commons, Movement and Mind-Body Therapies Commons, Orthotics and Prosthetics Commons, and the Physiotherapy Commons

Recommended Citation

Kyrylova, Anastasiia, "Development of a Wearable Mechatronic Elbow Brace for Postoperative Motion Rehabilitation" (2015). *Electronic Thesis and Dissertation Repository*. 3019.
<https://ir.lib.uwo.ca/etd/3019>

This Dissertation/Thesis is brought to you for free and open access by Scholarship@Western. It has been accepted for inclusion in Electronic Thesis and Dissertation Repository by an authorized administrator of Scholarship@Western. For more information, please contact wlsadmin@uwo.ca.

**DEVELOPMENT OF A WEARABLE MECHATRONIC ELBOW BRACE
FOR POSTOPERATIVE MOTION REHABILITATION**

(Thesis format: Monograph)

by

Anastasiia Kyrylova

Faculty of Engineering
Graduate Program in Biomedical Engineering

A thesis submitted in partial fulfillment
of the requirements for the degree of
Master of Engineering Science

The School of Graduate and Postdoctoral Studies
The University of Western Ontario
London, Ontario, Canada

© Anastasiia Kyrylova, 2015

Abstract

This thesis describes the development of a wearable mechatronic brace for upper limb rehabilitation that can be used at any stage of motion training after surgical reconstruction of brachial plexus nerves. The results of the mechanical design and the work completed towards finding the best torque transmission system are presented herein. As part of this mechatronic system, a customized control system was designed, tested and modified. The control strategy was improved by replacing a PID controller with a cascade controller. Although the experiments have shown that the proposed device can be successfully used for muscle training, further assessment of the device, with the help of data from the patients with brachial plexus injury (BPI), is required to improve the control strategy. Unique features of this device include the combination of adjustability and modularity, as well as the passive adjustment required to compensate for the carrying angle.

Keywords: brachial plexus injury, elbow, powered exoskeleton, wearable brace, rehabilitation, EMG, biceps and triceps.

*Dedicated to
all Ukrainians who
show that we are of the Cossack kin.*

Acknowledgements

I would like to express my deepest appreciation and sincerest gratitude to my supervisor, Dr. Ana Luisa Trejos, without whose guidance and persistent help, this dissertation would not be possible. Her wisdom and encouragement throughout the research were of great value. During this two-year journey of hard work, she kept the perfect balance between freedom and flexibility in the research on one side, and giving me motivation and directions when it was most needed, on the other side.

I would also like to thank the Research Engineer of the project, Abelardo Escoto, for sharing his knowledge through the design and prototyping phases. Your ideas and support helped me to improve the quality of my research. A big thanks goes to my research group, especially to Yue Zhou and to Tyler Desplenter, for their input in the project and for their critical analysis of my work. One more thanks goes out to the physiotherapist, Shrikant Chinchalkar (St. Joseph's Health Care London), for sharing his knowledge in upper limb rehabilitation. Additional thanks goes to the summer student Jolien van Gaalen for her help with the development and purchasing of the actuation system.

I wish to thank Dan Sweiger and Clayton Cook (University Machine Services) for their technical support and for lending me materials for my experiments. I would like to acknowledge the support from Dr. Rajni Patel (Canadian Surgical Technologies & Advanced Robotics research program) who provided the EPOS controllers for this project.

I am extremely grateful to all who have participated in my trials. More than 35 people have been involved in the data collection trials. This thesis would not have been possible to write without your help and time. Additional thanks goes to my friend Ievgeniia Morozova for lending me the photo equipment and for being the model for the demonstration video.

I would like to express my gratitude to the members of my advisory committee, Dr. Michael Naish and Dr. Thomas Jenkyn, as well as to my examination committee, Dr. James

Johnson, Dr. James Lacefield and Dr. George K. Knopf for their time and valuable comments.

I also want to thank my parents, Marina Kyrylova and Volodymyr Kyrylov, for their endless love and support. Above all, I would like to thank my husband Oleksandr Tymofieiev for never letting me doubt myself and for reminding me that there is a whole world outside of my laboratory. Thank you for being my muse, editor, proofreader, and technical support. And most of all, thank you for being my best friend.

Finally, the work reported in this thesis would not have been possible without the financial support of the Western Strategic Support for NSERC Success Grant and the Academic Development Fund, Western University and by the Natural Sciences and Engineering Research Council (NSERC) of Canada under grant RGPIN-2014-03815, for which I am grateful.

Table of Contents

Abstract.....	ii
Acknowledgements	iv
Table of Contents	vi
List of Figures.....	x
List of Tables	xiv
Nomenclature and Acronyms	xv
CHAPTER 1.....	1
 1 INTRODUCTION.....	1
1.1 Motivation	1
1.2 General Problem Statement	3
1.3 Research Objectives and Scope	3
1.4 Overview of the Thesis.....	4
CHAPTER 2.....	7
 2 LITERATURE REVIEW AND BACKGROUND	7
2.1 Brachial Plexus Structure and Lesions	8
2.2 Brachial Plexus Reinnervation	9
2.3 Portable Mechatronic Elbow Devices: State of the Art.....	12
2.3.1 Mechanical Design of Smart Elbow Devices for Rehabilitation.....	13
2.3.2 Actuation Systems for Wearable Elbow Powered Applications	17
2.3.3 Control Strategy of Actuation Systems in Motion Rehabilitation.....	19
2.4 Conclusions	23

CHAPTER 3.....	24
3 DESIGN OF THE WEARABLE ELBOW BRACE	24
3.1 General Design Specification	24
3.2 Design Constraints and Specification.....	25
3.2.1 Adjustability in Size	25
3.2.2 Payload and Torque Analysis	27
3.2.3 Weight of a Wearable Elbow Brace	28
3.2.4 Actuator Placement.....	28
3.2.5 Hinge Type	29
3.2.6 Arm Mounting	31
3.2.7 Safety Throughout the Rehabilitation Progress	31
3.2.8 User Requirements	32
3.3 Presentation of the Mechanical Design	32
3.3.1 Bearing Selection and Rated Life	33
3.3.2 2-DOF Motion of the Brace.....	35
3.3.3 Driver Selection.....	37
3.3.4 Motor–Gear Box Selection	40
3.3.5 Actuation System.....	41
3.3.6 Transmission System	44
3.3.7 Torque Amplifier	45
3.3.8 Material Selection	49
3.4 Conclusion	52
CHAPTER 4.....	53
4 WEARABLE ELBOW MECHATRONICS-ENABLED BRACE PROTOTYPE	53
4.1 Design Overview	53
4.2 Testing of the Mechanical Stoppers	58
4.3 Torque Amplifier Testing	61
4.3.1 Setup installation	63

4.3.1.1	Belt Installation.....	63
4.3.1.2	Cable Installation	67
4.3.2	Torque Transmission in Rehabilitation	68
4.3.2.1	Methods	69
4.3.2.2	Results and Discussion	70
4.4	Prototype Costs.....	74
4.5	Conclusions	75
CHAPTER 5.....		77
5	METHODS FOR DIGITAL SIGNAL PROCESSING OF EMG SIGNALS FOR MOTION PROFILE ESTIMATION.....	77
5.1	Rehabilitation Strategy Overview	77
5.2	Goals of Rehabilitation Modes	78
5.3	Signal Processing.....	79
5.3.1	Signal Filtering	80
5.3.2	Direction of Elbow Movement	81
5.3.3	Speed Estimation	82
5.3.4	Kalman Filter	84
5.3.4.1	Kalman Filter Design.....	84
5.3.4.2	Kalman Filter Application	85
5.4	Conclusions	87
CHAPTER 6.....		89
6	PROTOTYPE PERFORMANCE ASSESSMENT.....	89
6.1.	Rehabilitation Modes Assessment.....	89
6.1.1.	Data Collection	90
6.1.2.	Setup Installation	92
6.2.	Educational Mode	93
6.2.1.	Results	95

6.2.2.	Additional interpretation of the results	97
6.3.	Assistive Mode with PID Control	97
6.3.1.	Results	99
6.3.2.	Discussion.....	101
6.4.	Assistive Mode with Cascade Control.....	101
6.4.1.	Results	101
6.4.2.	Discussion.....	105
6.5.	Sources of Error and Limitations.....	106
6.6.	Conclusions	106
CHAPTER 7	108
7 CONCLUSIONS AND FUTURE WORK	108
7.1.	Contributions	109
7.2.	Future Work.....	110
REFERENCES	112
Appendix A	125
Rated Life of Bearings	125
Appendix B	128
Motor–Gearbox selection.....	128
Appendix C	132
Motor Specification	132
Appendix D	135
Bearing Specification.....	135
Permissions and Approvals	137
Curriculum Vitae	145

List of Figures

- Fig. 2.1. Brachial plexus (C5-C7) and muscles that motor the upper limb.
- Fig. 2.2. Elbow biomechanics.
- Fig. 2.3. Mechanical brace, Innovator X® (Össur).
- Fig. 2.4. Mechanical rehabilitation braces for post-operative management of brachial plexus injuries.
- Fig. 2.5. Mechanical design of an elbow wearable powered brace.
- Fig. 2.6. EMG sensors and electrodes.
- Fig. 3.1. Size variations of a human arm.
- Fig. 3.2. CAD model of the first prototype of the ME-Brace.
- Fig. 3.3. Actuator placement.
- Fig. 3.4. Elbow motion.
- Fig. 3.5. Polycentric hinge elbow.
- Fig. 3.6. Single-axis hinge elbow.
- Fig. 3.7. Various design of the trough of the cuffs.
- Fig. 3.8. CAD model of the device.
- Fig. 3.9. Bearing loading scenario.
- Fig. 3.10. Elbow Brace DOFs.
- Fig. 3.11. Mechanical stoppers.
- Fig. 3.12. Schematic diagram of mechanical stoppers performance.
- Fig. 3.13. Bevel gear and belt-pulley transmission for one motor-gear box combination.
- Fig. 3.14. Worm gear and belt-pulley transmission for one motor-gear box combination.
- Fig. 3.15. Spur gear and belt-pulley transmission for one motor-gear box combination.
- Fig. 3.16. Kinematic diagram of the transmission system.
- Fig. 3.17. Actuation system of the elbow powered brace.

- Fig. 3.18. Reverse payload and torque calculation diagram.
- Fig. 3.19. Diagram of the torque amplifier.
- Fig. 3.20. Transmission system.
- Fig. 3.21. Detachable motor housing.
- Fig. 3.22. Neoprene belts with a fiberglass cord.
- Fig. 3.23. Forces acting on the base for the forearm.
- Fig. 3.24. Displacement analysis of the base for the forearm.
- Fig. 3.25. Stress analysis of the base for the forearm.
- Fig. 3.26. FOS analysis of the base for the forearm.
- Fig. 3.27. Vacuum forming cuffs.
- Fig. 4.1. Prototype of the wearable mechatronic elbow brace.
- Fig. 4.2. Range of motion of the prototype.
- Fig. 4.3. Passive ROM to account for the natural carrying angle.
- Fig. 4.4. Mechanical stopper of the prototype.
- Fig. 4.5. Adjustment of the device for a specific forearm length.
- Fig. 4.6. Minimum and maximum elbow breadth.
- Fig. 4.7. Elbow breadth that the prototype can handle.
- Fig. 4.8. The setup for the assessment of the mechanical stoppers.
- Fig. 4.9. Components' distribution in the forearm simulator.
- Fig. 4.10. Front view of the forearm simulator.
- Fig. 4.11. Mean error \pm SD of angular displacement under different loads.
- Fig. 4.12. Selected pulleys for belt–pulley and cable–pulley transmission.
- Fig. 4.13. Belt deflection.
- Fig. 4.14. Metal tensioner for a cut belt.
- Fig. 4.15. Torsion spring as a tensioner.
- Fig. 4.16. Movable 3D printed tensioner.
- Fig. 4.17. Cable deflection.
- Fig. 4.18. Diagram of a marine camel knot.
- Fig. 4.19. Setup for transmission system testing.
- Fig. 4.20. Example of the response of the brace with the belt–pulley transmission to a constant velocity command.

- Fig. 4.21. Example of the response of the brace with Nylon® cable–pulley transmission to a constant velocity command.
- Fig. 4.22. Example of $\Delta\alpha$ distribution over time for the Nylon® cable–pulley transmission.
- Fig. 4.23. Response of the brace with Nylon® cable–pulley transmission to different constant velocity commands.
- Fig. 4.24. $\Delta\alpha$ distribution over time for the Nylon® cable–pulley under different speed conditions.
- Fig. 4.25. Example of the response of the brace with Nylon® cable–pulley transmission to a constant velocity command $n = 22.5^\circ/\text{s}$.
- Fig. 4.26. Example of $\Delta\alpha$ distribution over time for the Nylon® cable–pulley transmission when moving at a speed of $n = 22.98^\circ/\text{s}$.
- Fig. 5.1. Architecture of the control system.
- Fig. 5.2. Raw EMG data from biceps and triceps.
- Fig. 5.3. Angular position of a forearm (3 FE) after 2 Hz high-pass filtering.
- Fig. 5.4. Single-Side Amplitude Spectrum of raw EMG signal.
- Fig. 5.5. RMS EMG signal from BB and TB.
- Fig. 5.6. Direct mapping of RMS EMG and motion data.
- Fig. 5.7. Speed profile compared to RMS EMG.
- Fig. 5.8. LogD EMG signal from BB and TB.
- Fig. 5.9. Direct mapping of logD EMG and motion data.
- Fig. 5.10. Speed profile compared to logD EMG.
- Fig. 5.11. Example of brace response to a constant $22.5^\circ/\text{s}$ command speed for maximum 3.3 kg load.
- Fig. 5.12. Example of $\Delta\alpha$ distribution over time for maximum 3.3 kg load.
- Fig. 5.13. Drive system efficiency during the CPM test across different speed commands for a maximum load (3.3 kg).
- Fig. 5.14. Position fluctuation during the CPM test for a maximum load (3.3 kg).
- Fig. 5.15. Drive system efficiency during the CPM test across different speed commands for different loads.

- Fig. 5.16. Muscle activation dynamics.
- Fig. 5.17. Neural activation from BB and TB.
- Fig. 5.18. Pure mapping of net neural activation (BB-TB) and motion data.
- Fig. 5.19. Flowchart of data in Kalman filter,
- Fig. 5.20. Filtered and rectified EMG signal.
- Fig. 5.21. Normalized EMG signal from BB and TB.
- Fig. 5.22. Kalman Filter mapping of neural activation and motion data.
- Fig. 6.1. Example of placement of the EMG sensing system and the mechanical brace.
- Fig. 6.2. Experimental setup.
- Fig. 6.3. Schematic representation of the setup for assistive mode.
- Fig. 6.4. Schematic representation of the signal flow for educational mode.
- Fig. 6.5. Sample of data (ROM 0–90°) for the MATLAB-based forearm trajectory estimation.
- Fig. 6.6. Accuracy of training educational sessions for different cases.
- Fig. 6.7. Schematic representation of the signal flow for assistive mode.
- Fig. 6.8. Sample of data (ROM 0–90°) for the MATLAB-based application.
- Fig. 6.9. Brace response to an estimated speed profile for a sample of data.
- Fig. 6.10. Schematic representation of the improved signal flow for assistive mode.
- Fig. 6.11. Sample brace response to an estimated speed profile while the PID control was used.
- Fig. 6.12. Sample brace response to an estimated speed profile while the cascade control was used.
- Fig. 6.13. Error accumulation at different stages of the assistive mode.
- Fig. 7.1. Elbow brace housing.

List of Tables

- Table 2.1. Upper limb postoperative care and rehabilitation.
- Table 2.2. Commercially available mechanical braces.
- Table 2.3. Review of wearable devices for elbow rehabilitation.
- Table 2.4. Actuation and power transmission in wearable devices for elbow rehabilitation.
- Table 2.5. EMG-driven models for elbow motion quantification.
- Table 3.1. Anthropometric data for 95th percentile of the population.
- Table 3.2. Measured torque of an elbow at different conditions.
- Table 3.3. Grid analysis of drivers for a powered elbow brace.
- Table 3.4. Grid analysis of splitter transmissions.
- Table 3.5. Belt–pulley selection chart for 3 mm pitch GT2 belts.
- Table 4.1. Muscle weight distribution in the forearm phantom.
- Table 4.2. Grid analysis of belt tensioners.
- Table 4.3. Belt and cable performance assessment.
- Table 4.4. Prototype costs.
- Table 5.1. Sample performance of the education mode performance.
- Table A.1. Bearing specification.
- Table B.1. Gearhead selection for 3.6 Nm.
- Table B.2. Motor selection for gearhead 3.6 Nm.
- Table B.3. Motor–gearhead selection chart for 3.6 Nm.
- Table B.4. Gearhead selection for 17 Nm.
- Table B.5. Motor selection for gearhead 17 Nm.
- Table B.6. Motor–gearhead selection Chart.
- Table B.7. Dual option for gearhead 17 Nm.
- Table B.8. Dual option for motor–gearhead 17 Nm.

Nomenclature and Acronyms

Acronyms

ABS	Acrylonitrile Butadiene Styrene
BB	Biceps Brachial
BPI	Brachial Plexus Injury
CC	Correlation Coefficient
CPM	Continuous Passive Motion
DSP	Digital Signal Processing
DOF	Degree Of Freedom
EMD	ElectroMechanical Delay
FEA	Finite Element Analysis
FE	Flexion–Extension
FOS	Factor of Safety
EMG	ElectroMyoGraphy
KF	Kalman Filter
LNU	Learned Non-Use
MST	MusculoSkeletal Trauma
PM	Passive Motion
RMS	Root Mean Square
RMSE	Root Mean Square Error
ROM	Range Of Motion
SD	Standard Deviation
TB	Triceps Brachial

Variables

A	Cross section area of the cable
a	Center distance between the sprockets/pulleys
acc	Acceleration
B	Force
COM	Centre of mass for the lower arm and hand
D	Pitch diameter
d	Maximal permissible external diameter of the pulley/sprocket
d_w	Wire/rope diameter

E	Modulus of elasticity
EE	Elongation
EMD	Electromechanical delay
EMG_{RMS}	Root mean square of the EMG signal
F	Force
f	Factor
g	Earth's gravity
G_k	Correction of Kalman filter
h	Groove depth
i	Step
l_{la}	Lower arm length
l_{COM}	Distance from the elbow to the centre of mass for the lower arm and hand
l_{EC}	Distance from the elbow to the lower cuff of the device
l_h	Hand length
M	Mass
m_{forearm}	Mass of a forearm
m_{hand}	Mass of a hand
m_{load}	Mass of a load
n	Speed
N	Internal diameter of the pulleys/sprockets
N_{GH}	Gear ratio of a gearhead
P	Power transmission
P_D	Corrected power
P_k	Correction of Kalman filter
P	Power transmission
P_D	Corrected power
P_k	Correction of Kalman filter
Q	Force
Q_{KF}	noise
R	Center of gravity of the lower arm
R_{KF}	Noise for Kalman filter
R_a	Ratio of the amplifier
r_1	Distance from the center of large pulley to the point where the force Q is applied
r_2	Distance from the elbow pivot point to the <i>COM</i> of the forearm
r_3	Radius of the large pulley
time	Time
T	Torque
T_{IN}	Input torque to the transmission system
T_{OUT}	Output torques from the transmission system
T_M	Continuous output torque from a motor
T_{peak}	Design load
t	Span length
u	Neural activation
ws	Window size
X	Plane
X_k	Estimated position by Kalman filter
X'_k	Updated position by Kalman filter

z	Number of teeth
α	Angle between force Q and plane X
α_{EMG}	Coefficient of neural activation equation
β	Angle between force F and plane Y
β_{EMG}	Coefficient of neural activation equation
γ	Angle between force B and plane Y
ε	Angle between force F and plane X
θ	Angle between force F and plane Z
μ	Angle between force Q and plane Y
δ	Angle between force Q and plane Z
φ	Slip angle
η_G	Efficiency of the gear transmission
η_{GH}	Efficiency of the gearbox
η_{TA}	Efficiency of the torque amplifier
σ_{limit}	Stress limit
σ_{VM}	von Mises stress
$\Delta\alpha$	Change in position
$\Delta\tau$	Change in speed
Δ	Cable deflection

Units

Nm	Newton·meter
Hz	Hertz
N	Newton
m	Meter
A	Ampere
m/s	Meter/second
°/s	Degrees/second
g	Gram
N	Newton
W	Watt
rpm	Revolutions per minute
h	Hours
s	Second

CHAPTER 1

1 INTRODUCTION

Over 60 million people in North America require trauma-related care [1]. The major causes of musculoskeletal traumas in Canada between 2008 and 2009 were accidents (79%): the result of a fall (38%) or of motor vehicle collisions (41%) [2]. After hospitalization, many patients struggle to find a therapy that works for them. A common challenge for a patient during the recovery process is to follow a long-term home-based exercise program customized for each specific case. Failure to comply with the rehabilitation program and a lack of cooperation by the patient leads to chronic pain, limited range of motion and other unresolved issues. 55–75% of patients retain the limb impairment after 3–6 months [3].

Thus, a huge area in biomedical engineering known as robotic-aided-rehabilitation proposes alternative solutions for complex and time-consuming motion training programs. The attraction of using robotic-aided-rehabilitation is based on the idea that a smart device has the capability of measuring the patient's performance outside of the clinical settings and providing effective feedback both to the patient and to the therapist. Thus, the 24/7 supervision provided by a rehabilitation device is a promising option for patients with functional impairment that lack motivation during long-lasting home-based treatment.

1.1 Motivation

Musculoskeletal trauma (MST), as a result of a peripheral nerve injury, was reported in 2.8% among the trauma population [4]. One particular MST that requires extensive upper limb therapy results when the brachial plexus nerves are damaged [5]. Brachial plexus injury (BPI) produces sensory degradation that starts immediately after nerve lesion occurs. Thus, early surgical nerve reconstruction is recommended [6].

Due to the complexity of the human neuromuscular system, the postoperative recovery process may take 12–24 months. During the reinnervation, i.e., nerve regeneration after a lesion, sensory functions are based on the previous experience of cortex (the region of the brain that controls movements), i.e., new profiles of nerve impulses are not immediately associated with corresponding movements. Therefore, some patients are not able to lift their arm without external assistance despite the presence of neural activity in the muscles. As a result, BPI patients have to learn how to control the extremity by means of repetitive training with dynamic splints and mechanical braces [6]. However, despite the desire to restore functional activity of the impaired extremity, many patients tend to skip the follow up meetings with the therapist due to social and economic problems [7]. Additionally, patients do not provide enough information about the progress and frequency of muscle training at home. Thus, therapists have difficulties in correcting the rehabilitation equipment properly and maintaining or accelerating the recovery of the impaired limb.

Moreover, without constant professional feedback during the home-based therapy, a phenomenon called “learned non-use” (LNU) may occur [6]. During the daily activities, BPI patients learn to involve their non-affected limb due to repetitive failure to use of the affected one. Eventually, when the motor skills are changed, patients suppress to use their recovered limb even when full reinnervation takes place.

At the end of the rehabilitation, in 20–25% of BPI patients, only half of the functional skills are restored [8] or they continue with lifelong limb impairment [9]. As a result, they have a lower quality of life compared to the normal population [8] due to such factors as reduced family income, low emotional connection between family members and overall emotional instability and constant stress. Consequently, despite clinicians’ effort and patients’ willingness to recover, the current postoperative treatment strategies are limited when assisting BPI patients during home-based therapy. Thus, an automated method of muscle training control with remote clinicians’ supervision during the home-based training is a promising but still unexplored possibility to accelerate BPI patients’ recovery.

The constant communication between the patient and the therapist via an automated method of muscle training control will increase the patient’s motivation to perform all of the prescribed training exercises. At the same time, the therapist will be provided with the information on how the patient progresses or whether the patient’s program/equipment should be corrected.

The automated method of control may be achieved by using smart robotic technologies for assistive-rehabilitation that can measure patient's muscle activity, record progress and communicate with the therapist 24/7. However, despite the abundance of robot-assisted projects during the last years, there is still no consistency on how to design wearable mechatronic devices for upper limbs, nor is there information on how to apply them to the needs of patients with BPI. Hence, it is necessary to determine how to expand the application of robots to home-based muscle trainings for BPI patients, as well as to identify the role of a wearable mechatronic device in the postoperative rehabilitation process.

1.2 General Problem Statement

Nerve related trauma can involve connective tissues, muscles and tendons. Despite the variety of nerve lesions, physical therapy modalities and postoperative care, therapeutic exercise plays an essential role for BPI patients. Although active-assistive rehabilitation has been shown [10] to help restore musculoskeletal functionality, many patients are not compliant with their rehabilitation program due to social responsibilities, forgetfulness, lack of motivation, boredom and/or lack of instant feedback [7]. Thus, a promising option for this group of patients is a home-based therapy assisted by an interactive portable mechatronic device that 1) maintains patient motivation, 2) monitors and measures movements outside of a clinical setting and 3) provides motion assistance. Hence, it was proposed to design a wearable mechatronic brace for upper limb rehabilitation that can be used at any stage of motion training after surgical reconstruction of brachial plexus nerves.

1.3 Research Objectives and Scope

The main goal of this thesis is to design a mechatronic home-based device for postoperative muscle training that assists patients to perform desired motions and ensures that the motion is within a safe range. Since the brachial plexus nerves control all upper limb muscles including neck muscles, the focus of interest was narrowed down to the upper arm muscles that move the elbow joint.

The scope of the work includes the mechanical design of the proposed device and an assessment of the performance of the prototype. In order to identify the design requirements for the safe and effective motion therapy of the upper limb, a proper review of elbow biomechanics and the natural movement of this joint, standard postoperative techniques of

motion restoration currently used and prior art in elbow rehabilitation robotics were required. The design stage of the project includes following objectives:

- to identify technical specifications for the mechanical and actuation parts of the device;
- to develop and evaluate proposed design concepts;
- to select the most optimal solution for the mechanical and actuation parts of the device;
- to build a prototype of the proposed device;
- to setup and calibrate the actuation system of the prototype.

Since motion rehabilitation involves both passive and active training, three basic modes of postoperative treatments were considered as the main functions of the device: (1) passive (assistive) exercises, (2) assisted (assistive-as-needed) motions and (3) resistive (assistive-as-needed) exercises. All modes require a sensing system that quantifies patient's intention to move the upper limb. Therefore, a method of motion intention estimation that can be adapted for different exercise modes was designed as part of the current work. To achieve this goal, the following objectives were addressed:

- Sensing systems that quantify the patient's intention to move the upper limb were reviewed.
- A motion sensing strategy for BPI patients that undergo postoperative motion rehabilitation was selected.
- An elbow motion model that uses sensed data from the user and estimates the desired elbow position was designed and evaluated.
- The proposed elbow motion sensing model was integrated into the control system of the prototype.

Finally, an assessment of the mechatronic elbow brace performance can be achieved by evaluating reliability, accuracy and repeatability of the device response for the three modes under diverse conditions according to the specifications. Based on the results, further modifications to the device were proposed.

1.4 Overview of the Thesis

The structure of the rest of the thesis is as follows:

Chapter 2	Background: Provides an overview of elbow biomechanics and current strategies for postoperative elbow treatment. Literature Review: Summarizes the state of the art in portable rehabilitation robotics for elbow motion rehabilitation, as well as sensing strategies for motion detection.
Chapter 3	Device Design: Outlines the design and development of the prototype of the wearable elbow brace. A comprehensive decision making analysis of mechanical and actuation design was also described in this section.
Chapter 4	Device Prototype: Provides an overview of the wearable elbow mechatronics-enabled brace prototype. An assessment of the design features is described and discussed.
Chapter 5	Methods of Digital Signal Processing: Presents the work done towards the development of two rehabilitation modes of the wearable elbow brace. The educational mode was designed to mimic the training sessions with the therapist, while the assistive mode was developed for home use. This chapter includes the preliminary evaluation of two hypotheses used for estimation of a trajectory and a speed profile of the forearm motion.
Chapter 6	Performance Assessment: This chapter explains how the two postoperative modes were simulated using MATLAB scripts and duplicated in C++ Visual Studio project to test prototype performance. The results of the experiment were compared to the design goal. The prototype performance, as well as errors and limitations of the experiment, are discussed in this chapter.
Chapter 7	Concluding Remarks: Highlights the contributions of this thesis and proposed suggestions to refine the preferred design.
Appendix A	Rated Life of Bearings: Based on the findings in Section 3.3.1, calculation of the rated life of a bearing are presented in the Appendix.
Appendix B	Motor–Gearbox selection: This Appendix presents the summary of motor–gearbox selection according to actuation system specification in Section 3.3.4.

Appendix C	Motor Specification: This Appendix includes motor specification that was selected in Chapter 3.
Appendix D	Bearing Specification: This Appendix includes the specifications of the bearings selected in Chapter 3.
Permissions and Approvals	Presents proof of ethics approval for the trials that involved human subjects, as well as the supporting documents for the trials.

CHAPTER 2

2 LITERATURE REVIEW AND BACKGROUND

In order to develop the list of design requirements for a mechatronic elbow brace, the elbow biomechanics, current postoperative motion rehabilitation techniques, prior art in portable rehabilitation robotics for upper limb, as well as sensing strategies for motion detection were reviewed. The section presents a summary of the findings.

A comprehensive literature search was performed during the period of January to August 2014 and continuously updated during the period of September 2014 to April 2015 using Google Scholar, IEEE Xplore, SpringerLink Journals and PubMed. A diverse combination of the following keywords were used: elbow, powered, exoskeleton, brace, orthosis, wearable, portable, rehabilitation, EMG-driven, EMG model, EMG prediction, EMG biceps (BB) and EMG triceps (TB). The priority was given to papers published in the previous 5 years. A total of 154 papers formed a database, including 70 papers selected for the mechanical design review of powered elbow braces and 52 papers that review sensing systems for elbow motion and rehabilitation. Additionally, a review of the commercially available devices for upper arm and elbow rehabilitation was summarized in order to estimate cost constraints and to develop a custom-oriented design strategy.

The following section focuses on the basics of the upper limb neuromuscular structure (Section 2.1), a brief overview of the elbow motion restoration process (Section 2.2) and current methods for postoperative elbow motion rehabilitation strategies (Section 2.3). Based on the literature research in Section 2.3, Section 2.4 summarizes this chapter with an outline of the unresolved problems in upper limb motion rehabilitation for BPI patients.

2.1 Brachial Plexus Structure and Lesions

The sensory-motor innervation of the upper arm is provided by the brachial plexus nerves formed by the confluence of the ventral rami of the spinal nerve roots from C5 to T1. Considering the location of nerve dissection (nerve root, trunk, division, cord or musculocutaneous nerve), each scenario of muscle palsy will limit upper limb functionality.

As shown in Fig. 2.1, a lesion in the musculocutaneous nerve (Fig. 2.1 blue area in the brachial plexus nerves diagram) results in a palsy of three muscles: coracobrachialis, brachialis and biceps brachii (Fig. 2.1 blue area in the corresponding palsy diagram), which cause flexion movements at the elbow.

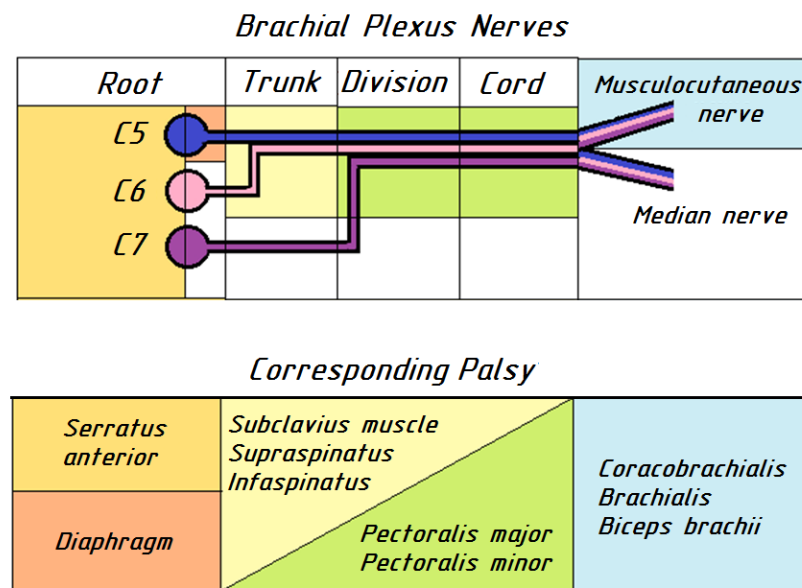


Fig. 2.1. Brachial plexus (C5-C7) and muscles that motor the upper limb.

As the contraction of the brachialis and biceps brachii muscles is diminished, the elbow loses its main function: to position the forearm in space. In normal circumstances, the elbow performs flexion-extension (FE) motions within 0–130° [10] (Fig. 2.2 A) in the sagittal plane with a gradual change of carrying angle within -5°–+15° [11] (Fig. 2.2 B) in the coronal plane (Fig. 2.2 C). During the normal elbow FE movement, a linear change in carrying angle was reported by Morrey and Chao in 1976 [12].

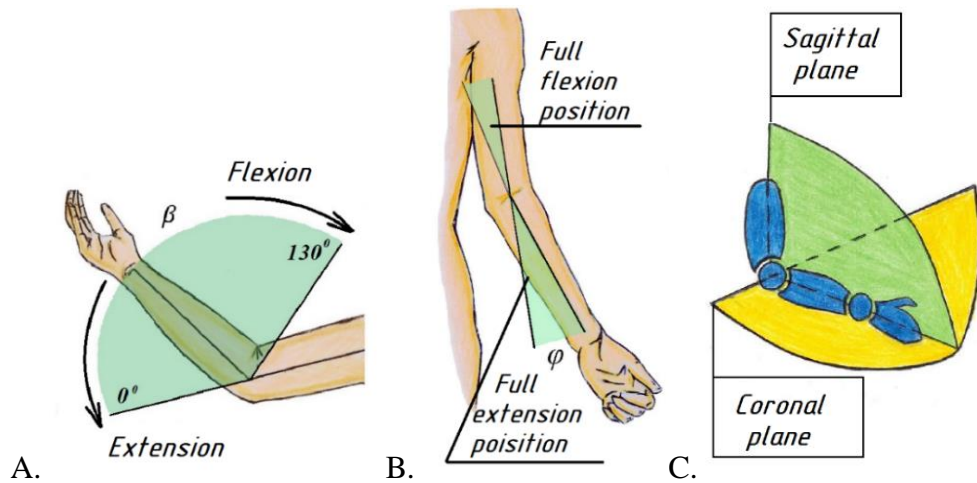


Fig. 2.2. Elbow biomechanics: φ - carrying angle, β - range of motion.

A. Active range of motion in the sagittal plane. B. Carrying angle in the coronal plane. C. Sagittal and coronal plane of the upper limb.

The inability to flex the elbow results in abnormal upper limb function and muscle atrophy. When flexion of the elbow becomes impossible to perform, an investigation of the nerves using electromyography (EMG) should be done. When the musculocutaneous nerve alone is injured, nerve repair is prescribed after a 3-month observation period [13].

2.2 Brachial Plexus Reinnervation

Since an injury can occur near the target muscle, nerves may recover in few months. If no improvement is observed, reconstructive surgery takes place.

Reinnervation, i.e., nerve regeneration after a lesion, is a complex and time-consuming postoperative process. The postoperative management starts with arm immobilization at 90° of elbow flexion (see Table 2.1, Phase I). The goals of Phase I are to protect the healing tissue and to decrease pain and inflammation. During this phase, patients are instructed to perform biceps isometric contraction to prevent muscle atrophy and neurophysiological alterations.

Slings and upper limb supports are usually provided by the therapist, see Fig. 2.3. The design is based on the therapist's experience and the patient's needs [14]. The polymer used for casting elbow splints can vary in price between \$2 and \$10 per unit [15]. Commercially available braces can also be proposed for immobilization. The price for an item starts at \$30 [16].

The other option is to use more advanced mechanical braces (see Fig. 2.3) that can fix the forearm in a certain position and are able to limit the range of motion (ROM) for different rehabilitation purposes. In this case, the brace has to be regulated and adapted to various stages and progress of the physical therapy [10]. The average price is \$260 [17].

In order to maintain muscle trophism and stretch denervated muscle fibers while the nerve recuperation progresses, passive movements are applied to the appropriate joint (see Table 2.1, Phase II). To promote the healing process, the physiotherapist manually helps the forearm to overcome gravity. As pain and edema subside, the amount of assistance is decreased [18]. In addition, postural education and balance retraining [4] help to decrease neuropathic pain, re-educate the cortex and promote return to normal activities.

Table 2.1. Postoperative care after brachial plexus nerve reconstruction.

Postoperative management	Equipment	Limitations
Phase I. Protection. Time: up to 6 weeks		
Arm is immobilized, i.e. no elbow movement. Biceps isometric contractions.	Static orthotic/splint [19], sling or mechanical brace (see Fig. 2.3).	(1) May be difficult for a nontherapist to position and/or adjust [19].
Phase II. Occupational therapy. Time: week 2 to 8 [19]		
Passive muscle training with therapist. Postural and full passive ROM education. Review of slings/ supports.	Dynamic orthotic/splint [19] or mechanical brace. Physical therapy [6].	(1) May be difficult for a nontherapist to position and/or adjust [19]. (2) Therapist can be available only at the clinic.
Phase III. Home-based muscle training program. Time: week 8 to 12–24 months [19]		
Maintain passive and active elbow ROM. Begin resistive exercises.	(1) Mechanical braces with elastic bands (see Fig. 2.4) or springs for home daily exercises.	(1) Constant adjustment of the elastic bands or springs are needed to ensure that the patient continues to progress. (2) Lack of professional feedback. (3) Failure to comply with the rehabilitation program.



Fig. 2.3. Mechanical brace, Innovator X® (Össur).

As the nature of recovery does not require long-term and constant physiotherapy, a daily home exercise program (see Table 2.1, Phase III) with continuously progressive strengthening regimes [4] supplements the physical therapy and later becomes the main rehabilitation activity. Although patients are encouraged to use their affected arm in their daily activity, the phenomenon LNU may occur [6]. However, if provided with sufficient opportunities to practice [21], [22], patients can restore motor performance.

Elastic bands, rubber bands (see Fig. 2.4), spring wires and springs are used as additional components in passive hinges to provide torque to a joint [23] at the resistive training stage. Regardless of the choice of an energy-storing component, the resistance must be progressive during the entire BPI rehabilitation. Additionally, as the patient's ROM may increase, changes in the resistance of the elastic components should be made. Since the length of the component and stiffness of the material change the amount of applied torque, the size of elastic components should be adjusted with respect to new conditions.



Fig. 2.4. Mechanical rehabilitation braces for post-operative management of brachial plexus injuries. St. Joseph's Health Care London, ON. ©2014 IEEE

Due to the constant stretching and relaxing of the elastic components, they experience cyclic deformation (cumulative damage to the material). Thus, the resistive properties of the material decreases over time and eventually the resistive component must be replaced. However, the frequency of periodic replacements may vary from case to case. Moreover, specific sensors for torque estimation has to be applied in order to check the level of damage to the material. Thus, in order to save time, the therapist simply installs a new component with known resistive properties instead of estimating the resistive properties of the material. Nevertheless, each new component will still experience cyclic deformation and, therefore, apply an unknown torque to the joint.

Even though elastic and resistive components are affordable and cheap, constant replacement or size adjustment is required to tailor the amount of torque applied to a joint, as the affected muscles get stronger, as the patient's ROM may increase during the training program and as the materials experience cyclic deformation.

At the end of the rehabilitation, a BPI patient will spend around \$300 for equipment rent and supporting materials. Additionally, since patients are limited to staying at home (due to the need of frequent clinical appointments and daily muscle training for 12–24 months), their income may decrease by an average of \$49,000 per year [24]. Even with increased effort and time, in 20–25% of cases, only half of the functional skills of BPI patients are restored [8] or lifelong limb impairment persists [9]. As a result, they have a lower quality of life compared to the normal population [8].

2.3 Portable Mechatronic Elbow Devices: State of the Art

Since the likelihood of a positive outcome from current BPI rehabilitation techniques is low, alternative ideas for muscle training programs that involve automated methods for controlling patients' movement control have been developed during recent years. This new concept can be accomplished by using smart robotic technologies for assistive-rehabilitation that can measure patient's muscle activity, record progress and communicate with the therapist 24/7. Even though multiple attempts to create a robot-assisted rehabilitation program were reported in recent years, there is no consistency on the optimal design for wearable robotics aimed to train muscles. Therefore, a review of smart elbow

rehabilitation mechatronic systems, as well as the types of actuation and sensing systems that can be adapted for BPI patients with upper arm palsy is summarized below.

2.3.1 Mechanical Design of Smart Elbow Devices for Rehabilitation

Systematic reviews confirm that powered assistive devices have high potential of improving upper limb functionality in neuromuscular rehabilitation [25]–[29]. Therapeutic exoskeletons for the upper limb were shown to be more effective on motor functional improvement than continuous passive motion (CPM) machines [30], and as efficient as the same amount of exercise performed with a therapist [31], [32]. Lo, *et al.* reported that more frequent and longer training with appropriate movements and intensities speed up the recovery process [33]. The latest reports [35]–[67] show that adapting assistive robotic therapy to home-based conditions is a promising way to increase patient's motivation to perform repetitive daily exercises. Home-based training with wearable rehabilitation devices has benefits over robot-based training in a clinical environment, since portable technologies can meet two criteria for a successful recovery [68]–[70]: (1) the device has to oversee the patient's performance and (2) it must provide regular feedback to the therapist.

Wearable assistive devices combine the advantages of the leading robotic technologies (high accuracy of motions, stable positioning of the forearm in space and high repeatability), with the clinical experience of therapists (customized rehabilitation programs and effective feedback), while maintaining independence from the clinical environment. Such possibilities inspired many research groups to develop wearable smart elbow devices [35]–[67] (see Table 2.3). However, the reviewed mechatronic systems have a number of limitations that are discussed below.

The overall mechanical design of the smart elbow systems is based on the type of the torque transmission system. Thus, reviewed mechatronic systems can be grouped in three categories (see Fig. 2.5):

- A. Rigid bars and one actuation system located on the lateral side of the upper limb, see Fig. 2.5 A.

B. Rigid bars are located symmetrically on both sides of the upper limb. One actuation system drives the brace from the lateral side, see Fig. 2.5 B.

C. Rigid bars are placed symmetrically on both sides of the upper limb. The actuation system transmits torque to both sides of the joint, see Fig. 2.5 C.

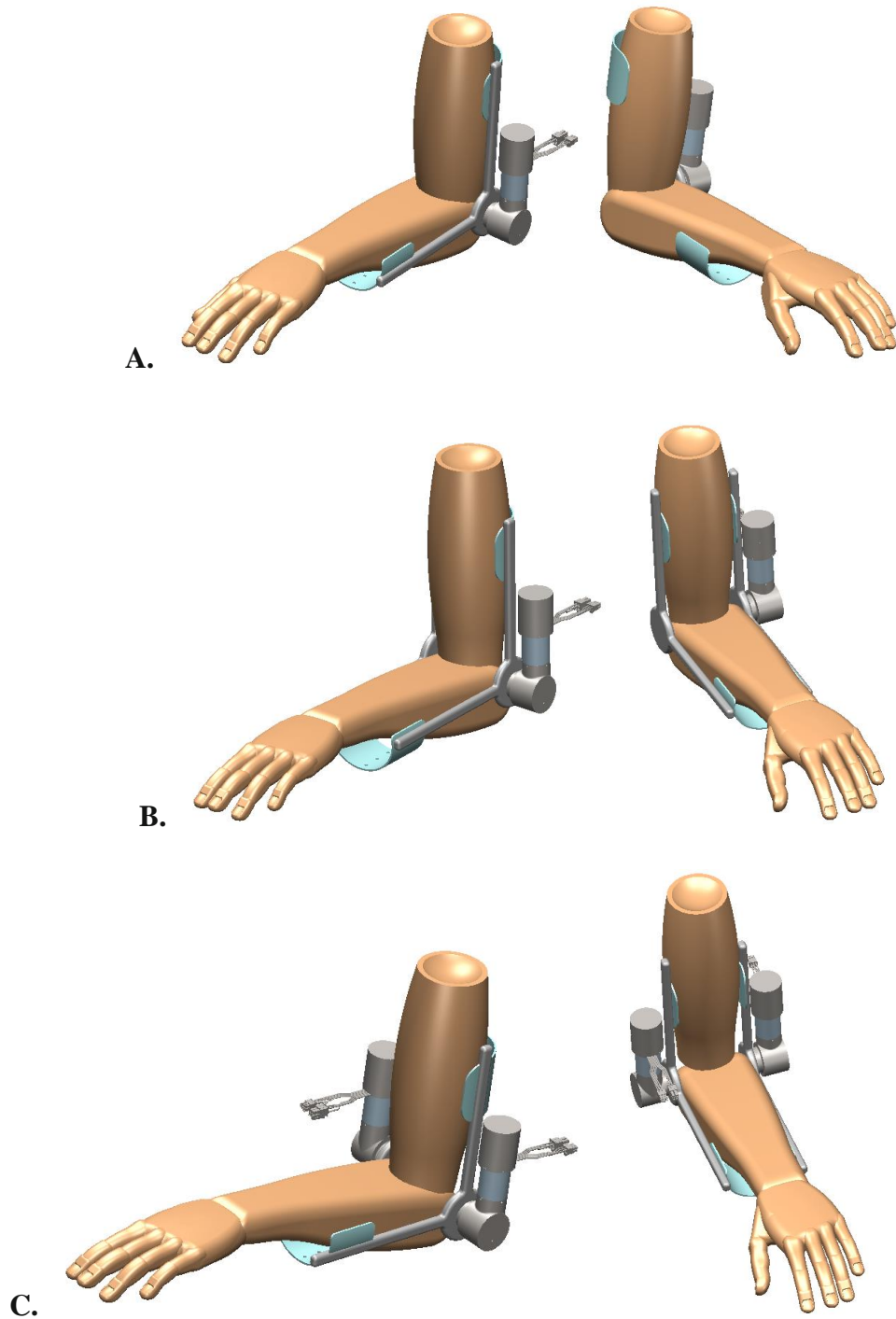


Fig. 2.5. Mechanical design of an elbow wearable powered brace.

Table 2.3. Review of wearable devices for elbow rehabilitation.

Ref.	General Information	Type	Limitations
[37]	Proposed device was designed to assist in recovery therapy of motor function about elbow joint.	A	No mechanical stoppers. No rigid cuffs. May slide off the arm. The design does not take into account the carrying angle.
[42]	A powered orthosis for upper limb training and functional support. The weight of the control system is distributed on the backside of the upper arm.	C	May slide off the arm. Actuators are limited in producing torque. Splints are not adjustable in size and position. No mechanical stoppers. The design does not take into account the carrying angle.
[43]	RAO, robotic arm orthosis, is a portable assistive device for the upper extremities. ROM was mechanically limited to 110 degrees. All structural components were fabricated out of an ABS derivative. A strap that goes over the user's right shoulder and underneath the left arm prevents slid-off effect. Portable battery.	A	No information about the weight of the prototype. The design does not take into account the carrying angle.
[47]	AVSER is an active variable stiffness exoskeleton robotic system with an active variable stiffness elastic actuator. The total weight is 1.6 kg. ROM: 0–150 degrees.	A	The weight of two motors and transmission mechanism may distort the device. No mechanical stoppers. May slide off the arm. The design does not take into account the carrying angle.
[48]	Powered elbow orthosis for rehabilitation. Can be used for three stages of the rehabilitation process: passive, active and interactive mode. Mechanical stops. The total weight is 1.1 kg.	A	The weight of two motors and transmission mechanism may distort the device. May slide off the arm. The design does not take into account the carrying angle.
[53]	A powered orthotic brace is designed to follow the natural motion of the elbow.	C	The backpack makes the exoskeleton too bulky. No mechanical stoppers.
[54]	An upper limb orthosis for rehabilitation. The materials are a combination of carbon reinforced plastics and polyamide PA6. A carrying system distributes the weight of the device on both shoulders.	A	No rigid cuffs. No mechanical stoppers.
[57]	A wearable robotic device that assists or resists the subject's joint torques. The weight is 2.5 kg (excluding a pneumatic servo valves and a compressor).	A	Transmission system limits the workplace. No mechanical stoppers. The design does not take into account the carrying angle.

Ref.	General Information	Type	Limitations
[58]	An exoskeleton system for elbow assistance. The total weight is 2 kg. The weight of the control system is distributed on the backside of the lower arm.	C	The elbow joint is not actuated in an extension direction. No mechanical stoppers. May slide off the arm. Cuff position is not adjustable. The design does not take into account the carrying angle.
[59]	An exoskeleton that provides elbow flexion–extension movements. The exoskeleton structure was built in aluminum. The weight is 2.9 kg.	A	No mechanical stoppers. May slide off the arm. The weight of the motor and transmission mechanism may distort the device. The design does not take into account the carrying angle.
[60]	NEUROExos is a portable version of the robotic elbow exoskeleton designed for the treatment of stroke survivors in acute/subacute phases. The weight of the control system and actuators are distributed on the backside of the upper arm.	B	No mechanical stoppers. May slide off the arm. Cuffs are not adjustable in position. The design does not take into account the carrying angle.
[62]	MAHI Exo II is an exoskeleton designed for rehabilitation of stroke and SCI patients. Mechanism allows changing the transmission from one side to the other.	C	The actuation mechanism makes the exoskeleton too bulky. No mechanical stoppers. May slide off the arm. Cuff size and position are not adjustable. The design does not take in to account the carrying angle.
[64]	An upper-limb power-assist exoskeleton. The total weight is 2.1 kg.	A	No mechanical stoppers. May slide off the arm. The design does not take into account the carrying angle.
[66]	My Own Motion E100 (Myomo) is a powered orthotic device designed to provide rehabilitation exercises. The weight of the wearable portion of the unit is 0.5 kg.	C	May slide off the arm. The design does not take into account the carrying angle. No mechanical stoppers.

Despite reduced weight, powered elbow braces Type A [37], [43], [47], [48], [54], [57], [59], [64] and Type B [60] can be distorted by the weight of the actuation system if they are not distributed across the arm. Due to this fact, the brace may slide down the arm or provide undesired additional torsion force to the joint. Uncontrolled assistance may result in joint deformity and limited ROM in the elbow coronal plane. The more advanced mechanical designs can be seen in mechatronic elbow braces Type C [42], [53], [58], [62], [66], [67]. The two-sided actuation system distributes the torque applied to the joint and

supports the forearm during FE movements in a synchronized manner. The resulting torque produced by the actuation system ranges between 10 Nm [43], [48] and 30 Nm [60].

One method increasing the reliability of a mechatronic system is to use an additional component, which duplicates the function of a part that can fail, i.e., to use a reserve component. Realistically only critical functions of the system should contain reserve components. In case of the powered elbow mechatronic system, the range of motion has to be constantly monitored and maintained within safe limits. Thus, if the control or the actuation systems fail to limit the patient to a specific ROM to the patient, a mechanical stopper will limit patient's ROM and therefore increase the system's reliability. Despite the benefits of reserve components, most of the reviewed projects [37], [42], [47], [53], [54], [57]–[60], [62], [64], [66], [67] did not pay attention to the reliability of the prototype.

Since the main function of an elbow brace is to support the forearm and help it to overcome gravity, the mechatronic brace should maintain the natural biomechanics of the elbow. Incorrect elbow positioning or movement during the rehabilitation program may cause alterations in joint anatomy and limitations of elbow motions. Hence, a simplified model of an elbow that has one degree of freedom (DOF) in the sagittal plane (see Fig. 2C) may trigger disease aggravation. **A 2-DOF model of an elbow motion** is the minimum requirement for a mechatronic brace as it includes active flexion-extension and passive adduction-abduction movements (driven by the bone structure of the elbow). Only two prototypes found in the literature [53], [54] met this requirement.

The last main limitation of the reviewed elbow braces is the lack of adjustable components [42], [58], [60], [62]. Fixed rigid cuffs and bars without a telescopic feature will dramatically decrease the adjustability of a device to different users.

2.3.2 Actuation Systems for Wearable Elbow Powered Applications

Smart elbow devices are aimed at delivering forces with high precision and repeatability. Thus, the choice of the actuation technology is a key decision for creating an efficient rehabilitation system. The most frequently used actuators are electromagnetic motors [35], [40], [41], [43]–[54], [58]–[62], [65]–[67], while less popular technologies include pneumatic muscles [37], [56], [57], [64], hydraulic drivers [42], [55], and shape memory

alloys [38]. A short summary of actuation systems used for powered elbow projects designed within the last 5 years is presented in Table 2.4.

Table 2.4. Actuation and power transmission in wearable devices for elbow rehabilitation.

Ref.	Type of actuator	Actuation and Power Transmission
[37]	Pneumatic actuator	Two artificial pneumatic muscles (Shadow Robot) on the lateral side of the upper limb. Maximum pull 20 kg.
[42]	Hydraulic drive	Hydraulically driven elbow training system: two miniaturized flexible fluidic actuators.
[43]	DC motor	Was designed to generate 10 Nm of output torque by a brushless DC motor with customized gearbox.
[47]	DC motor	One DC-motor is used to control the position of the joint, and the other is used to adjust the stiffness. Maximum output torque of 29 Nm.
[48]	DC motor	Two electric drives. The larger one, attached nearest to the joint allows the orthosis a maximum torque of 10 Nm. The smaller drive sets the compliance of the system. Clip-off actuator.
[53]	Motor	Cable-driven (Bowden cables) series elastic actuators with motors in the backpack.
[54]	DC motor	A 24 V Maxon Amax 22 DC motor with a 333:1 Maxon planetary gear and a 4:1 worm wheel gear drives the joint. The DC-drive can generate a torque of about 16 Nm.
[57]	Pneumatic actuator	Pneumatic actuators.
[58]	Motor	Six motors are placed on both sides of the forearm support part. Two wires connect the motors and the upper arm support part. Each motor produces 0.468 Nm. The gear ratio is 66:1.
[59]	DC motor	DC brushed motor produces mean torque of 45 Nm.
[60]	DC motor	DC servomotor (Maxon EC motor EC60, 400W) produces a maximum joint torque of 30 Nm. Harmonic Drive reduction stage (CPL-17A-080-2) has a reduction ratio of 80.
[62]	DC motor	Two high torque DC motors (Maxon RE65) with cable drives achieve a maximum torque of 11.61 Nm.
[64]	Pneumatic actuator	Two pneumatic muscles (SPCU-S-1, The Shadow Robot Company Ltd., London) connecting to the Nylon® axis drive rotate the joint of the device.
[66]	Motor	Two motors, each located on opposite sides of the joint, are connected to a drive assembly on the corresponding side of the joint. The actuation mechanism generates up to 14 Nm.
[67]		

Electric motors as part of assistive robotics are well studied due to their availability and high precision. However, the complexity of the mechanical coupling and heavy weight motivates researchers to use pneumatic muscles that have a better power to weight ratio. Despite the attractiveness of using simple and inexpensive pressure-driven muscles, the

biggest disadvantage is the pressure source, which can be noisy and heavy. Another alternative is the use of dielectric polymers that do not require an intermediate transducer and operates silently. Nevertheless, this type of actuation is the most expensive and requires high voltages. Accordingly, a report that describes an actuation system that has high feasibility and efficacy was not found. Hence, the choice of the actuation technology mainly relies on the experience of the design engineer and the design constraints.

2.3.3 Control Strategy of Actuation Systems in Motion Rehabilitation

For a wearable mechatronic device to be controlled, human interaction can be detected and transferred to the actuation system of the device. Human intent can be measured by a number of sensors [71]: position and motion sensors, force and pressure sensors, muscle activity sensors or brain activation sensors. Moreover, muscle activity sensors that measure cognitive human-robot interaction include EMG (electromyography) sensors, muscle stiffness sensors, muscle tenseness sensor, ultrasonic muscle activity sensors and mechano-myography sensors [71].

Surface EMG sensors (see Fig. 2.6) have been proposed as natural muscle interfaces for wearable mechatronic devices [72]. As EMG measurements have high sensitivity to muscle activity, they have been successfully used to measure fatigue [73] and to identify the operator's intention [72], [74]. Surface EMG recordings provide a safe, easy and noninvasive method that allows objective quantification of muscle energy [75].

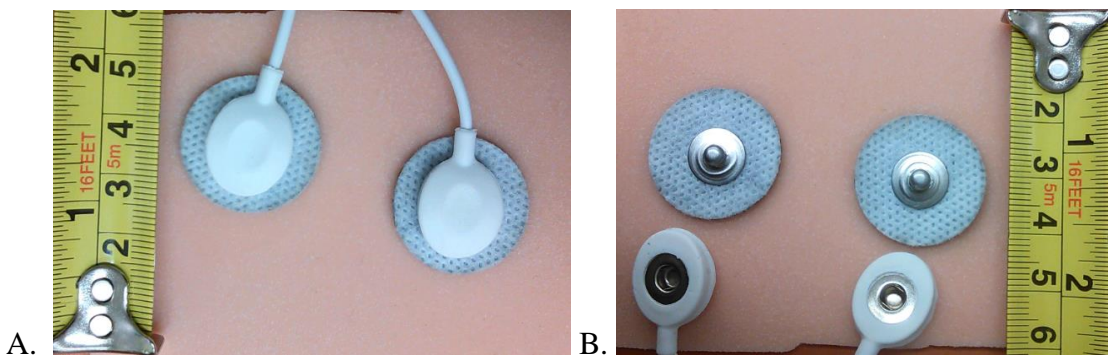


Fig. 2.6. EMG sensors and electrodes.
A. Assembled and placed on a silicone skin.
B. Sensors separated from the electrodes.

The raw EMG signal can be analyzed in one of four different approaches: amplitude, frequency, EMG-force relationship and amplitude probability distributions [77]. The

average, root mean square (RMS) and mean spike amplitude of band-passed EMG activity have been used to quantify the magnitude of muscle activity [78].

Over the past 5 years, several research groups have developed EMG-driven models that quantify upper arm muscle activity and provide elbow FE motion profiles [79]–[91] (see Table 2.5). The aim of the models is to describe limb motion as a function of its EMG signals. At first, Hill-based models used knowledge about the dynamics of individual sarcomeres within a fiber [93] to link extremity motion to muscle activity. Later, it was shown that a mapping technique (e.g. classification models, artificial neural networks or support vector machines) could achieve better accuracy (88.15–98.8%) than Hill-based models [81], [84], [87], [89], [90] that have 90.54–96.37% accuracy. On the other hand, mapping EMG signals directly to joint kinematics [79], [80], [83], [85], [86], [88], [91] requires a long individualized calibration process that must be updated as muscles strengthen. Thus, despite good accuracy, mapping models are complex and limited in their application.

The error of converting motion intention from EMG signals to motion profiles for these models [79]–[91] was estimated to be in the range of 1.20–11.85%. However, it is hard to compare the dynamic models' performance since a different number of EMG signals are used as input signals to the models. The most frequent and intuitive method of describing elbow motion is thought the EMG signals from the biggest flexor (BB) and biggest extensor (TB) [79], [83], [84], [87], [91]. The more advanced attempts involve adding the input signals from additional EMG sensors placed on the upper limb muscles: brachioradialis [85], [90] or forearm muscles [86]. Controversially, the simplified models were using only one input from BB [80], [81] or TB [88]. As a result, there is no standard rule for using EMG signals neither for describing dynamic elbow motion, nor for justifying why a certain group of muscles may result in better accuracy of prediction for EMG-driven models.

As human limb positioning and movements are controlled by receptors with specific precision, we are interested in the ability to assist during the motion with sensitivity equal to that of human joint positioning. The error of joint position sensing for the elbow is 2° [92]. An expert from St. Joseph's Health Care London, hand physiotherapist S. Chinchalkar, has confirmed that elbow FE position error can vary between 2° and 5° . As an average elbow ROM is 0 – 130° , the accuracy of limb positioning can be between 96% –98.5% (5° of error out of 130° is equivalent to 96% accuracy, and 2° of error out of 130° is equivalent to 98.5% accuracy). Therefore, an EMG-driven model will be considered effective and

stable if it can quantify the patient's intention to move within a specific accuracy of 96–98.5% for different ROMs.

Table 2.5. EMG-driven models for elbow motion quantification.

Ref.	Method	Muscles	Accuracy (%)	Limitation
[79]	Acceleration data and RMS of the EMG data was mapped with the help of a Kalman filter.	BB ¹ , TB ²	88.15	The model was designed to predict tremor, thus may be suitable only for fast motions. Low accuracy.
[80]	Artificial neural network.	BB	89.51	Low accuracy.
[81]	Modified Hill-based model and a Kalman filter.	BB	90.54	Low accuracy and long calibration process. The model was tested only for the EMG signal from the biceps.
[83]	Mapped model and a Kalman filter.	BB, TB	91.7	Low accuracy.
[84]	Classic Hill's model.	BB, TB	92.5	Low accuracy and long calibration process.
[85]	Artificial neural network that uses mechanomyography in combination with EMG.	BB, BRD ³	93	Low accuracy. The model was tested for isometric contractions.
[86]	Artificial neural network.	BB, TB, PM ⁴ , DA ⁵ , DP ⁶	93.8	Low accuracy.
[87]	Hill-type model.	BB, TB	94.78	The model was tested for moderate speeds.
[88]	Fuzzy-neuro modifier.	TB (BB was used for scaling the signal)	93.73	Low accuracy.
[89]	Hill's model [93] with a Calcium concentration rule.	BB short head, BB long head, TB long head, TB lateral head	96.03	Limited to isometric contractions at a stationary elbow position (90°).
[90]	Switching the model between two different modes (velocity and force).	BB, TB, BRD	96.37	The model is restricted to normal and high speeds (25–80°/s).
[91]	Mapping models.	BB, TB	98.8	It is not clear how the model will perform for a ROM between 90° and 130°.

¹ BB – biceps brachial.

² TB – triceps brachial.

³ BRD – brachioradialis.

⁴ PM – pectoralis major.

⁵ DA – deltoid anterior.

⁶ DP – deltoid posterior.

Accordingly, only three models [89]–[91] meet this requirement. Despite good accuracy, these models are restricted to specific exercise conditions: isometric contractions (i.e., stationary contraction of the muscles) [89], normal and high speeds [90] and limited ROMs [91].

2.4 Conclusions

Rehabilitation therapy of a neuromuscular injury consists of daily exercises, as they prevent joint stiffness and deformity, contractures, and increase the range of motion. However, due to muscle weakness, some patients may not be able to lift their limb without external help. To prevent muscle degradation a therapist or a rehabilitation robot assists with the exercise during the in-clinic-sessions, while a mechanical brace can immobilize the joint in a certain position the rest of the time. An alternative way is to use a smart home-based device that senses the patient's intention to move, assists him or her to perform the desired motion and ensures that the range of motion is within a safe limit. A number of research groups have developed powered elbow devices for home use, but only a limited number of projects can meet basic requirements for safe and effective therapy [35]–[67]. In order to mimic the natural biomechanics of the elbow, most devices consider the elbow FE movement as the only motion occurring at the joint. However, according to the review, a 2–DOF model of the elbow is the minimum requirement for a device to provide natural movements to the upper limb. Additionally, it was found that most existing prototypes do not assess the reliability of critical functions of the device. As ROM overshoots may damage the reconstructed nerve, a pair of mechanical stoppers was proposed to maintain a specific ROM even if the control or the actuation system fails.

EMG-driven models quantify upper arm muscle activity in order to convert EMG to elbow motion and force [79]–[91]. A device employing such models can use estimated motion profiles as commands to the actuators to assist in the movement. Nevertheless, current models are very complex, require long calibration processes and result in relatively low accuracy, which limits their applicability in motion-based rehabilitation systems.

Thus, the focus of current project is to adapt the mechanical design of wearable elbow devices presented in the literature review to the needs of BPI rehabilitation. The work includes the development of a simple sensing technique for elbow motion postoperative rehabilitation that can be integrated into the control system of an assistive device. The following chapter presents the design of the wearable elbow brace for motion rehabilitation.

CHAPTER 3

3 DESIGN OF THE WEARABLE ELBOW BRACE

As presented in the previous chapter, a promising option for postoperative elbow motion restoration is a smart elbow device that provides guidance while BPI patients perform the required exercises outside of the clinical setting. However, most projects designed within the last 5 years do not meet basic safety requirements or require further improvements in order to be used for BPI muscle re-education. Therefore, with the support of a hand therapist from the St. Joseph's Health Care London (London, ON) and based on the literature research presented in the previous section, a wearable elbow brace was designed. This chapter describes the design and development of the prototype.

3.1 General Design Specification

An elbow mechatronics-enabled brace has two major functions: 1) to assist movement of the upper limb when muscles are weak; and 2) to reduce muscle tone of spastic muscles to promote joint mobility [94]. To account for this, the force transmitting mechanism of the brace should provide a non-jerky motion compatible with the natural movements of the elbow. A list of mechanical constraints is described in Section 3.2. The final design is presented in Section 3.3.

3.2 Design Constraints and Specification

The following questions were considered in the design of an ergonomic wearable elbow brace that can be used in all stages of elbow rehabilitation after nerve surgery:

- (1) How should the device be adjusted in order to be used at all stages of the BPI rehabilitation?
- (2) How should the device support the affected upper limb?
- (3) What is the balance between the portability and the functionality of the device?

A detailed discussion of the design specifications is presented below.

3.2.1 Adjustability in Size

In order to account for anthropometric diversity, ergonomic design should accommodate a range of user dimensions, typically up to the 95th percentile of the population [95]. Hence, the ability to adjust fixators (i.e., straps, cuffs, splints, shells) and links is an essential feature of the proposed mechatronic device for BPI muscle training. Since the length of both the upper and lower arms differs for males and females (i.e., the location of the centre of mass for the lower and for the upper arm differs for males and females), size alteration of the device is critical, see Table 3.1 [96]–[98].

Table 3.1. Anthropometric data for 95th percentile of the population.¹

Parameter	Male	Female
Upper arm length (m)	0.389	0.358
Lower arm length (m)	0.312	0.268
Hand length (m)	0.205	0.189
Lower arm mass (kg)	1.66	1.24
Hand mass (kg)	0.63	0.50
Centre of mass for the lower arm and hand (%)*)	31.8	

* Distal orientation (i.e. direction from fingers to the elbow)

By supporting the forearm at its centre of mass, the elbow brace minimizes the acting on the lower arm and maintains static equilibrium of the affected arm. Since the training sessions with the rehabilitation equipment are conducted while the patient is sitting or standing, no torque is applied to the upper arm and, therefore, the role of the upper cuff is

¹ Anthropometric data for 95th percentile of the population has a normal distribution, i.e., the mean, median, and mode of the parameters shown in Table 3.1 are the same and within two standard deviations.

to position the device on the upper arm. To ensure that the position of the lower cuff can be adjusted to the location of the forearm's center of mass, positions of the lower cuff were calculated as follows:

$$l_{EC} = l_{com} - 0.5\text{cm} = (l_{la} + l_h) \cdot COM - 0.5\text{cm},$$

where l_{com} is location of the centre of mass, l_{la} is the lower arm length (cm), l_h is the hand length (cm), and COM is the centre of mass for the lower arm and hand (%), and, finally, the edge of the lower cuff l_{EC} was shifted distally to the elbow (-0.5 cm) in order to minimize high pressure points at the centre of mass. The forearm l_{COM} for females and males was calculated to be 11.5 cm and 13.4 cm, respectively, see Fig. 3.1A. The l_{EC} for the lower cuff is equal to 11 cm and 13 cm. Since BPI affects males more commonly than females [99] [100], an additional position of the lower cuff (14.5 cm) was included in the design specification, see Fig. 3.1A.

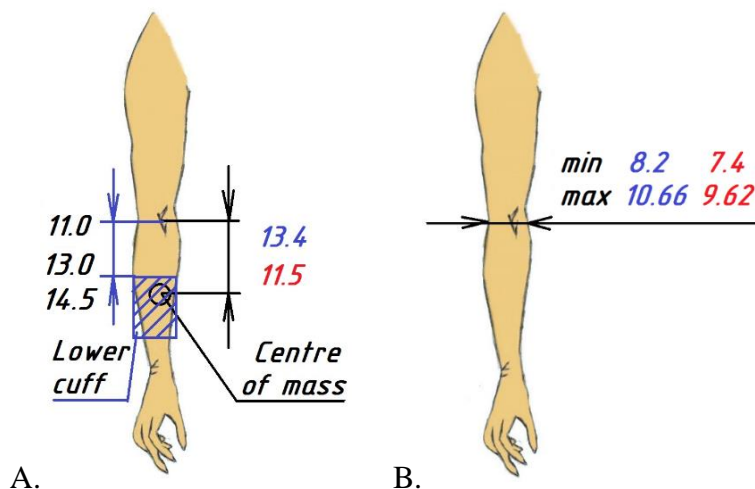


Fig. 3.1. Size variations of a human arm (cm).

- A. Right side: Distance from the elbow to the centre of mass for the lower arm and hand (calculated for 95th percentile of the population). Left side: Recommended distances from the elbow to the lower cuff (based on the l_{COM} location for 95th percentile of the population). B. Elbow breadth variations.**
Blue values for males, red values for females.

It is known that the elbow breadth for people 20 years and older is 8.2 cm for males and 7.4 cm for females (data for the 95th percentile of population) [101]. The presence of edema may increase interlimb discrepancy by 5%–30% [102]. Therefore, elbow breadth may fluctuate between 8.61 cm and 10.66 cm for males and between 7.77 cm and 9.62 cm for females. Based on this data, a two-sided elbow brace must be able to accommodate an elbow joint that is 7.4–10.66 cm in width, see Fig. 3.1B.

3.2.2 Payload and Torque Analysis

In musculoskeletal rehabilitation, daily exercises play an important role in the recovery process. Assistive and resistive motions are prescribed until the patient can lift a 1-kg load during the elbow FE movement. Thus, a smart elbow brace should be able to support the weight of the lower arm, 1-kg load and its own mass. To account for this, a torque analysis of a forearm that holds a 1-kg load in hand was performed, as follows:

$T = M \cdot g \cdot R$, $M = m_{\text{forearm}} + m_{\text{hand}} + m_{\text{load}}$, $R = (l_{\text{la}} + l_h) \cdot COM$, where T is the torque applied by the brace to support the lower arm and a load, $g = 9.8 \text{ m/s}^2$ (earth's gravity), M is the total mass that should be supported by the brace, R is the center of gravity of the lower arm, m_{forearm} is the mass of a forearm, m_{hand} is the mass of a hand, m_{load} corresponds to the combination of a 1-kg load and the weight of the lower part of the brace, l_{la} is the length of the forearm, l_h is the length of the hand, and COM is the center of mass of the lower arm.

Using these equations and the anthropometric data for the 95th percentile (Table 3.1), it was calculated that the actuator must be able to produce at least 5.3 Nm for males and 3.9 Nm for females to overcome gravity during the assistive and resistive training. However, it has been found in the literature that the torque measured during daily activities at the elbow exceeds this range [103], [104], see Table 3.2. Moreover, the daily activities require complex movements of the upper limb, which involve the shoulder, elbow and wrist. Since the elbow motions are not isolated from the movements of other upper limb joint, the forearm rotation (i.e., pronation–supination) significantly influences the torque produced by the elbow during the flexion–extension movements [105], as summarized in Table 3.2.

Table 3.2. Measured torque at the elbow under different conditions.

Measurement conditions	Torque	Ref.
Torque needed to hold an average forearm against gravity at a flexion angle of 90°.	3.1 Nm	[103]
Torque measured during activities of daily living.	5.8 Nm	[104]
Maximum torque measured in the range 0°–90° of the FE motion during reaching and lifting tasks.	7.0 Nm	
Maximum torque measured in the range 90°–120° of the FE motion during reaching and lifting tasks.	5.0 Nm	
Range of extra torque that the elbow produces during the FE (0–130°) while the motion is combined with the forearm rotation.	from 3.88 Nm to -3.2 Nm	[105]

As the maximum torque for elbow FE motion was found to be 10.88 Nm (i.e., 7 Nm [104] plus 3.88 Nm [105]), it was decided to design **an actuation mechanism that can produce 10 Nm** and will allow a patient to use the brace not only as a rehabilitation tool, but also as a helper during everyday activities while their muscles are weak or restricted.

3.2.3 Weight of a Wearable Elbow Brace

The mass of the mechanical parts and the control system of the brace should be distributed throughout the upper limb. Based on the discussions with an expert, the goal is to design **an elbow mechatronics-enabled elbow brace that weighs less than 1 kg** including the actuators and the control system. Portable batteries are considered as the main energy source for the device. Since these can be carried in a built in a waist belt, their weight can be excluded from the total weight of a device. The control and sensing systems are expected to weigh 0.1–0.2 kg.

The device should be fixed with a shoulder strap that goes over the patient’s shoulder and underneath the arm. Such strap will reduce the sliding effect, i.e., it prevents the brace from migrating down the arm. Having the mass distributed along the arm will reduce the inertial effect, which can be detrimental to the shoulder-neck section of a patient.

Other reviewed powered elbow orthotics and exoskeletons [35]–[67] are bulky and/or heavy. Thus, a promising option for the wearable rehabilitation system is to have detachable heavy components, i.e., to apply a “modular” design strategy. An easy “clip-on–clip-off” feature of the motor, for example, will decrease the weight of the brace for constant wear conditions. Additionally, the force applied to the affected arm can be increased or decreased by replacing the motor with an appropriate one. This allows customizing the actuation system for each specific rehabilitation program without changing the mechanical structure of the device.

3.2.4 Actuator Placement

The placement of the actuator with respect to the upper limb of a user is one of the critical design specifications. From experience the first prototype of the ME-Brace designed at the Wearable Biomechatronics Laboratory (see Fig. 3.2), it was learned that when the elbow

joint is actuated only on one side, it creates a twisting effect on the brace, thereby causing the brace to migrate from its actual location.

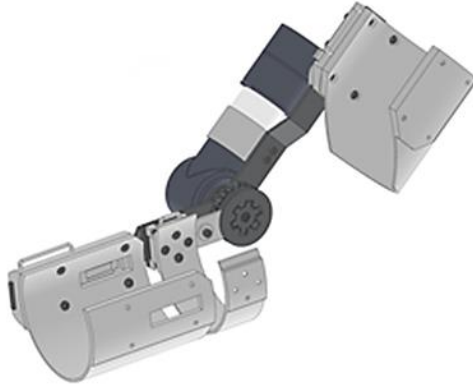


Fig. 3.2. CAD model of the first prototype of the ME-Brace.

To maintain the weight balance on both sides of the extremity, it was decided to place the actuator on the backside of the upper arm. As shown in Fig. 3.2, the weight of the actuator can be supported by a structure or a strap connected to the shoulder. Additionally, since the actuation system does not have to produce extra power to support its own weight, the size of the driver can be decreased.



Fig. 3.3. Actuator placement.

3.2.5 Hinge Type

The humerus, ulna and radius bones that act as a hinge form the elbow joint, see Fig. 3.4. While the ulna and the radius bones slide backwards and forwards along the head of the humerus, the center of rotation migrates. Displacement of the pivot point results from the

nature of the bone structure. Due to this fact, a polycentric hinge (Fig. 3.5) can be used to mimic natural elbow motion [106].

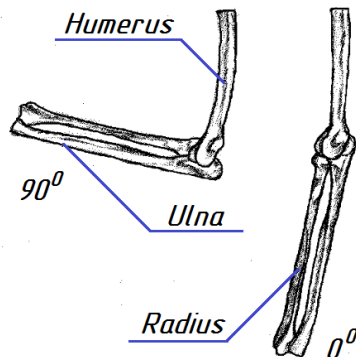


Fig. 3.4. Elbow motion.

Although the polycentric hinge makes it relatively easy to move the arm [107], the primarily articulation of the joint is made by the ulnar-humeral coupling [108], and, therefore, the elbow can be represented as a single-axis hinge (Fig. 3.6).

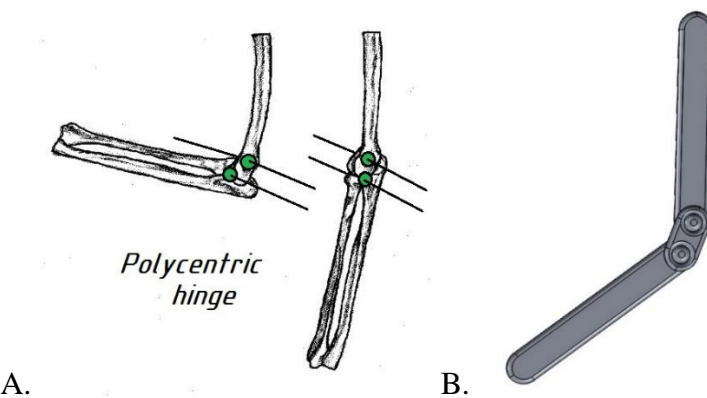


Fig. 3.5. Polycentric hinge elbow.

A. Elbow bones modeled as a polycentric hinge. B. Rigid polycentric hinge.

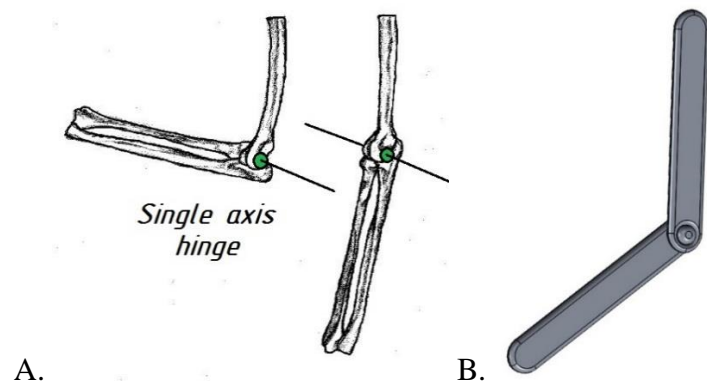


Fig. 3.6. Single-axis hinge elbow model.

A. Elbow bones modeled as a single-axis hinge. B. Rigid single-axis hinge.

Hence, a **single-axis hinge** was used for the design of the wearable mechatronic elbow brace.

3.2.6 Arm Mounting

The design of fixators with an appropriate width should minimize the high pressure points by maximizing the distribution of the force applied by the cuff. A **5-cm wide strap** should be used to ensure comfort and safety [98].

The trough of the cuffs, see Fig. 3.7, should be sufficiently deep so that the limb is well seated. A widely used practice is to make **the trough of the cuffs such that it extends slightly more than halfway up the sides of the limb** [98].

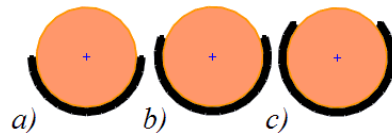


Fig. 3.7. Various design of the trough of the cuffs.

- a) The limb overflows the sides of the trough (40% of the limb's circumference);
- b) Slightly more than halfway up the sides of the limb (60% of the limb's circumference);
- c) Too difficult to position the cuff around the forearm or upper arm (70% of limb's circumference).

Since postoperative motions decrease wound edema by milking fluid out of the extremity, it is important to correct the trough of the cuffs periodically. Thus, the process of customizing cuffs should be easy and affordable to rehabilitation clinics. All materials contacting to the body should be nontoxic. Additionally, all corners should be rounded, as sharp edges may injure the skin.

3.2.7 Safety Throughout the Rehabilitation Progress

The strategy for treatment following surgery mainly includes pain management, decreasing edema and protection of the nerve coaptation site. To achieve these goals, upper limb immobilization is recommended. Thus, mechanical stoppers that can limit the elbow's ROM are considered for protection Phase I (Table 2.1). Based on the literature review in Chapter 2 and the experience of a hand therapist from the St. Joseph's Health Care London

(London, ON), the elbow's range of motion was divided in 26 sections, i.e. the increment for mechanical stopper position is equal to 5° . The proposed increment allows controlling the tension applied to the affected muscle by limiting the elbow ROM.

Additionally, the reliability of the proposed device can be increased by using the mechanical stoppers as safety reserve components in the torque transmission system. It was found that most wearable elbow braces simplify the brace design and avoid using duplicate components for critical features of the device [37], [42], [47], [53], [54], [57]–[60], [62], [64], [66], [67]. As a result, mechanical stoppers are important components of the elbow mechatronics-enabled brace for BPI rehabilitation that provide upper limb immobilization and increase the safety of the device.

3.2.8 User Requirements

A wearable device will become a part of the patient's daily life. This means that the appearance of the device should meet cosmetic and aesthetic needs. Thus, functional parts of the device should be covered by a detachable housing that makes it easy to clean the device. Another important factor for the user is the device portability. Despite the complexity of the proposed device, **the maximum setup time for the system should not exceed 3 minutes**. The setup time was selected based on an interview with an expert presented in [110].

3.3 Presentation of the Mechanical Design

The final design of the wearable elbow mechatronics-enabled brace for the upper limb is presented in Fig. 3.8. By using the SolidWorks Mass Analysis Tool, the total expected weight of the mechanical components and the actuation system was calculated to be 1.4 kg. Further explanation of the device components is presented in the following sections.

As it was outlined in Section 2.3.1, a 2-DOF model of an elbow motion is the minimum requirement for a mechatronic brace as it includes active flexion-extension and passive adduction-abduction movements. Thus, Section 3.3.1 presents summary of bearing selection process for the passive adduction–abduction elbow movements, while Sections 3.3.2–3.3.7 describe the process of designing the actuation system for the proposed

wearable elbow mechatronics-enabled brace. Additionally, a short summary of material selection is presented in Section 3.3.8.

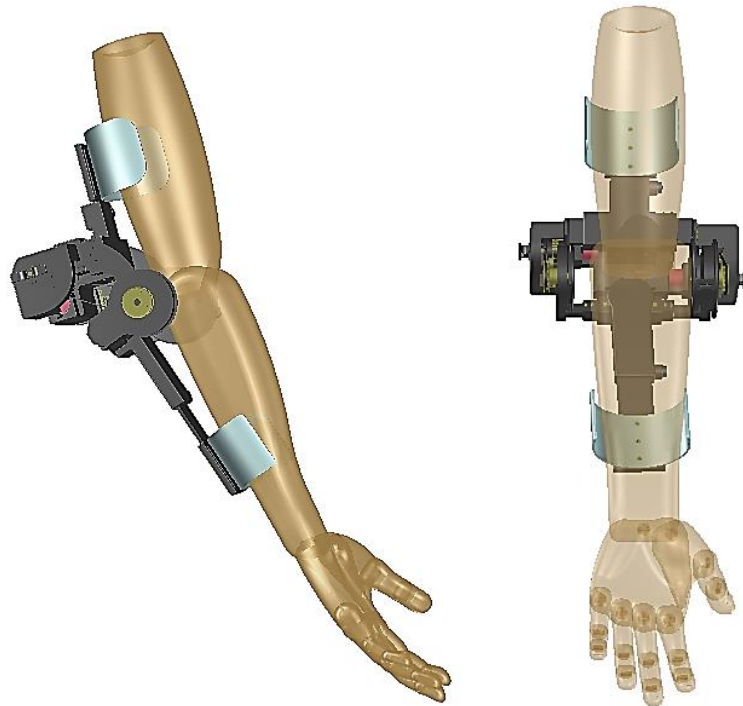


Fig. 3.8. CAD model of the device.

3.3.1 Bearing Selection and Rated Life

The passive adduction–abduction elbow movements require a properly selected bearing that minimizes friction energy losses between the lower link of the device that supports the weight of the forearm, the hand and the load and the surrounding structures (Fig. 3.9 A). The bearing selection process involves an analysis of the loads acting on the surface of the bearing and of the environmental conditions. Since the device should become a part of the BPI rehabilitation process, low levels of dust and external disturbances allows the consideration of low-cost sealed rolling-element bearings that do not require further lubrication.

The load conditions on the bearings are a combination of radial and axial loads, see Fig. 15 B. According to the loading scenario, active FE movements driven by the actuation system result in a 40 N radial load (i.e., 5 Nm at a 0.125 m distance). The weight of the forearm, the hand and the 1-kg load produce 25 N axial load on the bearing (i.e., 15 N from the lower arm and 10 N from the 1-kg load). Additionally, a 3 N axial load should account for the

external gentle disturbances. By knowing that the passive adduction–abduction motions are slow (e.g., 1142 rpm), the rated life of the bearing can be calculated according to Appendix D [111]. The goal of the calculation is to find a bearing that has the rated life of operation greater than the length of the rehabilitation process for a patient.

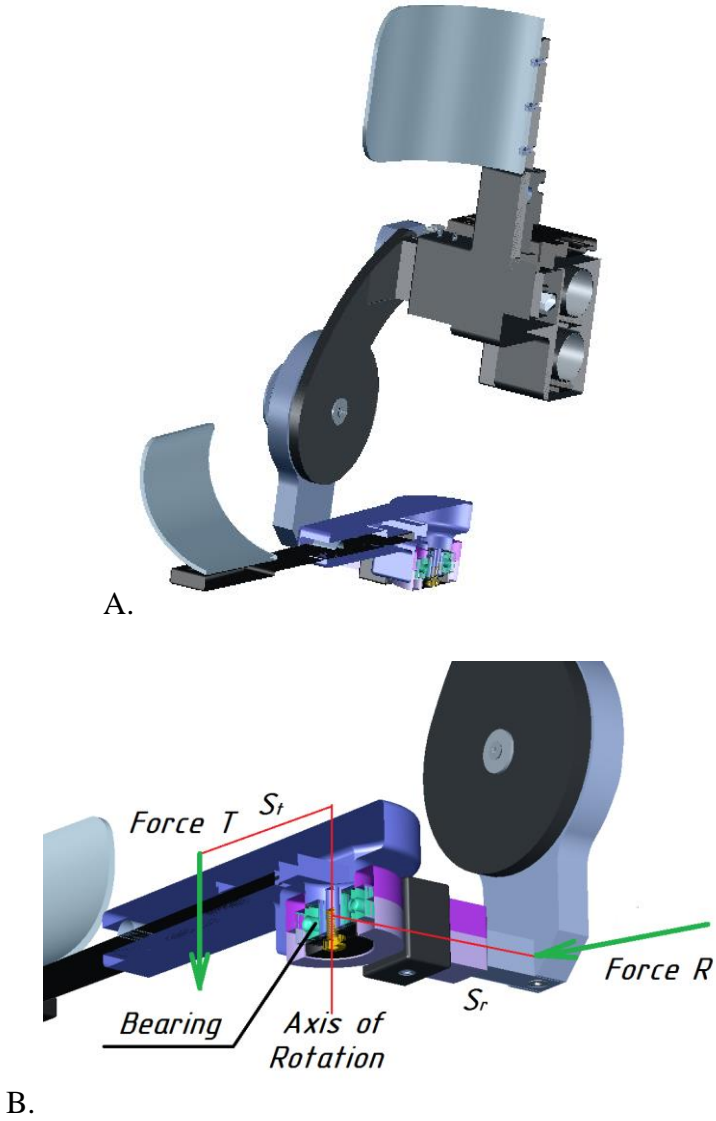


Fig. 3.9. Bearing loading scenario.
A. Section view. B. Forces acting on the bearing.

The seven-step process for calculating the rated bearing life is described in Appendix A. After several iterations, it was found that the 5908K390 Stainless Steel Ball Bearing from the McMaster-Carr catalogue satisfies the design requirements. The calculated rated life of the bearing was 10,056 h (i.e., 14 months of constant use), which is equal to the expected rehabilitation time for BPI.

3.3.2 2-DOF Motion of the Brace

The main ROM (Fig. 3.10 A and B) of the elbow brace was limited by the customized internal gear and mechanical stoppers that are coupled to the gear's teeth, see Fig. 3.11. A metal pin **1**, secured in a plastic housing **3**, can be moved along the inner gear **2** within the grooves of the surrounding parts to a certain position by applying a force to the button **4**. A screw **5** fixes the position of the inner gear **2**. Thus, bar **6** that transmits the force to the forearm can only move between two pins **1** meshed with the inner gear **2**. Since the single-axis hinge elbow design was modified to meet all design requirements, the position of bar **6** has a 90° shift with respect to the position of the forearm, see Fig. 18. Hence, a start position (0°) of the forearm corresponds to a -90° position of bar **6**.

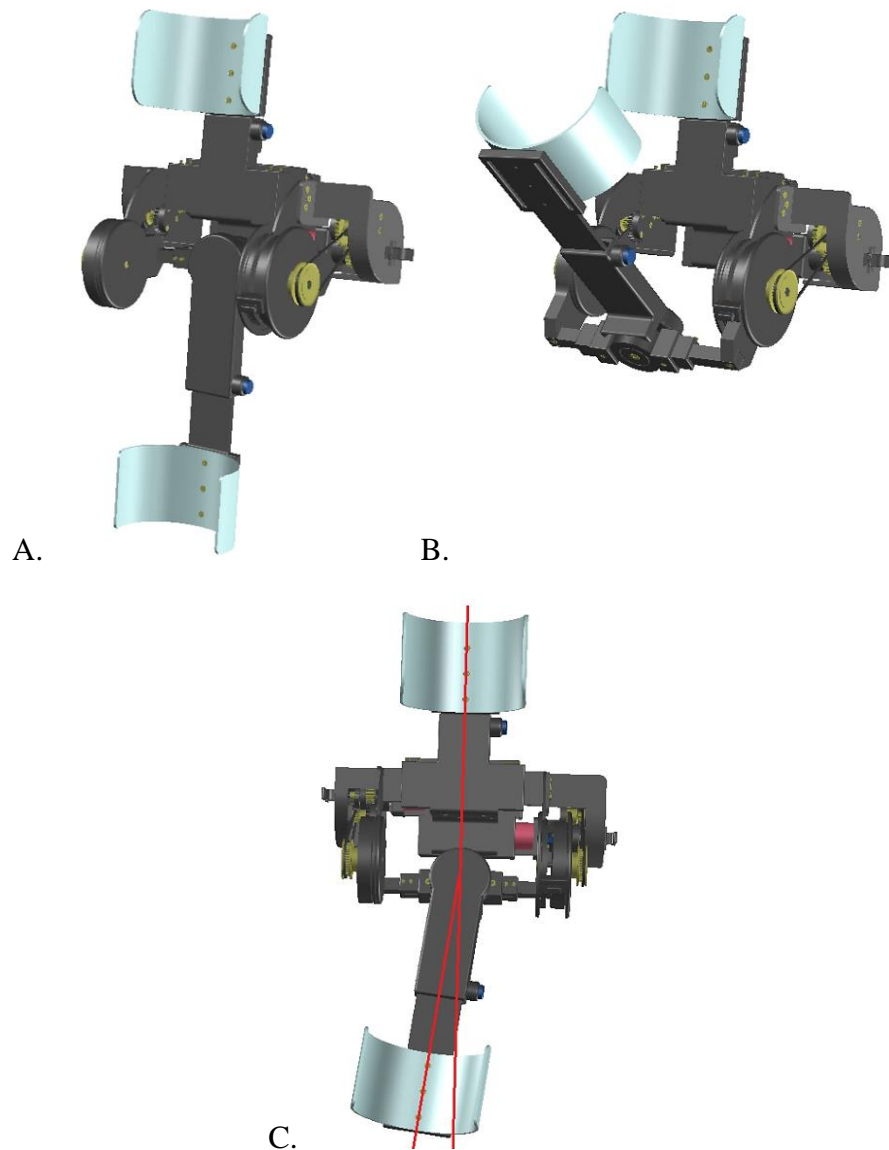


Fig. 3.10. Elbow brace DOFs.

A. Full extension. B. Full flexion. C. Carrying angle.

As it was discussed in Section 3.3.1, the passive movement of the forearm in the coronal plane was achieved by using a stainless steel ball bearing that allows the lower link of the device to move within $\pm 12^\circ$, see Fig. 3.10 C.

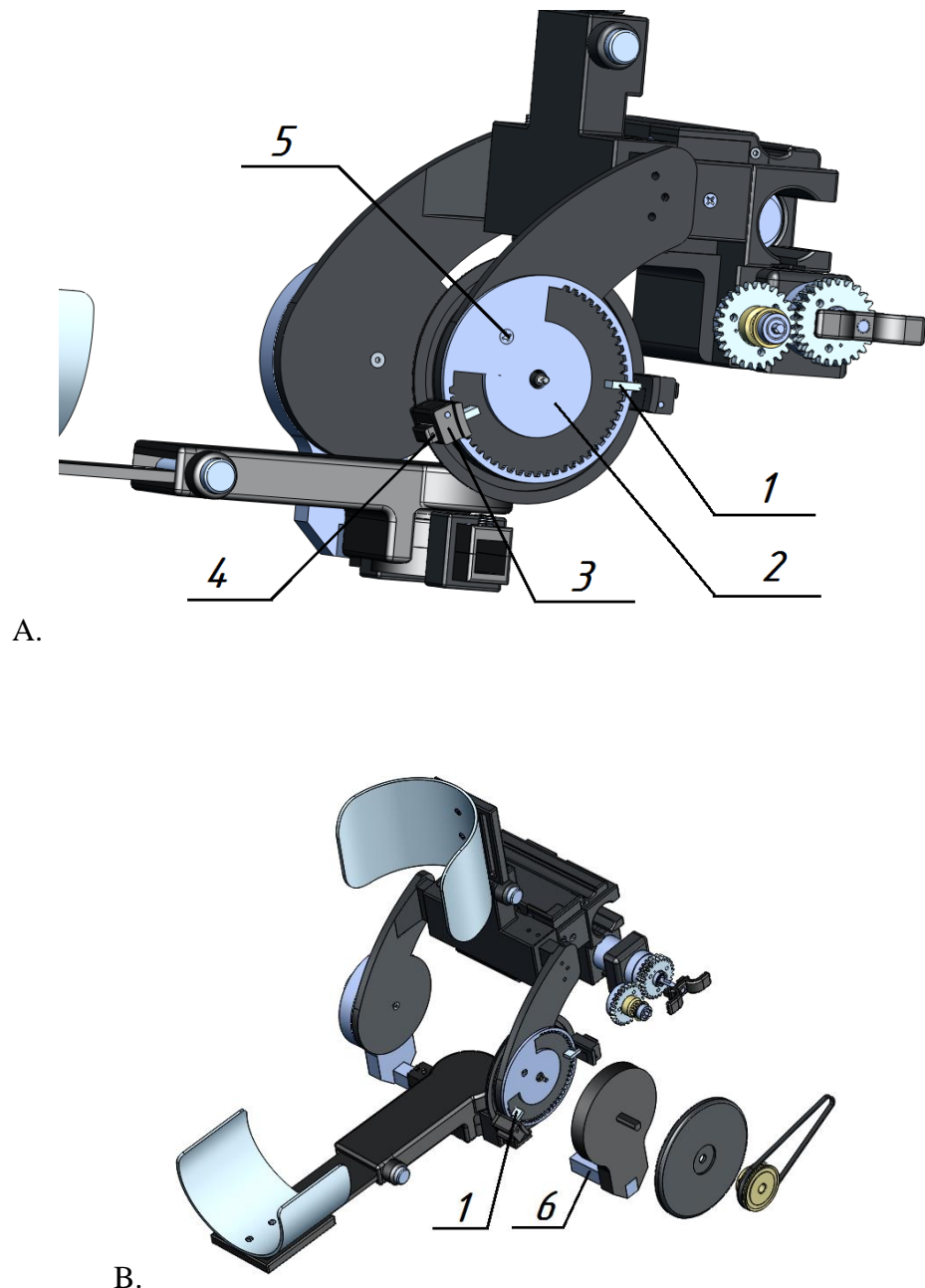


Fig. 3.11. Mechanical stoppers.
1 – pin, 2 – inner gear, 3 – pin housing, 4 – button, 5 – screw, 6 – bar.

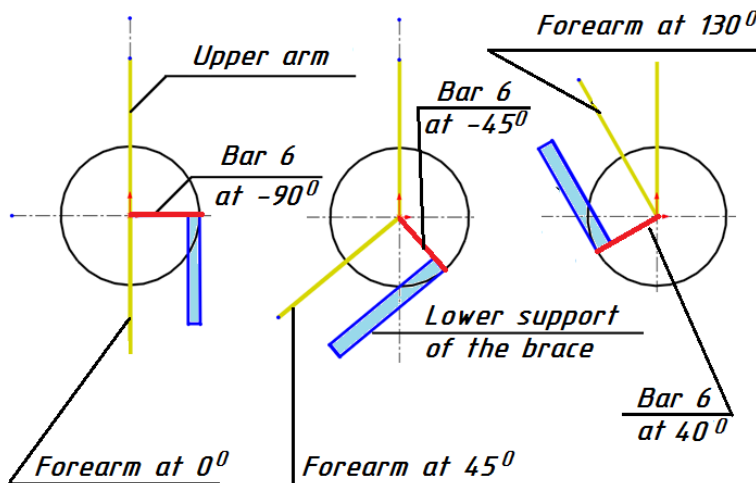


Fig. 3.12. Schematic diagram of the performance of the mechanical stoppers.
The red line is the bar 6. The yellow lines are the upper arm and the forearm. The blue bar is the lower part of the elbow brace that supports the weight of the forearm, the hand and the load. The position of the forearm at 0° corresponds to the position of the bar at -90° . The position of the forearm at 45° corresponds to the position of the bar at -45° . The position of the forearm at 130° corresponds to the position of the bar at 40° .

3.3.3 Driver Selection

As defined in Section 2.3.2, the device should produce 10 Nm in order to provide support to the affected arm during the training sessions and everyday activities. Based on the literature review presented in Chapter 2, the wearable devices for upper limb rehabilitations use DC motors, pneumatic muscles, hydraulic drives and smart materials for torque generation. As no consistency in driver selection was found in the reported projects [35]–[67], the grid analysis method was used to narrow down driver options, see Table 3.3. High priority (scaling factors 3 and 4) was assigned to the torque output, weight, and size criteria. A medium scaling factor of 2 was chosen for safety, easy installation, and weight of the control system. The cost of the prototype was chosen as less critical among other criteria (scaling factor of 1). Each type of actuator was assigned with a score for each criteria (where 1 means that the design requirements is not met by the actuator, 2 means that the design requirement is met, and 3 means that the property of the actuator exceeds the design requirement). The final scores was calculated as a sum of criteria score multiplied by the scaling factor.

The motor–gear box combination and smart materials were eliminated based on the low final score achieved by them (31 and 32 respectively). Both options were not addressing the main requirement: the torque specifications. Pneumatic muscles and

pneumatic/hydraulic drives require large housings due to the nature of the pressure-driven actuators. This makes them bulky, despite the high power-to-weight ratio. Therefore, the final score of a motor–gear box drive with a transmission system was higher (39) than the pneumatic muscles and pneumatic/hydraulic drives (36 and 34 respectively) due to having the best power density (torque-to-weight ratio) among the remaining drivers.

Table 3.3. Grid analysis of drivers for a powered elbow brace.

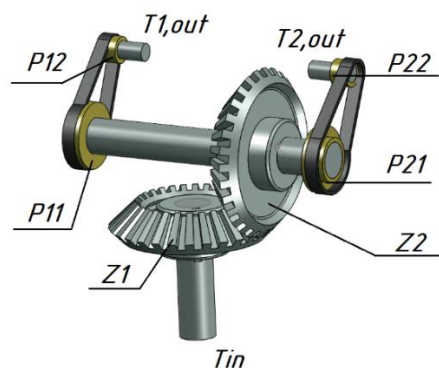
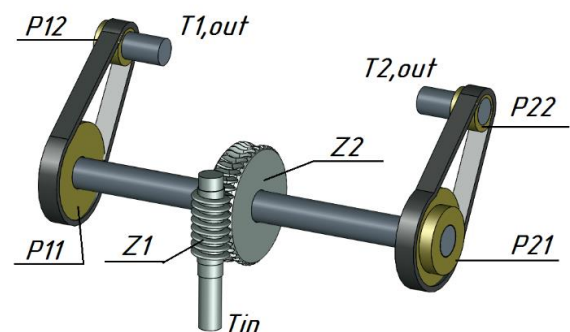
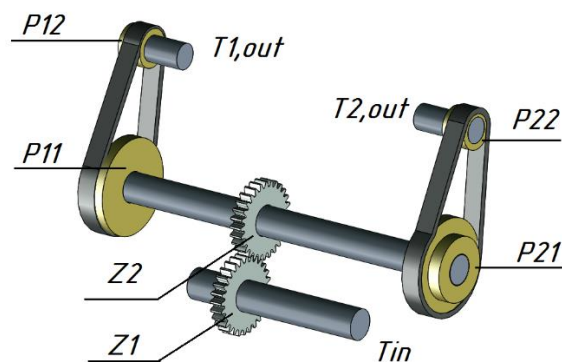
	Scaling factor	Motor and gear box	Final score	Pneumatic muscle	Final score	Pneumatic/Hydraulic drive	Final score	Smart materials	Final score	Motor, Gear box, Transmission system	Final score
Torque output	4	1	4	3	12	3	12	0	0	3	12
Weight	3	2	6	3	9	2	6	3	9	2	6
Size	3	2	6	0	0	0	0	3	9	2	6
Safety	2	2	4	2	4	2	4	1	2	2	4
Cost	1	1	1	3	3	2	2	0	0	1	1
Ease of installation	2	3	6	3	6	3	6	3	6	3	6
Weight of the control system	2	2	4	1	2	2	4	3	6	2	4
			31		36		34		32		39

According to the literature review, smart elbow braces that are driven from both sides of the elbow should provide more stable assistance during a movement compared to one-sided driven prototypes. Hence, a number of design concepts for an actuation system that splits torque (i.e., symmetrically transmits half of the torque to several directions) from a motor–gear box combination were analyzed, see Table 3.4.

Gears with intersecting axes and parallel axes typically have 98%–99% efficiency (η_G) [111], while efficiency of gears with nonparallel and nonintersecting axes may vary between 30% and 90% [111]. Hence, due to excessive friction, worm gears were eliminated from further analysis, see Table 3.4.

Table 3.4. Grid analysis of splitter transmissions.

	Scaling factor	Bevel Gear (Fig. 3.13)	Worm Gear (Fig. 3.14)	Spur Gear (Fig. 3.15)
Complexity of transmission (1 – complex, 2 – straightforward)	1	1	1	2
Efficiency of transmission (1 – less than 50%, 2 – between 50% and 95%, 3 – greater than 95%)	2	6	2	6
		7	3	8

**Fig. 3.13. Bevel gear and belt-pulley transmission for one motor–gear box combination.****Fig. 3.14. Worm gear and belt-pulley transmission for one motor–gear box combination.****Fig. 3.15. Spur gears and belt-pulley transmission for one motor–gear box combination.**

Since spur gears are easy to find, inexpensive, and efficient, a spur gear was chosen as the optimal. It should also be mentioned, that beveled gears can be noisy when operating at high speeds. Thus, may be inappropriate for home-based devices.

3.3.4 Motor–Gear Box Selection

The kinematic diagram of the transmission system in presented in Fig. 3.16. The output torques from the transmission system, $T_{1,2 \text{ OUT}}$, can be found as:

$$T_{\text{IN}} = T_M \cdot N_{\text{GH}} \cdot \eta_{\text{GH}}$$

where T_{IN} is the output torque from the gearhead that is attached to the motor, T_M is the continuous output torque from a motor, N_{GH} is the gear ratio of a gearhead, η_{GH} is the efficiency of the gearhead.

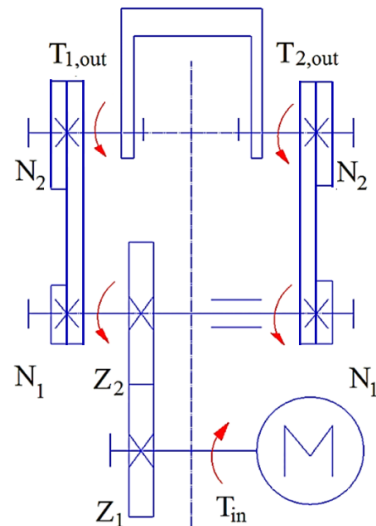


Fig. 3.16. Kinematic diagram of the transmission system.

The output torque from the transmission system, $T_{1,2 \text{ OUT}}$, can be calculated as follows:

$$T_{1,2 \text{ OUT}} = \frac{(T_{\text{IN}} \cdot \eta_G)}{2} \cdot \frac{N_2 \cdot \eta_{\text{TA}}}{N_1}$$

where η_{TA} is the efficiency of the torque amplifier and η_G (0.98) is the efficiency of the gear transmission, N_1 and N_2 are the diameters of the pulleys of a torque amplifier ($\frac{N_1}{N_2}$ ratio is 3). The efficiency of the torque amplifier is assumed to be $\eta_{\text{TA}} = 0.95$. Substituting the corresponding values into this equation gives:

$$5 = \frac{X \cdot 0.98}{2} \cdot \frac{3 \cdot 0.95}{1}$$

$$X = 3.58 \text{ Nm.}$$

Therefore, 3.58 Nm torque is required from the output shaft of the driver to get 10 Nm torque applied to the forearm. The exerted force is applied symmetrically from both sides of the forearm. According to the required torque from the gearhead, a summary of the catalogue search is presented in Appendix B. As a result of the driver's analysis, two motor-gear box combinations can be used for the current project: Maxon Planetary Gearhead 143995 + Maxon EC-max 22 283840 or Maxon Planetary Gearhead GP 32 166979 + Maxon A-max 26 110192. The preference was given to the first option with dual drivers, since this configuration results in more possible solutions for the transmission system.

3.3.5 Actuation System

Two brushless DC Maxon motors (EC-max22, continuous torque 0.0108 Nm) combined with planetary gears (GP22C, gear ratio 333:1 and maximum efficiency 49%) can produce 1.76 Nm per each combination. In order to achieve 10 Nm, a custom transmission system was designed, see Fig. 3.17.

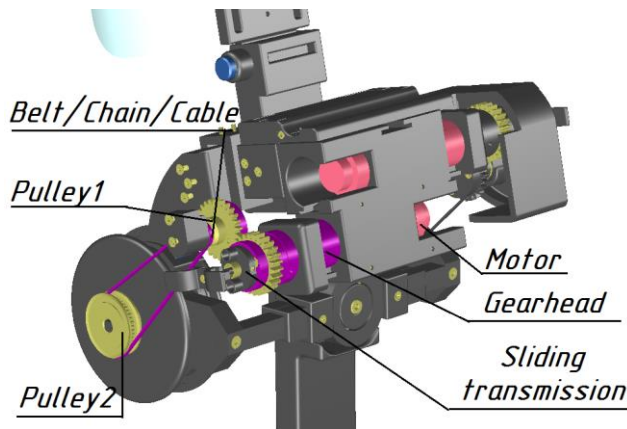


Fig. 3.17. Actuation system of the smart elbow brace.

The torque is transmitted through a gear set (efficiency 0.98%, maximum continuous torque 1.727 Nm) and through a torque amplifier (e.g. belt/chain/cable and pulleys system) that increases the output torque from 1.727 Nm up to 5.42 Nm:

$$\frac{T_1}{T_2} = \frac{N_1}{N_2}$$

where T_1 is input torque to the transmission system, T_2 is the output torque from the transmission system, N_1 and N_2 are the diameters of the pulleys of a torque amplifier ($\frac{N_1}{N_2}$ ratio is 3). The final output torque from the actuation system is $T_{\text{OUT}} = T_2 \cdot 2 \cdot \eta_{\text{TA}} = 5.42 \text{ N} \cdot 2 \cdot 0.95 = 10.29 \text{ Nm}$ for the worst-case scenario.

The reverse calculation will estimate whether torque T_2 can lift the weight of the brace, the patient's lower limb and a 1-kg load in the hand for a particular brace design.

A combination of forces F , Q and B act on the brace, see Fig. 3.18; where $F = mg$, m is the mass of lower part of the brace, the mass of patient's forearm and hand plus the mass of the load in the hand; $g = 9.8 \text{ m/s}^2$; r_2 is the distance from the elbow pivot point to the COM of the forearm; Q is a force generated by the drive system of the brace; r_1 is the distance from the center of large pulley to the point where the force Q is applied; B is the force generated by a large pulley; and r_3 is the radius of the large pulley.

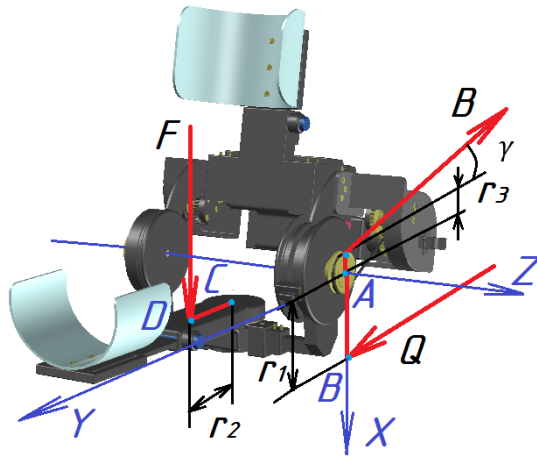


Fig. 3.18. Reverse payload and torque calculation diagram.

The balance condition at 90° can be described as follows:

$$\sum x_i = 0, \sum y_i = 0, \sum z_i = 0, \sum M_{iA} = 0;$$

$$Mx_A: \bar{Q} \cos \alpha + \bar{F} \cos \varepsilon = 0, \quad My_A: \bar{Q} \cos \mu + \bar{F} \cos \beta = 0, \quad MZ_A: \bar{Q} \cos \theta + \bar{F} \cos \delta = 0;$$

where $\alpha = 90^\circ$ is the angle between force Q and plane X ;

$\varepsilon = 0^\circ$ is the angle between force F and plane X ;

$\mu = 0^\circ$ is the angle between force Q and plane Y ;

$\beta = 90^\circ$ is the angle between force F and plane Y ;

$\theta = 90^\circ$ is the angle between force F and plane Z ;

$\delta = 90^\circ$ is the angle between force Q and plane Z ;

$$\sum M_{iA} = 0 + \bar{F} \cos \varepsilon + \bar{Q} \cos \mu + 0 + 0 + 0 = 0;$$

In other words, the brace will stay at the 90° position if

$$F \cdot \cos \varepsilon \cdot COM + Q \cdot \cos \mu = 0,$$

where CD (COM) is the distance from the elbow to the centre of gravity of the forearm and hand (0.145 m for females and 0.164 m for males), and Q has to be equal to the output torque from the actuation system B . Therefore, the relation between Q , B and F can be represented as follows:

$$Q = \frac{F \cdot 1 \cdot 0.145}{1} = 0.145F_f \text{ and } Q = \frac{F \cdot 1 \cdot 0.164}{1} = 0.164F_m$$

$$\bar{Q} + \bar{B} \cdot \cos \gamma = 0;$$

where $\gamma = 5.92^\circ$ is the angle between force B and plane Y that was measured according to Fig. 3.19, B is the output torque from the actuation system (10.29 Nm).

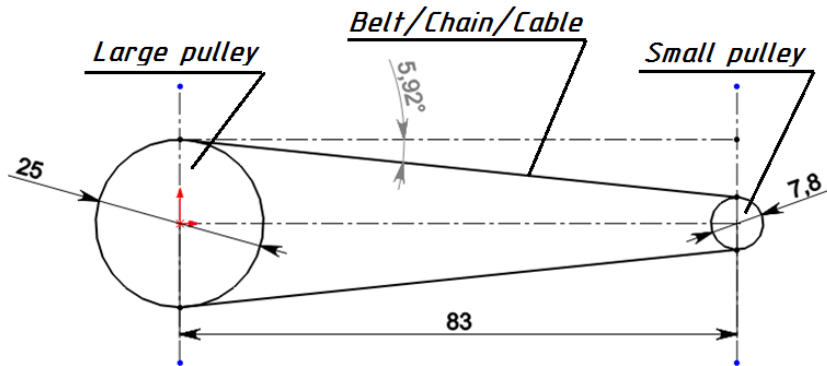


Fig. 3.19. Diagram of the torque amplifier. Dimensions are in mm.

$$0.145F_f = B \cdot \cos \gamma, F_f = \frac{10.29 \cdot 0.99}{0.145} = 6.83 \cdot B = 70.26 \text{ N};$$

$$0.164F_m = B \cdot \cos \gamma, F_m = \frac{10.29 \cdot 0.99}{0.164} = 6.04 \cdot B = 62.15 \text{ N}.$$

$$m_f = 7.17 \text{ kg}; m_m = 6.34 \text{ kg},$$

Since the estimated load is larger than the required load ($7.17 \text{ kg} > 2.5 \text{ kg}$ for females and $6.34 \text{ kg} > 2.9 \text{ kg}$ for males), the reverse calculation proved that the designed brace is capable not only for a BPI rehabilitation, but also can be used during daily activities.

3.3.6 Transmission System

Three hubless gears (SPD/SI, 2024 Aluminum alloy, Module 1, 26 Teeth, 20° Pressure Angle) were used in the torque transmission system to allow the motor to be coupled and decoupled from the transmission system, Fig. 3.20, component 1, 2 and 11.

To decouple the motor, the user has to shift gears 1 and 2 manually. By locking the selected gear pair 1–2 and 11 to the output shaft of component 6 inside the transmission, the torque from the shaft of the gearhead 12 is directly transmitted through the motor coupler 14 to the torque amplifier (components 8, 9 and 10). As the handle 5 is pulled away from motor, the shaft 4 pulls gears 1–2 away from the motor coupler 14 and unlocks the transmission system. Both subsystems (1–5 and 6–8, 11, 13) are connected to a wall of a housing (not shown on the Fig. 3.20). In order to minimize torque losses, bearings 3, 7 and 13 were used to decrease friction.

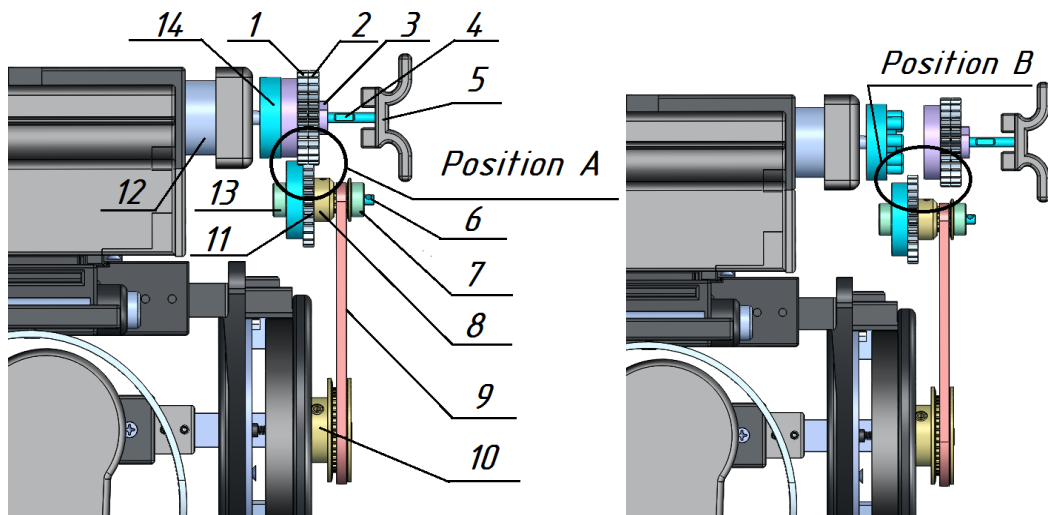


Fig. 3.20. Transmission system. Position A – coupled. Position B – decoupled. 1 – gear Z1, 2 – gear Z2, 3 – bearing B1, 4 – shaft, 5 – handle, 6 – shaft, 7 – bearing B2, 8 – small pulley/sprocket, 9 – belt/chain/cable, 10 – large pulley/sprocket, 11 – gear Z3, 12 – motor holder, 13 – bearing B3, 14 – motor coupler.

In the decoupled mode (Position B, Fig. 3.20), the motors and their housing can be easily detached from the device (Fig. 3.21). Then, the user has the option to either move the forearm within a specific ROM or to fix it in a certain position.

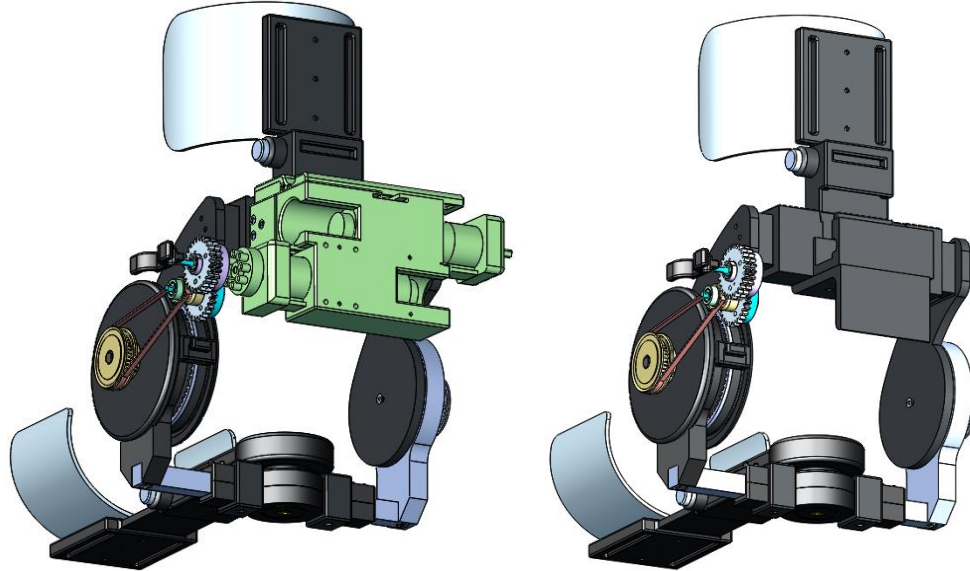


Fig. 3.21. Detachable motor housing.

3.3.7 Torque Amplifier

As part of the transmission system, a torque amplifier is required to achieve 10 Nm in total from both sides of the device. During the design stage, the ratio of the amplifier was selected as $R_a = 3$. Thus, the diameter/teeth/grooves ratio between the driver pulley/sprocket and the driven one should be at least 3. The amplifier has to include a belt, chain or a cable that actually conveys the power from the driver to the driven shaft. In order to select the best option, three types of torque amplifiers were analyzed and designed for further testing.

The initial input values for torque amplifier selection are: the torque $T = 1.75$ Nm, the driving speed $n_1 = 10$ rpm, the ratio of the torque amplifier $R_a = 3$, the center distance between the sprockets/pulleys $a = 83$ mm, maximal permissible external diameter of the larger pulley/sprocket $d_2 = 80$ mm, and the maximal permissible external diameter of the smaller pulley/sprocket $d_1 = 20$ mm.

3.3.7.1 Timing Belt–Pulley Transmission

The design load T_{peak} can be determined by multiplying the torque on the smaller pulley by a service factor S : $T_{\text{peak}} = T \cdot S = 1.75 \cdot 2 = 3.50 \text{ Nm}$, where $S = 2$ for small pitch synchronous drives [113]. According to the belt technical information [113], a 3 mm pitch GT2 belts are the smallest potential choice for the computed T_{peak} .

The pulleys size was computed according to the following algorithm:

- 1) The number of grooves was selected according to the SDP/SI manufacturer's documentation [113].
- 2) The larger pulley combination was found based on the following criterion: the ratio between the diameter of the smaller pulley and the larger pulley should not be less than 3.
- 3) A belt was selected if two criteria were met:
 - (a) the distance between the centers of the pulleys should not be less than 83 mm;
 - (b) the number of teeth in contact with the belt should not be less than 6 for both pulleys.

The rated torque for the smaller pulley multiplied by the appropriate belt width factor and applicable belt length factor should be equal or larger than the computed T_{peak} . Based on the size constrains for the torque amplifier (Section 3.3.7), three combinations of the small and larger pulleys can be used in the torque amplifier, see Table 3.5.

Table 3.5. Belt–pulley selection chart for 3 mm pitch GT2 belts.

Small pulley Number of grooves and Pitch diameter, mm	Larger pulley Number of grooves and Pitch diameter, mm	Belt Number of teeth and Length Correction Factor	Belt Width, mm and belt width factor	Calculated torque, Nm
16; 10.19 mm	48; 45.84 mm	89; 0.95	6 mm; 1.00	1.50
			9 mm; 1.50	2.25
			12 mm; 2.00	3.00
			15 mm; 2.50	3.75
18; 17.19 mm	56; 53.48 mm	94; 0.95	6 mm; 1.00	1.75
			9 mm; 1.50	2.62
			12 mm; 2.00	3.50
			15 mm; 2.50	4.37
			6 mm; 1.00	2.09
20; 19.10 mm	60; 57.30 mm	98; 1.00	9 mm; 1.50	3.14
			12 mm; 2.00	4.18
			15 mm; 2.50	5.23

According to the calculated torque that the belt-pulley can transmit, the SDP/SI Aluminum Alloy Timing Pulley with grooves $N_1=56$ and $N_2=18$ in combination with 3 mm pitch GT2 belt 12 mm width that has 94 teeth was found to be the best space saving option.

3.3.7.2 Chain–Sprocket Transmission

The power transmission of a chain–sprocket combination can be found as:

$$P = \frac{T \cdot n_1}{9550}$$

where T is the input torque to the transmission system, n is an average speed of force transmission, °/s.

$$P = \frac{1.75 \cdot 10}{9550} = 0.002 \text{ kW.}$$

According to the DIN curve [114], chain M106 Single (DIN ISO – 10B1) with chain pitch 16 satisfies the power requirements. The recommendation is to have 11–13 teeth of a sprocket for chain speed under 4 m/s. A sprocket with less than 11 teeth is not used for power distribution. Therefore, the number of teeth $z_1 = 11$ of a small chain wheel corresponds to a power coefficient $f_1 = 1.72$ [114]. The transmission ratio of a large sprocket to a small sprocket $R = 3$ corresponds to a power coefficient $f_2 = 1.0$ [114]. The effect of the shock factor $Y = 2.5$ [114] corresponds to a power coefficient $f_3 = 1.59$ [114]. The ratio of center distance (a) to chain pitch (p) $\frac{a}{p} = \frac{83}{16} = 5.19$ corresponds to a power coefficient $f_4 = 1.18$ [114]. Chains that move with speed less than 4 m/s have a power coefficient $f_5 = 1.4$ [114]. The resulting power coefficient is $f_R = f_1 \cdot f_2 \cdot f_3 \cdot f_4 \cdot f_5 = 1.72 \cdot 1.00 \cdot 1.59 \cdot 1.18 \cdot 1.4 = 4.52$. Thus, the corrected power is $P_D = P \cdot f_R = 0.002 \text{ kW} \cdot 4.52 = 0.01 \text{ kW}$. The chain M106 Single (DIN ISO – 10B1) with chain pitch 16 still satisfies the power requirements. The technical details of the selected chain driver are: 33.81 mm of the smaller pitch diameter and 100.21 mm of the larger pitch diameter.

3.3.7.3 Cable–Pulley Transmission

The cable drivers combine unique features: no backlash, high stiffness and low friction [115]. Easy installation and cable flexibility allows designing the smallest torque amplifier for the current brace transmission.

Since the cable–pulley option does not require specific pulley dimensions, a set of general constraints for pulley selection can be described as follows:

- a) the diameters of the two pulleys should satisfy the ratio criteria ($R = 3$);
- b) the overall force applied through the rope to the pulley should be taken into account in order to eliminate pulley deformation;
- c) the groove depth should be equal to 1.5 of the cable diameter;
- d) the slip angle φ , the minimum angle of wrap required to support the applied load, can be calculated according to [115]:

$$\varphi = \log\left(\frac{T_2}{T_1}\right) \approx 1^\circ$$

where T_2 – output torque from the cable-driven system, T_1 – input torque to the torque amplifier. A Nylon® rope with breaking strength 9.1 kg and $\emptyset = 0.25$ mm (Micron, Cortland Line Company Inc.) was selected as a cheap representative of lifting ropes.

3.3.7.4 Comparison of Torque Amplifiers

Section 0 showed that the chain–sprocket option cannot be used with the designed transmission system due to the large size of both sprockets. The cable–pulley option is the most easily implemented combination due to pulley size flexibility. However, the selected rope and belt have different material properties: Nylon® (Polyamide 66) can be stretched (about 10% elongation at 30% of breaking strain) and has fair moisture resistance (moisture regain is 4–4.5%) [116], [117], while neoprene belts with a fiberglass cord (Fig. 3.22) have high resistance to elongation and good tear resistance, but a high modulus of elasticity (difficult to bend) [113].

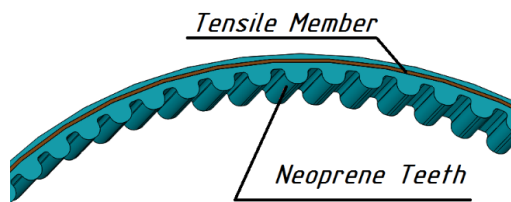


Fig. 3.22. Neoprene belts with a fiberglass cord.

Since both belt–pulley and cable–pulley combinations can potentially be used in the transmission system; a real world comparison and assessment is required and is presented later in Section 4.2.

3.3.8 Material Selection

The material selection preference was given to nontoxic materials such as aluminum, plastic and polyester. They are inexpensive, lightweight, easy to machine and widely used in the hand rehabilitation practice. Even though only a few cases have reported contact allergy to aluminum [118], the skin of the user will only be in contact with the plastic and polymer structures. This will ensure that the risk of an allergic reaction is minimized.

The components of the prototype were built out of acrylonitrile butadiene styrene (ABS) plastic in a Dimension Elite 3D Printer or manufactured from 6061/7075 aluminum bars. The material assigning process was based on the results of the Finite Element Analysis (FEA) under loads in the SolidWorks Simulation Module. Each component was analyzed according to the function in the device, external forces from the user and a Safety Factor (FOS). The results of the FEA analysis of each part (e.g., Fig. 3.23) are provided in the form of displacements (e.g., Fig. 3.24) and stresses (e.g., Fig. 3.25). An example of the FEA analysis is described below.

The base for the forearm (Fig. 3.23) supports the weight of the lower arm and the 1-kg load, while its ribs act as limiters for the carrying angle. Thus, it was assumed that a weight of 5 kg was supported by the base during everyday activities. According to the displacement analysis, the maximum deflection of the base was found to be 0.1126 mm (red zone in Fig. 3.24 A). The deflection will result in acceptable 0.52° displacement of the carrying angle (Fig. 3.24B).

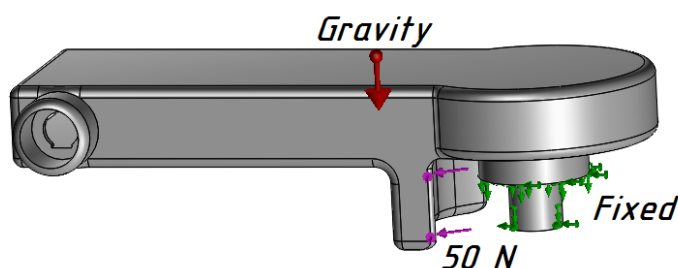


Fig. 3.23. Forces acting on the base for the forearm.

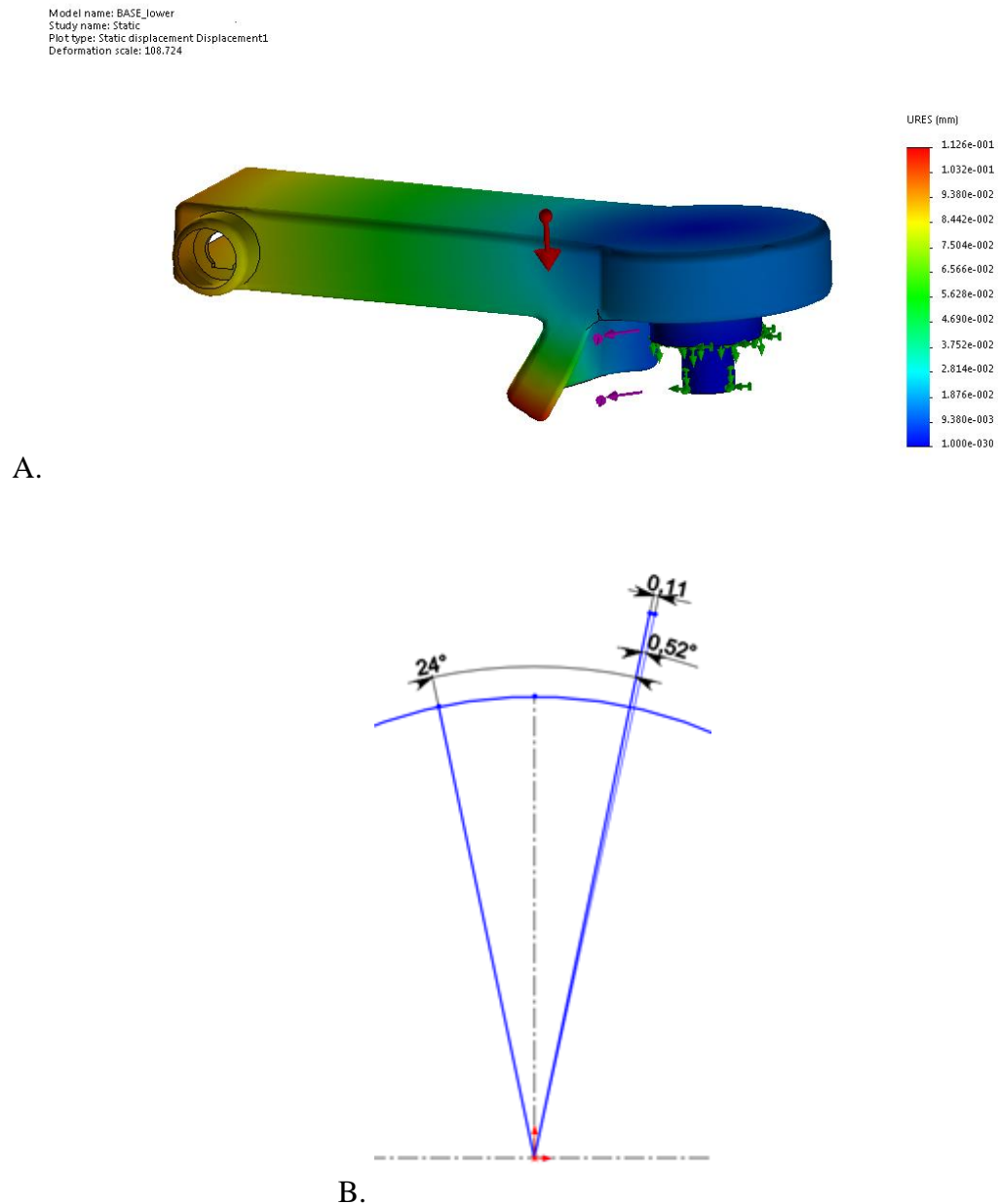


Fig. 3.24. Displacement analysis of the base for the forearm.

- A. Deflection analysis of the base (red zone corresponds to 0.1126 mm deflection).**
- B. Displacement of the carrying angle (0.52°).**

The von Mises-Hencky theory states that “a ductile material starts to yield at a location when the von Mises stress σ_{VM} becomes equal to the stress limit σ_{limit} ” [119]. Therefore, by knowing the stress limit of a material (i.e. yield strength), a FOS failure criteria for the components of the proposed device can be determined as $\frac{\sigma_{VM}}{\sigma_{limit}} > 4$, where σ_{VM} is calculated in the SolidWoks Simulation Module (Fig. 3.25). An example of the FOS analysis is presented in Fig. 3.26. The simulation shows that the base for the forearm made

from ABS plastic will not stretch or contract under loads and therefore will not fracture since the FOS is greater than 4 (blue area in Fig. 3.26).

Cotton and polypropylene bandages were used as interface materials for lining and padding. All selected materials either do not absorb moisture and odours, or are easily washable [94].

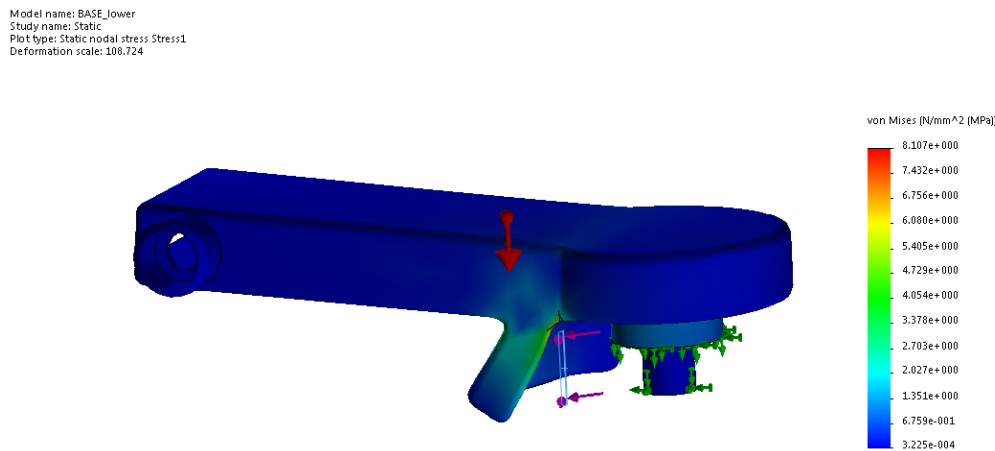


Fig. 3.25. Stress analysis of the base for the forearm.

Model name: BASE_Lower
Study name: Static_2c_По умолчанию-)
Plot type: Factor of Safety Factor of Safety1
Criterion: Max von Mises Stress
Red < FOS = 4 < Blue

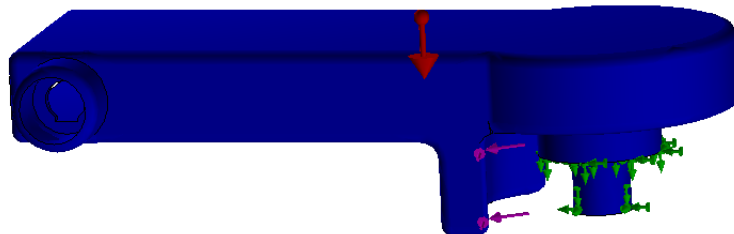


Fig. 3.26. FOS analysis of the base for the forearm.

A polyester sheet was used for forming the cuffs, as it is flexible, low-cost and common in rehabilitation clinics. A press-vacuum machine Formech 300XQ (Fig. 3.27) was used for cuff customization.

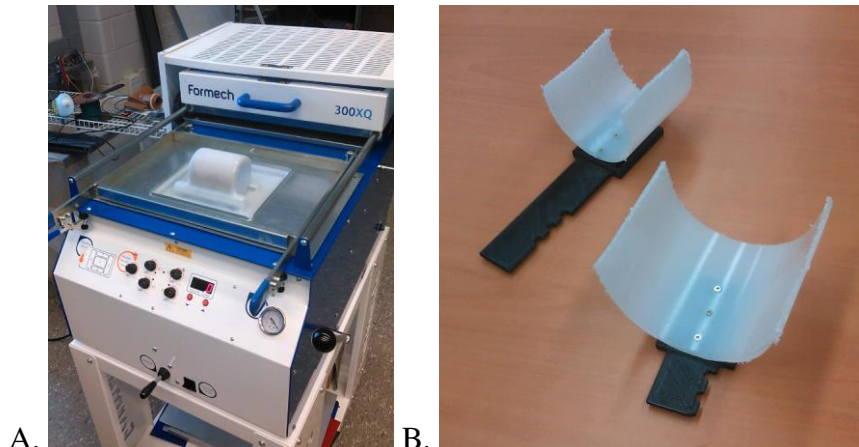


Fig. 3.27. Vacuum-forming cuffs. A. Formech 300XQ. B. Formed cuffs.

3.4 Conclusion

This chapter described the design and development of the wearable elbow brace. Technical specifications for the mechanical and actuation parts of the device were identified based on the literature review and discussions with a hand therapist. Different design concepts were considered and the best solution for the mechanical and actuation parts of the device were selected. In order to verify and test the developed device, a prototype was built and tested. The following chapter presents the resulting prototype and an evaluation of its performance.

CHAPTER 4

4 WEARABLE ELBOW MECHATRONICS-ENABLED BRACE PROTOTYPE

One of the goals of this project was to make the first prototype of the elbow brace as fault-free as possible. For this reason, the previous Chapter presented the work done towards developing the list of mechanical constraints and analyzing the results of static simulations in SolidWorks. Nevertheless, an evaluation of the performance of separate subsystems of the device under the real-world stresses and loads is required in order to provide smooth motions to the forearm of a BPI patient. Thus, Section 4.1 and Section 4.2 outline how the prototype meets the mechanical design specification. Section 4.3 describes how the best option for the torque transmission system was selected. Finally, Section 4.4 summarizes the budget for the prototype development and assembly.

4.1 Design Overview

A first prototype of the designed wearable elbow brace is presented in Fig. 4.1. The total weight of the device is 1.4 kg, while the mechanical structure that can be used for immobilization purposes weights 0.6 kg. The weight exceeds the design requirement of 1 kg and is higher than commercially available mechanical braces for immobilization (e.g., mechanical brace, Innovator X® (Össur) weights 0.4 kg). Despite this, the overweight of the prototype is a justifiable tradeoff since the proposed device offers a number of

advantages, as will be described in Section 4.2 and Section 4.4. Moreover, a shoulder strap can be used to compensate for extra weight of the device, see Fig. 4.1B.



Fig. 4.1. Prototype of the wearable mechatronic elbow brace.

- A. Side view of the prototype.**
- B. View from the back showing the overall width of the brace.**

The mechanical design requirements were verified as shown in Fig. 35–Fig. 39. The natural elbow motion is achieved by mimicking a 2-DOF single-axis hinge type elbow model, as follows:

- (1) The position A and B (Fig. 4.2) corresponds to the *full range of elbow motion in the sagittal plane*, i.e., from 0° in position A to 130° in position B.
- (2) Position C and D (Fig. 4.3) accounts for the *carrying angle that changes during forearm motion in the coronal plane from -12° to $+12^\circ$* . This passive change of carrying angle provides comfortable FE movements driven by the bone structure of the elbow joint.
- (3) Mechanical stoppers, see Fig. 4.4, limit the elbow motion in the sagittal plane, i.e., flexion–extension. *Each mechanical stopper provides a 5° step increment*, see Fig. 4.4B.

The prototype can be adjusted to a wide range of upper limb sizes, as follows:

- (1) The *forearm length can be varied from 25 cm to 32 cm*. Button 1 allows setting 3 positions of Link 1 (Fig. 4.2A and Fig. 4.5) that correspond to 25 cm, 28.5 cm and 32 cm

of forearm length. If extra length is required, Link 1 can be easily replaced with a new longer version without any other design updates.

(2) *The upper arm length can be adjusted from 36 cm to 39 cm.* Button 2 allows setting 2 positions of Link 2 (Fig. 4.2 B) that correspond to 36 cm and 39 cm of upper arm length. If extra length is required, Link 2 can be easily replaced with a new longer version without any other design updates.

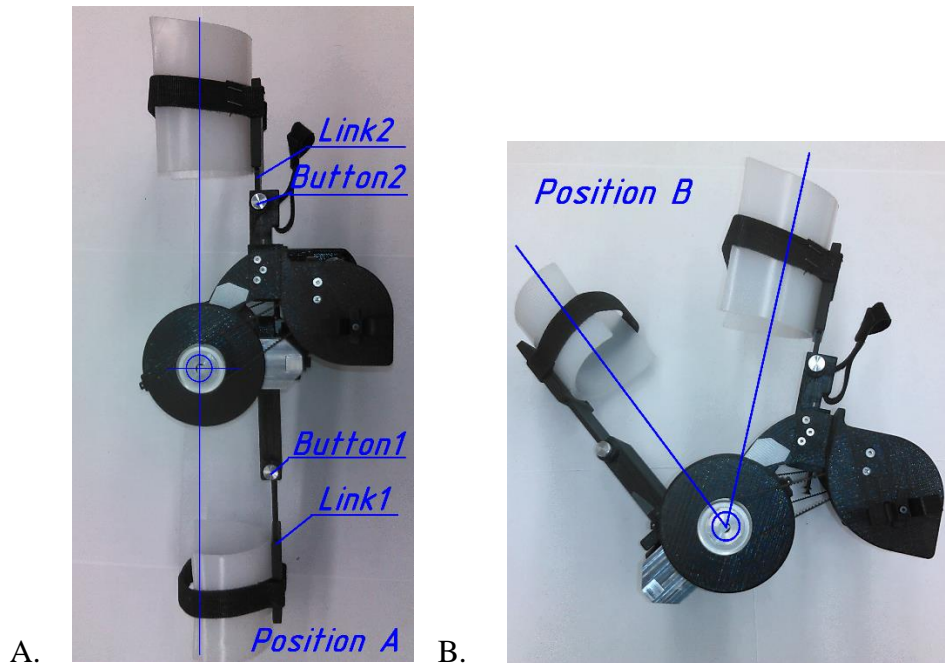


Fig. 4.2. Range of motion of the prototype.
A. Position A – full extension. B. Position B – full flexion.

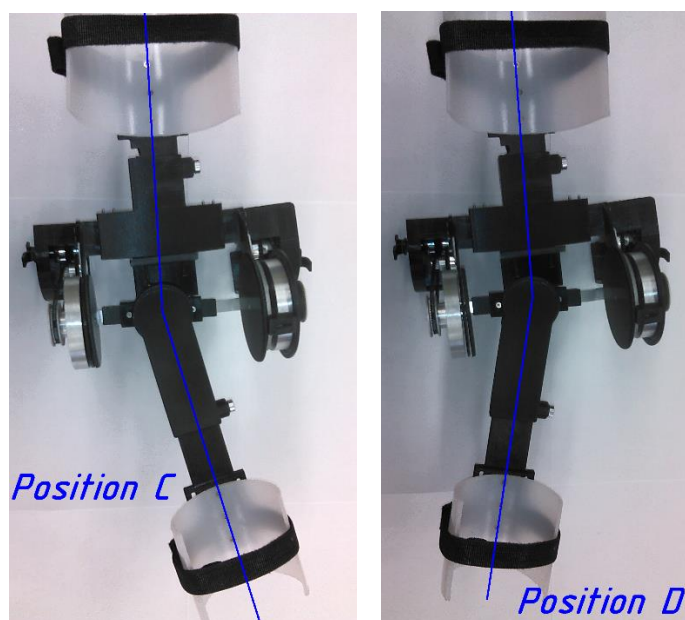


Fig. 4.3. Passive ROM to account for the natural carrying angle.

(3) The elbow breadth can be adjusted from 85 mm to 125 mm, see Fig. 4.6. However, due to the padding that will cover the brace surfaces that contact the skin, the actual space for the elbow is between 74 and 114 mm, see Fig. 4.7.

(4) The cuffs, see Fig. 3.27B, can be formed according to the unique forearm and upper arm circumference of each user. They are flexible, light weight and can be easily screwed onto Link 1 and Link 2 of the device, see Fig. 3.27 B.

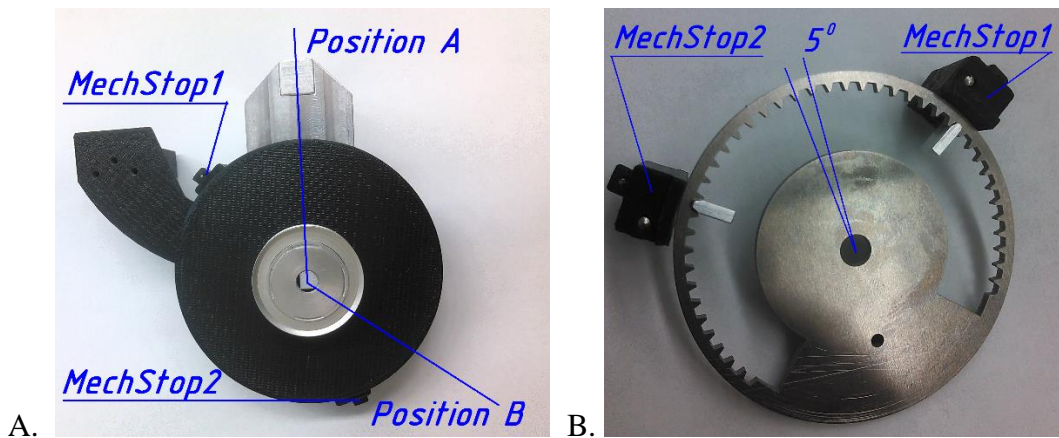


Fig. 4.4. Mechanical stopper of the prototype.

- A. Side of brace with the external part of the mechanical stoppers.
- B. Customized aluminum gear with two mechanical stoppers.

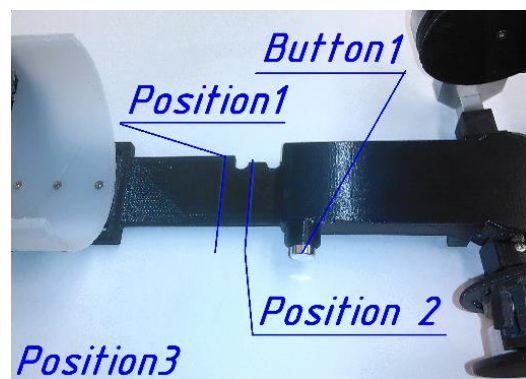


Fig. 4.5. Adjustment of the device for a specific forearm length.



Fig. 4.6. Minimum and maximum elbow breadth.

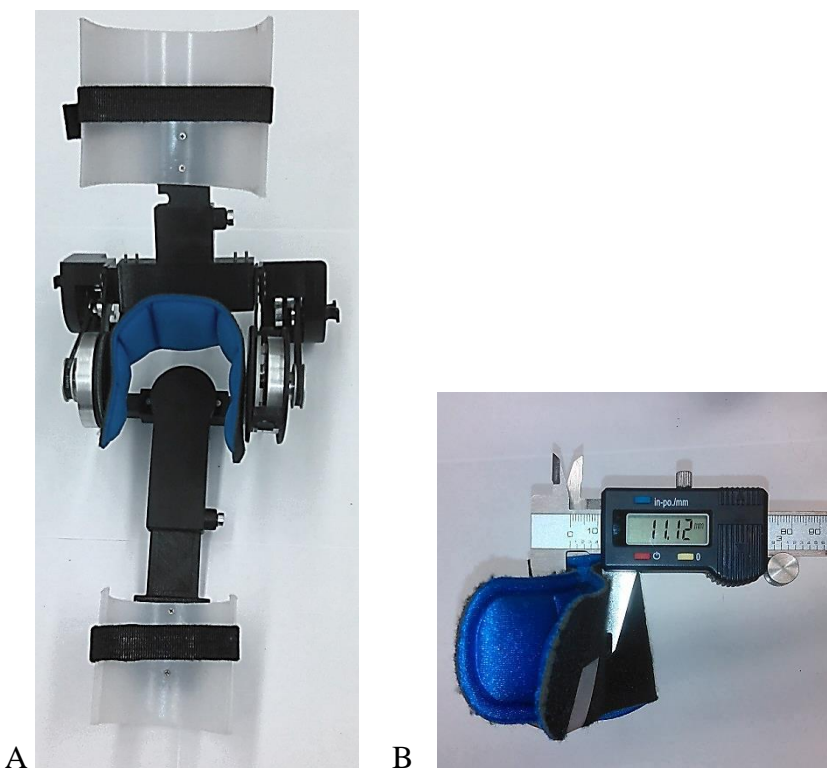


Fig. 4.7. Elbow breadth that the prototype can handle.

A. A possible padding for increasing comfort of a user. B. Thickness of padding.

The prototype can be resized in 1–3 minutes depending on skill level and experience of the user.

4.2 Testing of the Mechanical Stoppers

The mechanical stoppers have two functions: (1) to protect the affected forearm during the reinnervation process, i.e., to immobilize it, and (2) to act as safety reserve components in the torque transmission system. Thus, an assessment of the performance of the mechanical stoppers should include not only scenarios in which the brace is loaded with the weight of a human arm, but also cases in which an additional load (e.g., carrying a 0.5 or 1 kg load for resistive training) is held by the patient. To achieve this, a test that estimates how well the mechanical stoppers perform was designed and presented in this section. The results were compared with the performance of the market-available mechanical brace for immobilization, Innovator X® (Össur) shown in Fig. 2.3.

To assess the accuracy and repeatability of the immobilization phase with the help of the assembled mechanical stoppers, the elbow brace was fixed to a base as shown in Fig. 4.8. A forearm phantom that mimics muscle weight distribution for females and males [120], see Table 4.1, was used for tests. The forearm phantom was constructed from modeling clay (Play-Doh), metal components as shown in Fig. 4.9 and a wooden bar (0.2 kg). The forearm muscles were divided into three groups, see Table 4.1, and the final formed muscles were wrapped over a wooden bar connected to a single-axis hinge, see Fig. 3.6. An additional weight that corresponds to the hand weight of females and males was fixed to the end of the wooden bar. The forearm phantom was covered with silicone, as shown in Fig. 4.10. The total weight of the females forearm phantom (1.74 kg) and the males' version of the phantom (2.23 kg) mimics the lower arm weight for the 95th percentile of the population (see Table 3.1).

Table 4.1. Muscle weight distribution in the forearm phantom.

Group of muscles	Calculated weight (g)	Weight of modeling clay (g)	Weight of used metal part (g)	Length of the longest muscle in group (cm)
Wrist flexors for males forearm phantom	900	300	600	24.9
Wrist flexors for females forearm phantom	480	300	180	24.9
Finger flexors for females/males forearm phantom	430	200	230	24.5
Wrist extensors for females/males forearm phantom	330	100	230	22.2

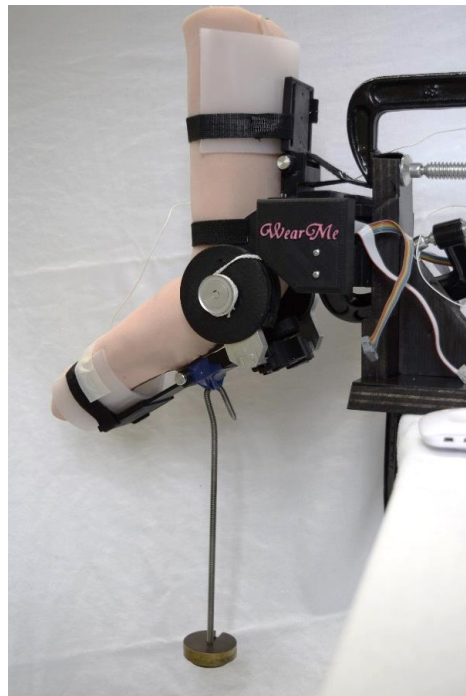


Fig. 4.8. The setup for the assessment of the mechanical stoppers.
Photo credits: Hilary Luo.



Fig. 4.9. Components' distribution in the forearm simulator.

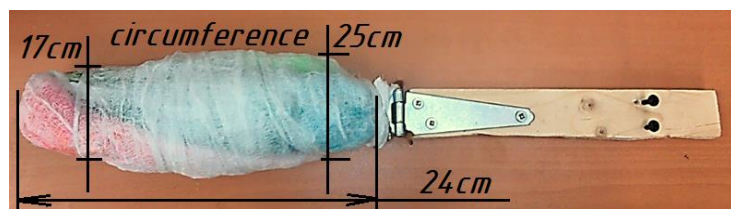


Fig. 4.10. Front view of the forearm simulator.

The test was conducted for three loads: (1) the weight of a female or a male forearm, (2) the weight of a female or a male forearm plus 0.5 kg applied to the center of gravity of the forearm, and (3) the weight of a female or a male forearm plus 1 kg applied to the center of gravity of the forearm. Each test was repeated 3 times for both the elbow brace and for the mechanical brace.

The angular position was recorded with the help of a motion sensor built into the Myo Gesture Control Armband (Thalmic Labs®). Recorded data was saved with the help of

open source software called Myo Capture, and later was processed in MATLAB (MathWorks, Inc.). The accuracy was calculated as the mean error between the initial position of the forearm in the brace and the measured position after a load was applied. Repeatability is presented as the standard deviation observed in tests for each load. The results are summarized in Fig. 4.11, where the mean error of angular displacement and the standard deviation under different conditions are shown for the prototype and the mechanical brace Innovator X®.

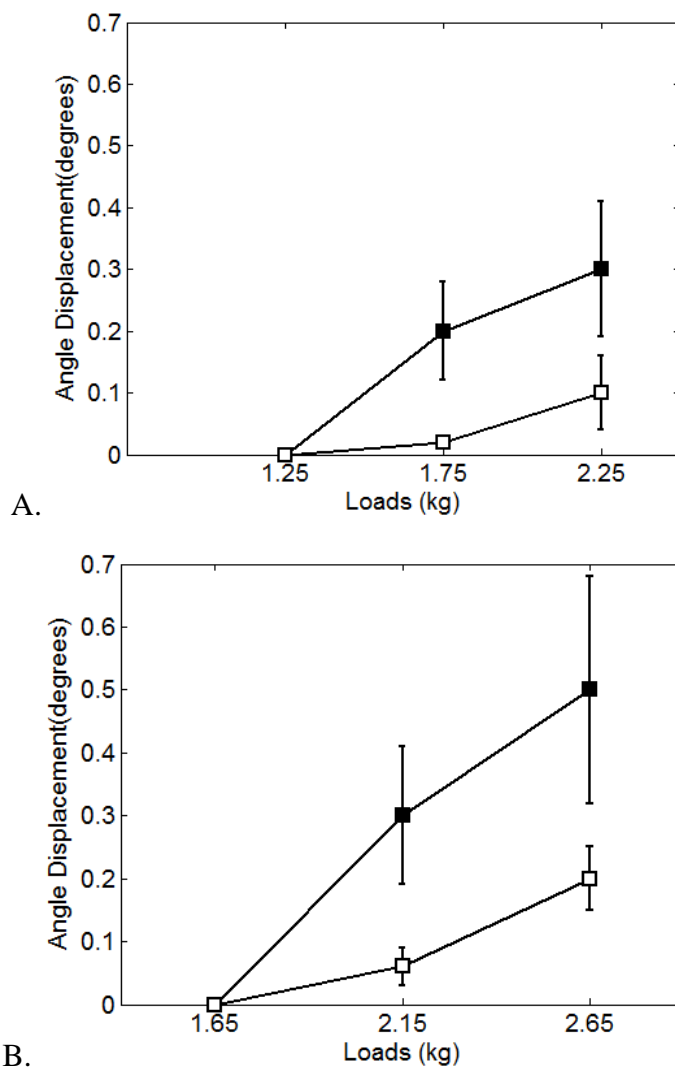


Fig. 4.11. Mean error \pm SD of angular displacement under different loads. □ – prototype of the wearable elbow brace, ■ – commercially available mechanical brace. A. Loads start at the weight equal to the weight of female forearm and hand (1.25 kg) and progress until 2.25 kg, which mimics resistive training with a 1-kg load in the hand. B. Loads start at the weight equal to the weight of male forearm and hand (1.65 kg) and progress until 2.65 kg, which mimics resistive training with a 1-kg load in the hand.

Since the maximum mean error obtained for each scenario for the elbow brace (0.1° for conditions in Fig. 4.11A and 0.2° for conditions in Fig. 4.11B) does not exceed the mean error for the mechanical brace Innovator X® for the same loads (0.3° for conditions in Fig. 4.11A and 0.5° for conditions in Fig. 4.11B), it can be concluded that the proposed device can be used to prevent motion beyond a certain range following nerve reconstruction surgery in order to protect the affected arm.

4.3 Torque Amplifier Testing

As it was mentioned before (Section 3.3.7.4), both belt–pulley and cable–pulley combinations can potentially be used in the transmission system. Hence, a test was designed to identify the best option for a torque amplifier, see Section 3.3.7.

To compare the cable and the belt options, the conditions were maintained throughout the test. Thus, the weight of the load applied to the lower link of the device was kept constant (the weight of the lower link of the device, which is equal to 0.2 kg). According to the calculations in Section 3.3.5, the force acting on the lower link of the device F can be found as $F_f = 6.83 \cdot B$ for females and $F_m = 6.04 \cdot B$ for males, where B is the total output torque from the transmission. Therefore, by knowing the mass of the weight that the pulley moves, $m = 0.2$ kg, the torque B acting on the belt/cable–pulley transmissions can be found as follows:

$$F_f = 6.83 \cdot B = m \cdot g = 1.96 \text{ N}, B = 0.28 \text{ Nm},$$

$$F_m = 6.04 \cdot B = m \cdot g = 1.96 \text{ N}, B = 0.34 \text{ Nm}.$$

As the calculated torque ranges between 0.28 Nm and 0.34 Nm, the largest number can be safely selected for all possible cases. Hence, torque amplifiers located on both sides of the device should transmit 0.17 Nm each.

In order to minimize changes in the transmission system during the test, it was decided to use the same small and the large pulley, which can transmit 0.17 Nm for both cable and belt options, as follows:

- (1) A large Aluminum Alloy Timing Pulley with $N_1=25$ mm, $h_1 = 5$ mm (2 mm (GT2) Pitch, 40 Teeth, 6mm Bore, 2 Flanges/With Hub, Aluminum Alloy Timing Pulley for 3mm Wide Belt, SDP/SI), and

(2) A small Aluminum Alloy Timing Pulley with $N_2=7.8$ mm, $h_2 = 5.7$ mm (2 mm (GT2) Pitch, 14 Teeth, 3 mm Bore, 2 Flanges/With Hub, Aluminum Alloy Timing Pulley for 3 mm Wide Belt, SDP/SI), see Fig. 4.12.

The ratio $\frac{N_1}{N_2} = \frac{25}{7.8} = 3.2$, the external diameter of the larger pulley $d_2 = 30.7$ mm and the external diameter of the smaller pulley $d_1 = 12.80$ mm satisfy the torque amplifier specifications outlined in Section 3.3.7. The groove depth was calculated as the difference between the outside diameter and the pitch (inner) diameter (Fig. 4.12).

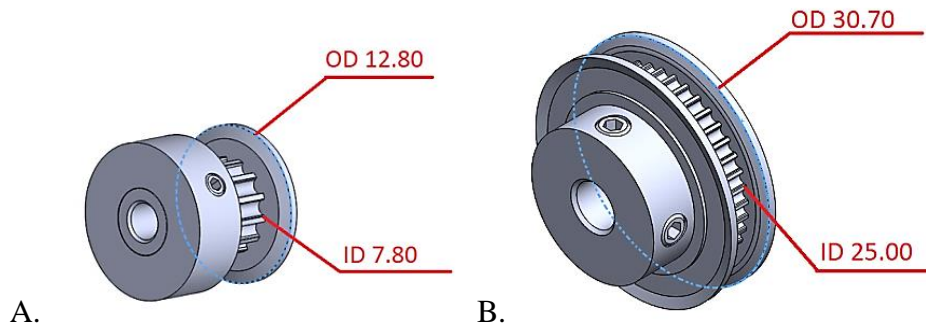


Fig. 4.12. Selected pulleys for belt-pulley and cable-pulley transmission. Dimensions are in mm. A. Small pulley. B. Large pulley.

The selected pulleys can be used with a Nylon® rope of an appropriate cross sectional area. The cross sectional area of a rope, πR^2 , is directly related to its breaking strength: $\delta \sim \pi R^2$.² Therefore, the ratio of the loads and the ratio of the area for a small and a large rope should be equal to the following equation:

$$\frac{f}{F} = \frac{d^2}{D^2}$$

where f and F are the loads of a small and a large ropes, d and D are the diameters of a small and a large ropes. By knowing that a Ø12.5 mm Nylon® rope has a breaking strength of 40 kN, the diameter of a Nylon® rope that can withstand 0.0057 kN (0.17 Nm/0.03 m as

² Assuming that a cable is circular, then its cross sectional area is πr^2 (where r is the radius of a small cable). So a larger cable would have a cross sectional area of πR^2 , (where R is the second cable's radius). This means that the breaking strength of two cables with the same mechanical properties is the ratio of their radii (or diameters) squared:

$$\delta_{\text{small rope}} = \frac{f}{\pi r^2}, \delta_{\text{larger rope}} = \frac{F}{\pi R^2}; \frac{\delta_{\text{small rope}}}{\delta_{\text{larger rope}}} = \frac{f}{\pi r^2} \div \frac{F}{\pi R^2}; \frac{f}{F} = \frac{r^2}{R^2} = \frac{d^2}{D^2}.$$

Torque/Radius of a pulley) can be calculated. Incorporating a safety factor of 3 (non-critical application), yields the following relationship:

$$\frac{0.0057 \cdot 3}{40} = \frac{d^2}{12.5^2}$$

Isolating for d , it was found that a Nylon® rope of Ø0.25 mm in diameter satisfies all requirements.

A 2 mm (GT2) Pitch, 110 Teeth, 3mm wide singles Neoprene belt with Fiberglass cords was selected as a representative of a GT2 belt family that can be used with the selected pulleys shown in Fig. 4.12. The current belt–pulley configuration can generate the following:

$$T = 0.12 \text{ Nm} \cdot 0.65 \cdot 0.7 \cdot 3.2 = 0.17 \text{ Nm/side},$$

where 0.12 Nm is the rated torque for the smaller pulley [113], 0.65 is the belt width factor, 0.7 is the belt length factor, 3.14 is the torque amplifier ratio. Hence, the selected belt–pulley combination can transmit 0.34 Nm.

4.3.1 Setup installation

Due to unique properties of the timing belt and the selected Nylon® rope, an appropriate tensioning needed to be implemented. Thus, the following sections describe the specific process of belt installation (Section 4.3.1.1) and cable installation (Section 4.3.1.2) that was done prior to testing.

4.3.1.1 Belt Installation

Proper tensioning of V-belts is the most important factor for a long, satisfactory operation of a transmission system [121]. Slippage, causing rapid belt and sheave wear, and loss of productivity result from insufficient tension, while excessive stress on the belts, bearings, and shafts and reduced efficiency are the effects of excessive tension. As a rule, belt deflection should not exceed $t/64$ per mm of span length [121], [122]. This can be checked using either a deflection gauge or a steel ruler [122], see Fig. 4.13.

The required span length can be calculated as described in [121]:

$$t = \sqrt{a^2 - \left(\frac{D-d}{2}\right)^2}$$

where t is a span length in inches; a is the distance between pulley centres (83 mm); D is the large pitch diameter (30.7 mm); and d is the small pitch diameter (12.8 mm). For the current project, the span length is as follows:

$$t = \sqrt{83^2 - \left(\frac{30.7 - 12.8}{2}\right)^2} = 82.51 \text{ mm}$$

The allowed deflection distance is equal to $t/64 = 82.51/2.52 = 1.29 \text{ mm}$.

Since the measured deflections from the belts of both transmission systems ($t_1 = 14.18 \text{ mm}$ and $t_2 = 13.28 \text{ mm}$) are larger than the allowed value, a tensioner needed to be applied.

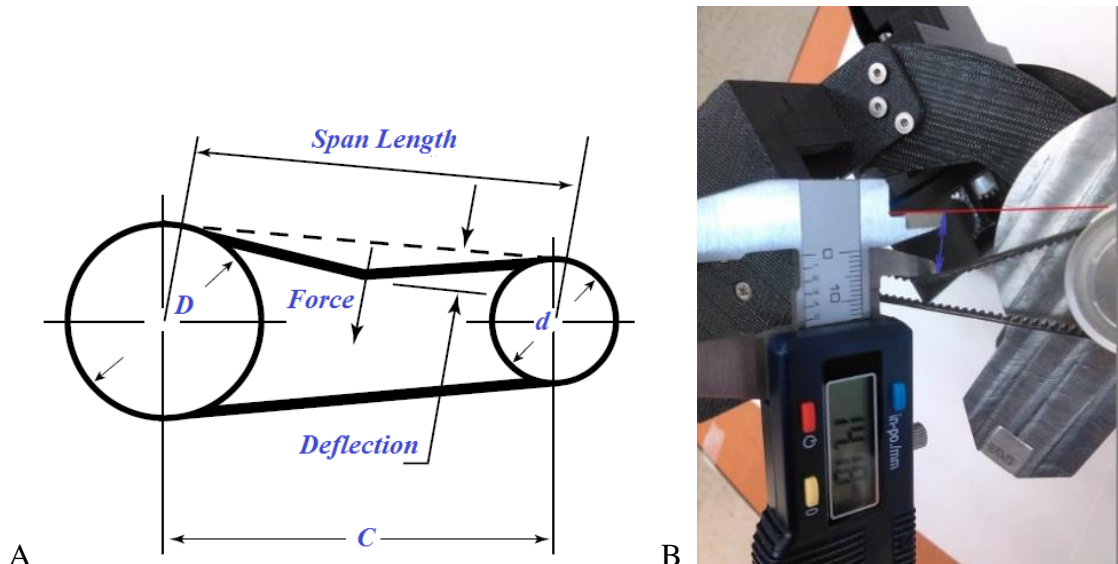


Fig. 4.13. Belt deflection. A. Diagram of a belt deflection measurement.
B. Measured deflection on the belt-pulley transmission.

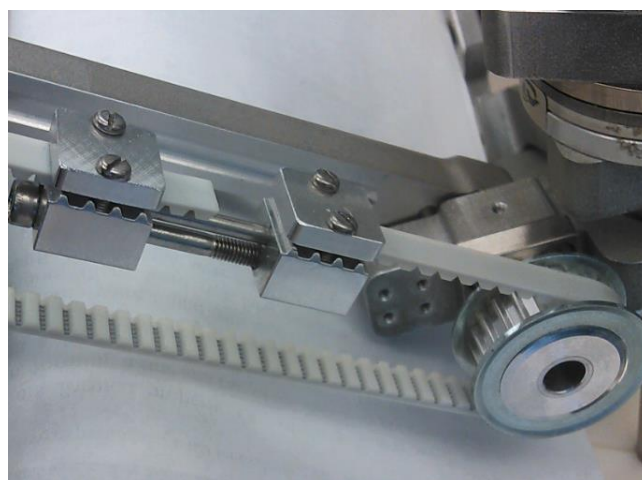
A grid analysis method was used to select the tensioner type, see Table 4.2. High priority was assigned to the weight/size and adjustability criteria. Medium and low weight was given for easy installation and cost criteria.

Table 4.2. Grid analysis of belt tensioners.

	Scaling factor	Stationary roller tensioner	Movable metal tensioner for a cut belt	Movable torsion spring tensioner	Movable 3D printed tensioner
Weight/Size	3	6	6	9	9
Adjustability	3	6	6	3	6
Cost	1	1	1	2	2
Easily installed	2	2	2	4	4
		15	15	18	21

The stationary tensioner and the metal tensioner for a cut belt (Fig. 4.14) were eliminated based on the low score. Due to the need for an additional mechanism that connects the transmission housing and a roller tensioner, stationary roller tensioner requires a lot of space and complex assembly.

On the other hand, movable tensioners that move with the belt and cannot travel over the timing pulley can be an option if the transmission only moves back and forth within a specific distance. A movable tensioner can be made by modifying a torsion spring, see Fig. 4.15. However, it is hard to accurately adjust spring leg length to create a specific tension. Therefore, the Grid Analysis showed that the most sensible option for the current project is a movable 3D printed tensioner (Fig. 4.16).

**Fig. 4.14. Metal tensioner for a cut belt.**

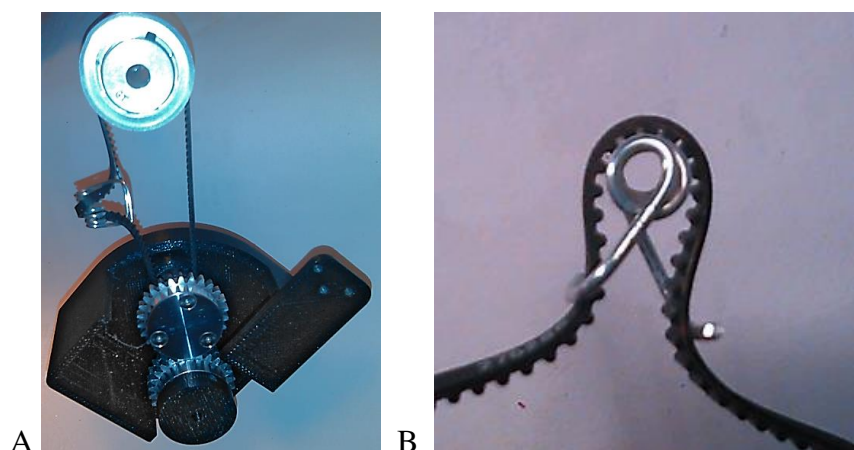


Fig. 4.15. Torsion spring as a tensioner

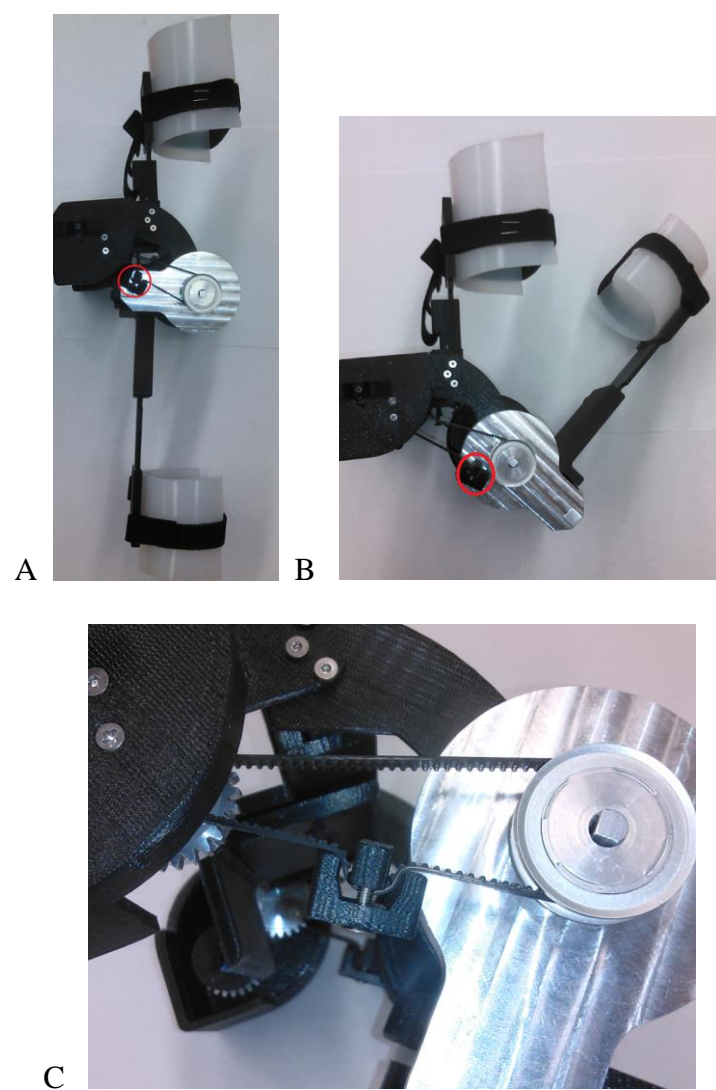


Fig. 4.16. Movable 3D printed tensioner.

- A. Tensioner position at full extension.**
- B. Tensioner position at full flexion.**
- C. Close up of the belt tensioner.**

4.3.1.2 Cable Installation

Properly tensioned closed-circuit cable drive provides good power transmission with no backlash [123]. Such trait is important for a system that regularly applies torque in a changing direction. However, to minimize changes in the drive system of the device, an open circuit cable-pulley transmission was selected for simplicity. The cable diameter was measured as $d_w = 0.25$ mm and the groove depth was calculated as $h = 1.5 \cdot d_w = 0.35$ mm. The elastic deflection of this cable (Fig. 4.17), measured at its center, fixed from two sides can be calculated as follows [124]:

$$F = \frac{4\Delta EA}{a}, \Delta = \frac{F \cdot a}{4EA} = \frac{1.83}{4 \cdot 4000 \cdot \pi \cdot (\frac{0.25}{2})^2} = \frac{83}{785} = 0.11 \text{ mm}$$

where Δ is the cable deflection, F is the force acting on the center of the cable during measurement, a is the measured length of the cable between the centers (Section 3.3.7), E is the modulus of elasticity (4 GPa), and A is the cross sectional area of the cable equal to $\pi(\frac{d_w}{2})^2$.

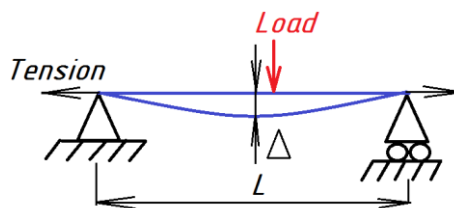


Fig. 4.17. Cable deflection.

The marine camel hitch (Fig. 4.18) was used to fix the rope in the groove of the pulleys. This knot is known for its ability to self-tie on cylindrical and flat objects while the load applied to the hitch might shift from one direction to another.



Fig. 4.18. Diagram of a marine camel knot.
Photo credit: Ingl Kiselov.

4.3.2 Torque Transmission in Rehabilitation

The calculations in Section 4.2 showed that the selected belt–pulley and cable–pulley combinations can easily move the unloaded brace. In order to determine the best option, the brace velocity was compared with the control command (constant speed). In the best-case scenario, the acceleration of the brace should be equal to zero:

$$acc_i = \frac{n_i - n_{i-1}}{\Delta t} = 0$$

where acc_i is the acceleration at time moment i , n_i is the velocity at time moment i , Δt is the time between moment i and $i - 1$. However, in the real world situation, the brace will experience deformations, stresses, disturbances and loads. Therefore, the final movement of the brace may not be smooth. Since jerky motions of the extremity can cause severe pain [125], a numerical limit of acceleration (quantitative measurement of jerky motions) was determined based on the findings in [126] and [127].

Konczak, *et al.* [126] showed that healthy individuals (mean age 61.1 ± 11.6 yrs.; 13 male, 15 female) can have a 0.2° position sense threshold, i.e., humans are not able to distinguish elbow movements that are less than 0.2° . On the other hand, humans can respond to a disturbance within 5–10 Hz [127]. In other words, an individual may recognize a change in the elbow position only every 0.1–0.2 s (where 0.1 s corresponds to 10 Hz and 0.2 s corresponds to 5 Hz). As a result, any movement of the elbow made slower than 0.1 s ($\Delta\tau$) or that resulted in less than 0.2° ($\Delta\alpha$) of elbow position change will be ignored by the cortex, and therefore no pain can be associated with such movements. As a result, the position change of the brace should not exceed $\Delta\alpha$ limit (0.002°) within each $\Delta\tau$ moment of time (0.001 s = 1 ms). In this case, the frequency of sensory stimulus would not exceed the pain receptor's threshold [128] and, therefore, it is speculated that it may be interpreted by the cortex as a non-painful motion (additional testing would be required to confirm this assumption). Additionally to the $\Delta\alpha$ limits that quantify smoothness of brace movement, the efficiency of the speed transmission (ratio of the command speed to the brace speed) should be at least 95%.

4.3.2.1 Methods

In order to test the designed transmission with a belt/cable–pulley combination, a closed-loop control system that contains a PC and two EPOS 24/5 Motion Controllers (Maxon Motors) was designed, see Fig. 4.19.

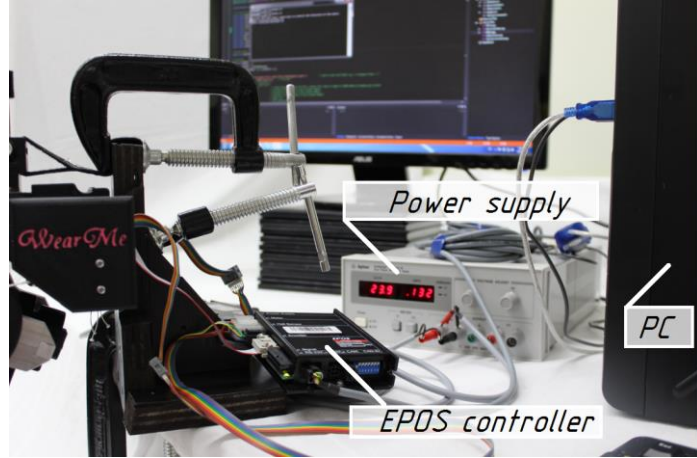


Fig. 4.19. Setup for transmission system testing. Actuators connected to the EPOS 24/5 controller, power supply and PC.

The EPOS 24/5 controllers receive velocity commands ($12000^{\circ}/\text{s}$) from the PC and actuate the appropriate Maxon Planetary Gearhead (Part No. 143995, Maxon Motors) through the coupled Maxon EC-max 22 (Part No. 283840, Maxon Motors). Once the velocity command is issued to the EPOS 24/5, internal PID controllers that use signals from an encoder that tracks the desired motor velocity. The gains for the PID controller were tuned to achieve a fast response of the motor for a specific velocity with the help of the Maxon software ($P=282$, $I=14$, $D=0$), where the target settling time was assigned to be 25 ms, the dead time 5 ms, and the velocity step 2000 rpm (12000°). The final velocity of brace can be calculated as follows:

$$n_{\text{brace}} = \frac{n_{\text{motor}}}{333 \cdot 3.14} = \frac{12000}{1045.62} = 11.47 \text{ } ^{\circ}/\text{s},$$

where 333 is the speed reduction ratio of Maxon Planetary Gearhead and 3.14 is the speed reduction ratio of the torque amplifier. More details about the control system (hardware and software) are provided in Section 6.

A constant speed (2000 rpm) was used to test the belt and the cable within the entire ROM (0–130°). The test was repeated 10 times³ with the same conditions for each transmission. The brace response was recorded with the help of a motion sensor used with the Biosignalsplus sensing platform (Plux®). The data were saved and later converted to an array of angular displacements with the help of “OpenSignals” (Plux®) and MATLAB (MathWorks Inc.) software.

4.3.2.2 Results and Discussion

After a motion profile was extracted from each trial, see Fig. 4.20 green area, the average velocity n , the average acceleration acc and the average $\Delta\alpha$ were calculated in MATLAB (MathWorks Inc.) and summarized in Table 4.3. Samples of data for the belt–pulley and the cable–pulley transmissions are shown in Fig. 4.20 and Fig. 4.21, respectively. The average velocity $n = 11.33^\circ/\text{s}$ shown in Fig. 4.20 and the average velocity $n = 9.95^\circ/\text{s}$ shown in Fig. 4.21 were calculated as a mean value of position changes within 1 ms divided by 1 ms across the green area. A sample of the $\Delta\alpha$ distribution over time for the Nylon® cable–pulley transmission is shown in Fig. 4.22, where the maximum $\Delta\alpha$ (0.0008°) is not exceeding the acceptable value (0.002°).

A small acceleration ($acc = 0.25^\circ/\text{s}^2$ for the cable transmission and $acc = 0.31^\circ/\text{s}^2$ for the belt combination) in both cases corresponds to a good mechanical response to a control signal. The test showed that the belt transmission has 98% efficiency of speed transmission (the ratio of output and input velocity, i.e., $11.21^\circ/\text{s} / 11.47^\circ/\text{s}$), while the Nylon® cable showed only 87% of speed transmission efficiency ($9.96^\circ/\text{s} / 11.47^\circ/\text{s}$). Despite the low efficiency of the speed transmission, the cable showed better repeatability ($0.1^\circ/\text{s}$ vs. $0.21^\circ/\text{s}$) and lower acceleration ($0.25^\circ/\text{s}^2$ vs. $0.31^\circ/\text{s}^2$) throughout the tests. Moreover, the mean $\Delta\alpha$ was lower for the cable transmission, as shown in Table 4.3.

³ The number of test repetitions with the same conditions for each transmission was limited to 10 times due to time constraints.

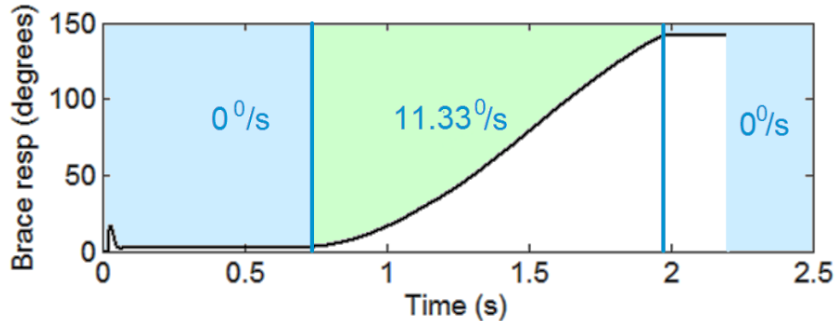


Fig. 4.20. Example of the response of the brace with the belt–pulley transmission to a constant velocity command. The average velocity $n = 11.33^{\circ}/s$ was calculated as the mean of position changes within 1 ms divided by 1 ms across the green area. Time $t=0$ refers to the moment at which the recording from the sensor started.

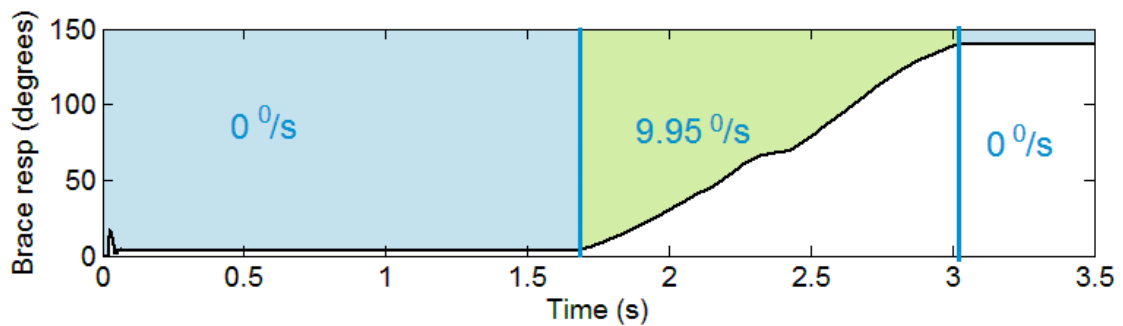


Fig. 4.21. Example of the response of the brace with Nylon® cable–pulley transmission to a constant velocity command. The average velocity $n = 9.95^{\circ}/s$ was calculated as the mean of position changes within 1 ms divided by 1 ms across the green area. Time $t=0$ refers to the moment at which the recording from the sensor started.

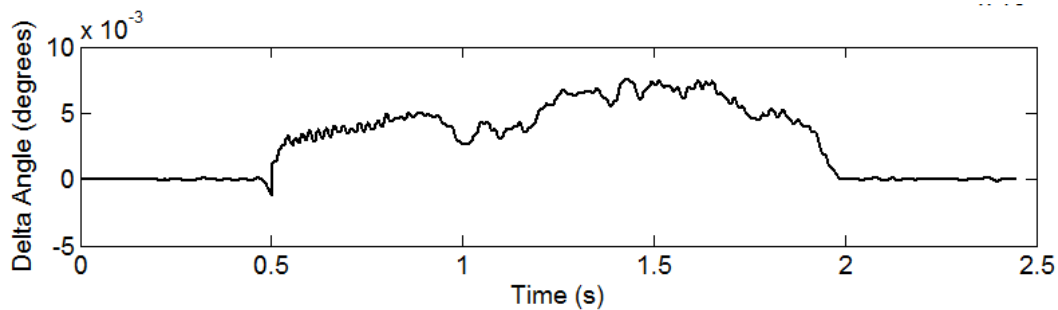


Fig. 4.22. Example of $\Delta\alpha$ distribution over time for the Nylon® cable–pulley transmission.

Table 4.3. Belt and cable performance assessment.

	Average velocity \pm SD, $^{\circ}/s$	Average acceleration \pm SD, $^{\circ}/s^2$	Mean $\Delta\alpha \pm$ SD, degrees
Belt	11.21 ± 0.21	0.31 ± 0.023	0.0032 ± 0.0032
Nylon® cable	9.96 ± 0.1	0.25 ± 0.028	0.0020 ± 0.0044

Both options considered above for the transmission system have advantages and limitations. However, the ability of Nylon® rope to perform smooth movements overweighs its limitation in speed efficiency. Moreover, high rope elongation, as observed in Fig. 4.21 explains the poor efficiency of speed transmission. Since the elongation EE at 90° (position where cable absorbs shock loading) is in inverse ratio to the cross sectional area of cable, the speed efficiency of the cable can be increased by increasing the cable diameter.

The rope diameter was increased in 0.25 mm increments until the speed efficiency achieved acceptable values. The iterations were stopped when the cable was formed from six 0.25 mm Nylon® ropes twisted as one wire. Tests with the new cable (1.5 mm diameter) were conducted with the unloaded brace for a speed range of 10–25°/s. The results of the cable-pulley transmission performance are summarized in Fig. 4.23 and Fig. 4.24. The mean speed efficiency across all speed conditions was $95.45 \pm 1.63\%$, while none of the mean $\Delta\alpha$ across all speeds exceeded the maximum allowed value of 0.002° . An example of the brace response to a $22.5^\circ/\text{s}$ speed command and corresponding $\Delta\alpha$ distribution are shown in Fig. 4.25 and Fig. 4.26, respectively.

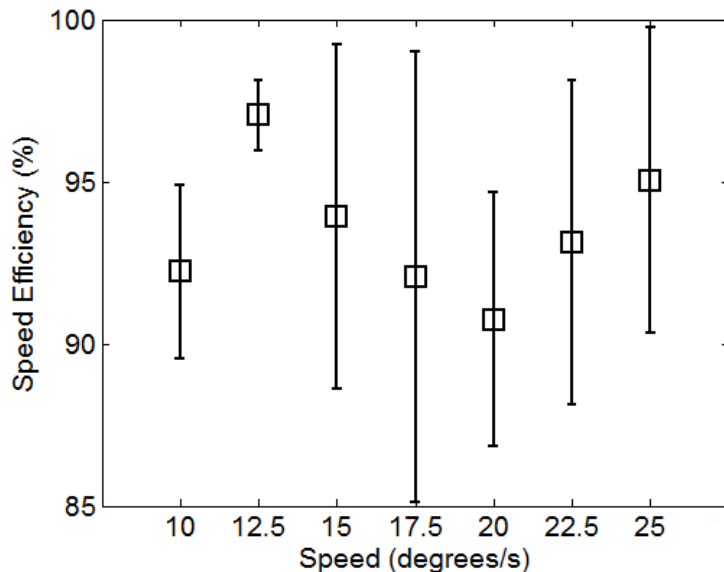


Fig. 4.23. Response of the brace with Nylon® cable-pulley transmission to different constant velocity commands. Each speed efficiency value is the mean value of 10 calculated speed efficiencies for a specific speed. The mean speed efficiency across all speed conditions is $95.45 \pm 1.63\%$.

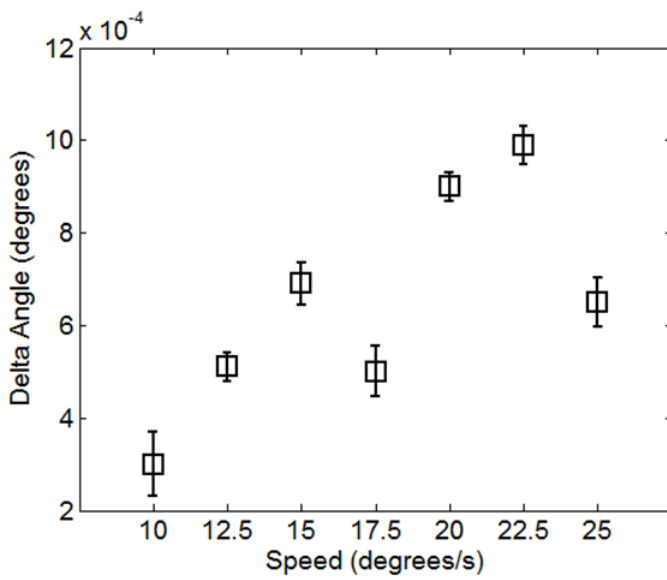


Fig. 4.24. $\Delta\alpha$ distribution over time for the Nylon® cable-pulley under different speed conditions. Each delta angle value is the mean value of 10 calculated delta values for a specific speed. The mean $\Delta\alpha$ across all speeds does not exceed the maximum allowed value of 0.002° .

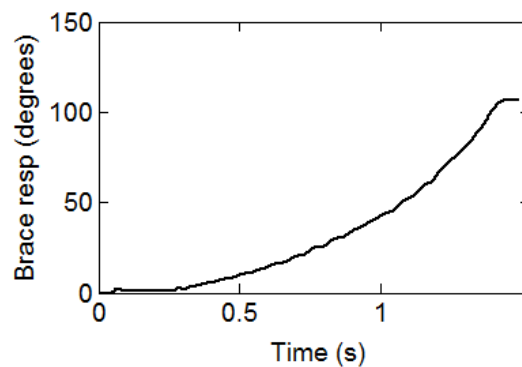


Fig. 4.25. Example of the response of the brace with Nylon® cable-pulley transmission to a constant velocity command $n = 22.5^\circ/\text{s}$. The average velocity of $n = 22.98^\circ/\text{s}$ was calculated as the mean of position changes within 1 ms divided by 1 ms.

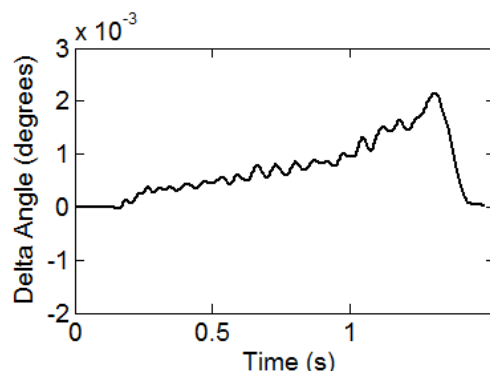


Fig. 4.26. Example of $\Delta\alpha$ distribution over time for the Nylon® cable-pulley transmission when moving at a speed of $n = 22.98^\circ/\text{s}$.

According to the results, the new cable performs smooth movements with acceptable speed efficiency (compared to the previous test with 0.25 mm rope). Therefore, the cable–pulley system was used as the torque amplifier for the current prototype.

4.4 Prototype Costs

Although none of the reviewed wearable elbow mechatronics-enabled devices found in the literature reported financial constraints, the cost of the final prototype (Table 4.4) can be compared with a market available MyoMo system [67] (\$7,500) that provides active-assisted motion support for the upper limb for stroke patients. The overall cost of machining, assembling, purchasing components and labor work resulted in \$5,600 per unit. By adding a 20% profit to the prototype cost, the final price \$6,800 is still below the \$7,500 level. Moreover, the cost can be reduced when the brace moves from the prototype stage to production (e.g. from \$5,600 to \$4,400 if components are purchased from wholesale companies).

Table 4.4. Prototype costs.

Item	Cost
ABS thermoplastic, 1 kg	\$40.00
3D printing service	\$50.00
Aluminum 7075 and 6061, machine shop service	\$2,300.00
Standard components	\$100.00
Gears	\$75.00
Dry EMG electrodes	\$185.00
Accelerometer	\$3.00
Pulleys	\$33.00
Cables	\$10.00
Motors, gearheads, encoders	\$1,260.00
Internal 12V 800mAh rechargeable NiMH battery	\$5.00
Polyester for cuffs and machining	\$50.00
Velcro straps and padding materials	\$35.00
Control system	\$500.00
Assembly	\$500.00
Testing	\$500.00
Profit (20%)	\$1,128.00
Total	\$6,767.50

4.5 Conclusions

A wearable mechatronic elbow brace was designed and a prototype was constructed. The weight of the device exceeded the design specification of 1 kg. However the 0.4 kg of overweight can be compensated with a shoulder strap. The extra weight resulted from a complex metal torque transmission that adds flexibility in the application of the device. Therefore, the prototype weight is a justifiable trade-off.

The brace mimics the 2-DOF single-axes hinge type elbow motion model and employs electromagnetic actuators and a customized transmission system for generating 10 Nm distributed to both sides of the joint (device Type C, see Section 2.3.1). The elbow brace can be adjusted to a wide range of lengths of upper limbs. Telescopic links can be manually moved to a specific position according to the anthropometric length of female's and men's upper limb length. Replaceable polyester cuffs make the device more affordable and comfortable for patients. The prototype can be adjusted to a new user in 1–3 minutes depending on the skill level and experience of a user. The weight of the actuation system is symmetrically distributed on the backside of the upper arm. Additionally, the benefits of this device over existing prototypes can be summarized as follows:

1. The drivers can be easily removed from the elbow brace by pulling a spring-loaded handle that decouples the transmission system from the output shafts of the gearheads, allowing (a) to remove transmission and actuation systems and use the device as a mechanical brace at the immobilization phase, (b) to use the decoupling handle as an emergency stopper, (c) to decrease the weight of the device in cases when the rehabilitation process requires active exercises only a few times a day, (d) to replace/test the actuation system without reassembling the construction. Other devices found in the literature implement stationary coupling of the actuation system to the device with limited or no emergency decoupling.
2. A 2-DOF elbow motion model with active flexion–extension and passive carrying angle was used for the elbow brace design. Thus, the device provides natural elbow motion and decreases alterations in joint anatomy and limitations of elbow motions. Although Vaca Benitez, *et al.* [54] also used a “passive comfort joint” to account for the carrying angle, the system is limited to active rehabilitation and has no emergency mechanical stopper.

3. A shoulder strap that goes over the patient's shoulder and underneath the arm prevents the slide-off effect. Such feature is critical for a wearable elbow brace since the pivot point of the elbow and the device should be aligned as precisely as possible through all the process of the rehabilitation. Failure to maintain this condition may trigger elbow deformation.

The results of the transmission system tests showed that the belt transmission has 98% of speed efficiency, while Nylon[®] cable of 1.5 mm in diameter showed 95% of speed transmission efficiency. Moreover, the cable showed better repeatability ($0.1^{\circ}/s$ vs. $0.21^{\circ}/s$) and lower acceleration ($0.25^{\circ}/s^2$ vs. $0.31^{\circ}/s^2$) throughout the tests. Additionally, position drift of the brace $\Delta\alpha$ was lower for cable transmission. This means that the cable-driven transmission may result in less muscle spasm than the belt-driven system. Therefore, it was decided to use a cable driven system for the torque transmission system.

The following chapter describes the next stage of the design process, i.e., the development of a control system for the assistive and resistive modes of the wearable mechatronic elbow brace.

CHAPTER 5

5 METHODS FOR DIGITAL SIGNAL PROCESSING OF EMG SIGNALS FOR MOTION PROFILE ESTIMATION

The previous chapters presented the design of the wearable elbow brace that forms the basis of the mechatronic system. Although the device meets all of the mechanical requirements, it is necessary to assess how the device interacts with a user. In order to do so, a sensing system is required to control the actuation system of the device (as discussed in Section 2.3.3). As the sensed data cannot be intuitively interpreted, digital signal processing techniques that extract useful information from the EMG signal are presented in the following chapter.

5.1 Rehabilitation Strategy Overview

A control strategy is required on the last stage of the reinnervation process, i.e. home-based daily exercises. At the beginning of the training program, a patient is encouraged to contract affected muscles and move the forearm against gravity. Since the cortex of BPI patients is not responding to the neural activity from the restored nerve (more details in Section 1.2, Section 2.1 and Section 2.2), training with EMG feedback enhances the muscle re-education process. Such training requires the patient to contract affected muscles, while an EMG device activates an alarm that indicates when the EMG signal overshoots a specific threshold. While the alarm is on, the therapist moves the forearm in order to re-educate the cortex to recognize the neural activity from the new nerve. Thus, the option of operating

the control system in **educational mode** has to be included in order to mimic training sessions with the therapist incorporating EMG feedback to promote the healing process.

As the affected arm starts to respond to muscle contractions, a patient is challenged to move his or her forearm without external support. At the moment when the patients cannot lift the forearm while the muscles continue to contract, the patient is instructed to help his or her affected arm with the non-affected one, i.e., assist the affected arm to perform the desired motion. Such training should be designed as the **assistive mode** of the control system of the proposed device. The training starts with unloaded exercises and progresses to 1-kg load exercises.

Thus, the control system of the device should have two modes that are consequentially used as the BPI patient progresses from the educational stage to the assistive training stage. Each mode requires the implementation of a sensing system that can quantify muscle activity as feedback to the control system. In order to design such human-machine interface, Section 5.2 outlines the list of goals for the two rehabilitation modes. Section 5.3 describes how the sensed data should be processed and used in each of two modes.

5.2 Goals of Rehabilitation Modes

For motion rehabilitation, the **speed settings should be set to the lowest value (10–25°/s)** for the device to avoid sudden overshoots in the achieved elbow ROM and in order to protect weak muscles and the reconstructed nerves from overstretching, which may result in pain. The device should work in one of two modes at a time. The first mode, educational, is aimed at detecting neural activity from restored nerves and, when the neural signal exceeds a specific value, the actuation system has to move the forearm in the desired direction with a pre-set speed. Hence, an EMG-based method that detects whether the desired trajectory has changed during the motion is proposed for the **educational mode** and presented in Section 5.3.2.

After the cortex of the patient is re-educated to recognize neural activity from the reinnervated muscles, the next goal is to train the affected muscles to contract as naturally as possible. Thus, the affected arm has to perform smooth elbow flexion–extensions with an accuracy in limb positioning between 2° and 5°. Therefore, the goal of the device in the **assistive mode** is to convert the EMG signal from the patient's muscles into a motion (speed) profile with at least **95% accuracy for a full ROM**.

The signal flowchart is shown in Fig. 5.1, where the BioSignalPlux (EMG and/or accelerometer) sensors are connected to the user. Data from the sensors are used to estimate the trajectory of motion for the educational mode or the speed of motion for the assistive mode. The desired trajectory/speed is transferred to the actuation system through the motion controller. The loop closes on the motion sensor that verifies whether the mechanical system achieved the desired position/trajecotry.

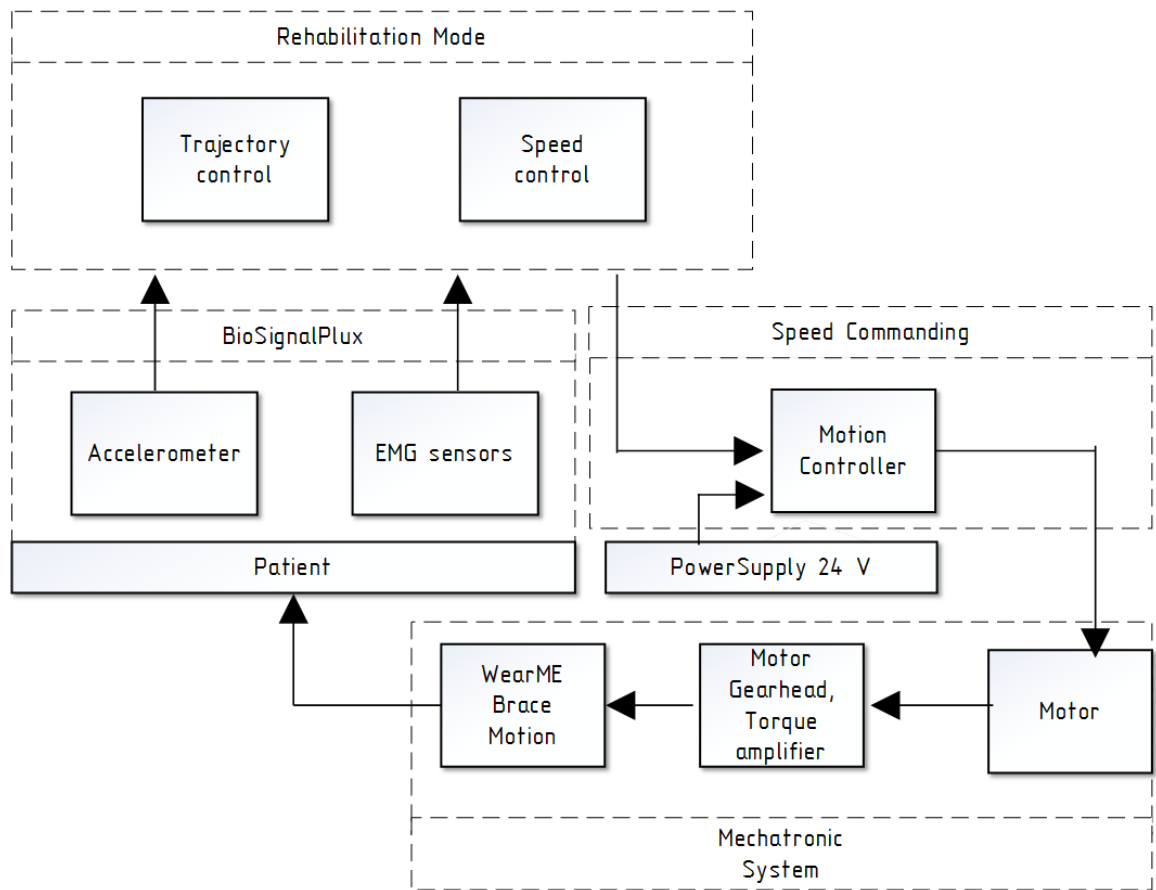


Fig. 5.1. Architecture of the control system.
Trajectory control is used for the educational mode.
Speed control is used for the assistive mode.

The frequency response of the control system has to be at least 5 Hz, since it will allow patients to use the device without noticing a delay between their intention to move and the brace response [127].

5.3 Signal Processing

Data sensed from a patient has two major noise components: electromagnetic noise and motion artifact (e.g., electrode movement on the skin or movement of wire leads) [131].

Once the signal is converted into a digital form, digital signal processing (DSP) is used to restore the signal and/or remove noise. A customized DSP technique for sensed data is described in the sections below.

5.3.1 Signal Filtering

As the raw EMG signal (Fig. 5.2) is often contaminated with direct current noise generated at the electrode – skin junction [132], an appropriate signal filtering is required to extract important EMG signal information. SENIAM's (Surface EMG for a Non-Invasive Assessment of Muscles, 1999) recommendations for EMG filtering include the use of a high pass filter with a 10–20 Hz cutoff frequency. Thus, the raw EMG data was high-pass filtered with 4th order Butterworth filter (as recommended in [78]) to remove any artifacts from the recorded signal.

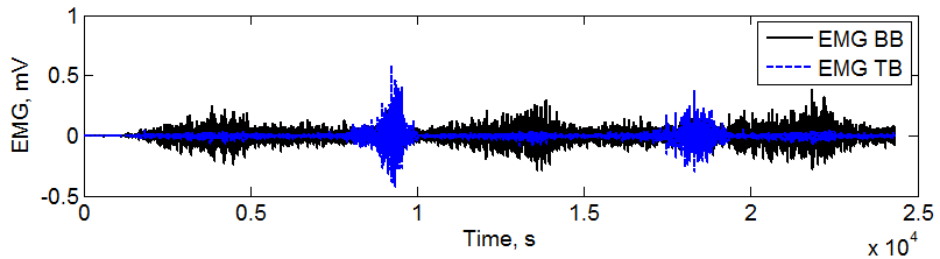


Fig. 5.2. Raw EMG data from biceps and triceps.

The raw three-axes data from the accelerometer should be high-pass filtered with a 2nd order Butterworth filter with a cutoff frequency of 2 Hz in order to reduce the motion artifact, gravitational artifacts and high frequency noise (as recommended in [133]) and finally, converted to angular displacements, see Fig. 5.3. The angular position in Fig. 5.3 corresponds to the EMG signal in Fig. 5.2. In order to find a method that maps information from the EMG sensing system to forearm's motions, the three-axes position data was converted to the distance traveled by the forearm as a function of time, see Fig. 5.3B.

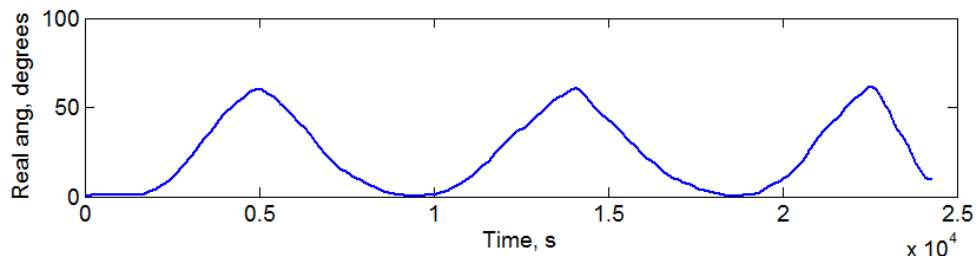


Fig. 5.3. Angular position of a forearm (3 FE) after 2 Hz high-pass filtering.

5.3.2 Direction of Elbow Movement

It was shown in the literature that the RMS of the EMG signal from the lower limb muscles implemented in a neuro-fuzzy modifier could be used as indicators of patient's intension to change the direction of movement [76]. As mean of RMS EMG correlates with muscle strength (CC=0.903) [77], it was proposed to use RMS EMG peaks to detect when the forearm reaches desired position during flexion (i.e. maximum muscle contraction due to the need to deceleration the forearm) and to identify when the forearm reaches full extension (i.e. maximum triceps contraction due to the need to decelerate the forearm). Thus, a simple peak-based method was designed for the educational mode of the control system for detecting a moment when the direction of the forearm should be reversed. The RMS signal of EMG data (Fig. 5.5) was described in [77] and can be found as:

$$EMG_{RMS} = \sqrt{\frac{1}{ws} \sum_{i=1}^{ws} EMG(i)^2}$$

where $EMG(i)$ is the raw EMG voltage signal, and i is the step number within the window of data (ws). A 250–500 ms window of data (ws) is recommended in [78]. An example of the RMS of the EMG signal that corresponds to Fig. 5.2 and Fig. 5.3 is shown in Fig. 5.5. The direct mapping of RMS EMG from Fig. 5.5 to the corresponding position data from Fig. 5.3 shows that the RMS peaks of the EMG signal imply two events: (1) when the elbow reaches the maximum flexion position, and (2) when the elbow extension results in full forearm stop, see Fig. 5.6. For this strategy, no overlapping analysis windows were used.

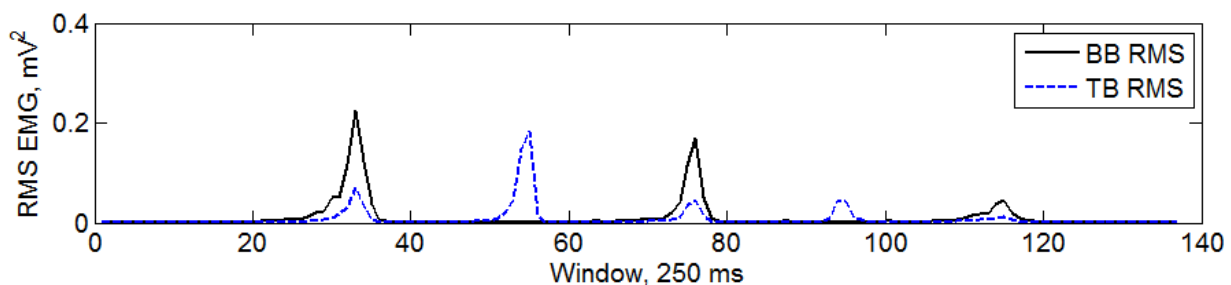


Fig. 5.5. Sample RMS EMG signal from BB and TB. Calculation based on the EMG data of one individual (Fig. 5.2) that was collected during three elbow FE movements (Fig. 5.3). Signal filtering was done as outlined in Section 5.3.1. RMS EMG from TB was amplified (Gain=20).

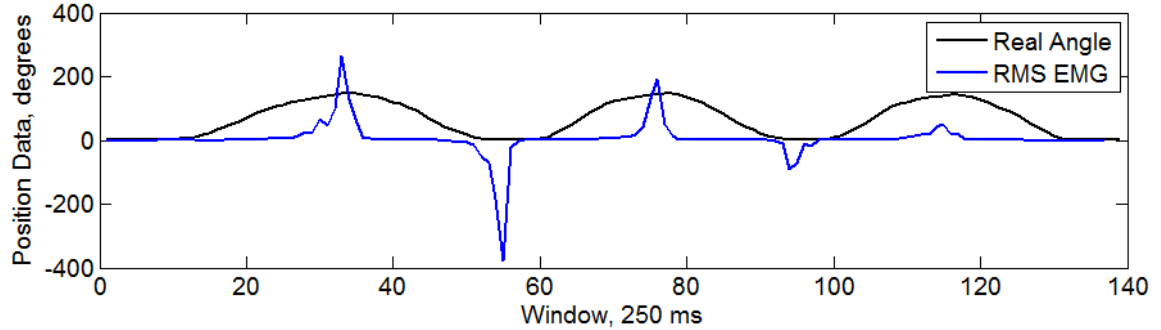


Fig. 5.6. Direct mapping of RMS EMG and motion data.
Net RMS EMG=(RMS BB – RMS TB)·100.

More information can be found if the RMS of the EMG signal is compared with the speed profile of the same motion (Fig. 5.7). The method estimates the moment when the speed crosses the zero line with a delay equal to a window size t .

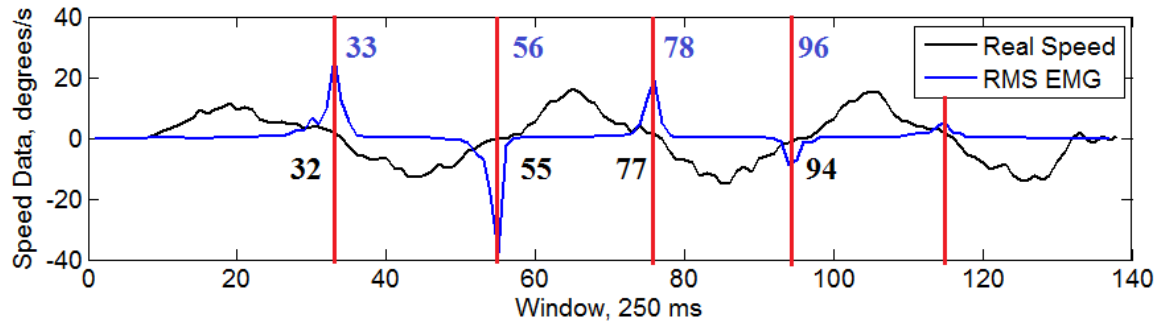


Fig. 5.7. Speed profile compared to RMS EMG.

5.3.3 Speed Estimation

The dynamics of the muscle tissue can be divided into activation dynamics and contraction dynamics [148] (Fig. 5.16).

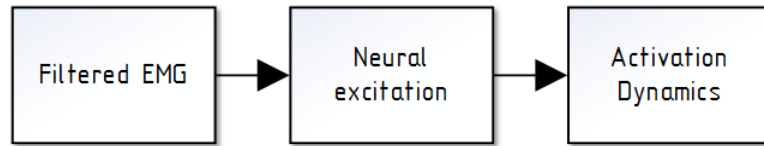


Fig. 5.16. Muscle activation dynamics.

Neural activation $u(t)$ is known to be a function of its recent history. A second-order equation that shows the relation between neural activation $u(t)$ and EMG signal $EMG(t)$ can be represented as [155], [156]:

$$u(t) = \alpha_{\text{EMG}} \cdot e(t - EMD) - \beta_{1\text{EMG}} \cdot u(t - 1) - \beta_{2\text{EMG}} \cdot u(t - 2),$$

where EMD is electromechanical delay, α_{EMG} , $\beta_{1\text{EMG}}$ and $\beta_{2\text{EMG}}$ are coefficients defined as following [143]:

$$\begin{aligned}\beta_1 &= \gamma_1 + \gamma_2, \\ \beta_2 &= \gamma_1 \cdot \gamma_2, \\ \alpha - \beta_1 - \beta_2 &= 1,\end{aligned}$$

where $|\gamma_1| < 1$, $|\gamma_2| < 1$.

Since the normalized EMG signal $EMG(t)$ is out of phase with the muscle force [157], there is an electromechanical delay between the time of the EMG and that of the corresponding force. This interval is assumed to represent the propagation of the action potential along the muscle, the excitation–contraction coupling process, and the stretching of the muscle's fibers [158]. The electromechanical delay is affected by the initial muscle length [160] and muscle loading [161], while fatiguing exercise lengthens the delay [162]. The EMD has been reported to range from 10 ms to about 100 ms [163]. Very often, a fixed EMD of about 70 ms is taken into account to relate EMG to muscle force [147]. The shortest EMD (16 ms) was recorded by testing voluntary biceps activation of elbow flexion using an accelerometer for motion sensing [158]. However, in general clinical practice the difference in timing is inconsequential [158]. Thus, for this project, EMD is assumed to be zero.

Based on the EMG data of one individual (Fig. 5.2) that was collected during three elbow FE movements (Fig. 5.3), an example of the neural activation is shown in Fig. 5.17. However, despite promising results (Fig. 5.18) of pure mapping the net neural activation to the corresponding motion profile, a method that minimizes error was developed in the following section.

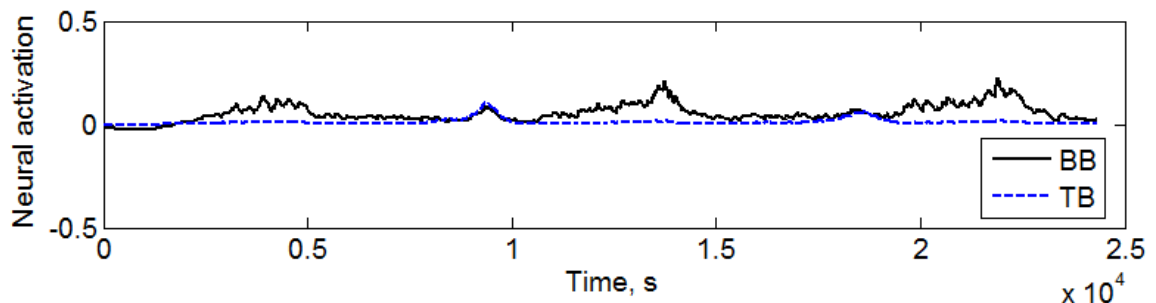


Fig. 5.17. Neural activation from BB and TB.

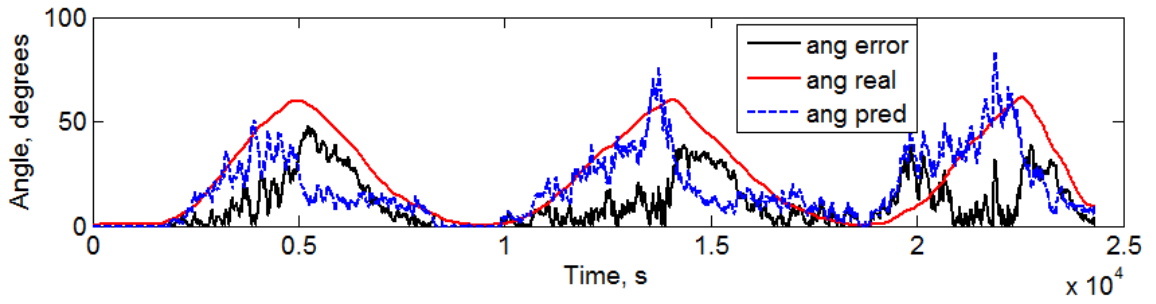


Fig. 5.18. Pure mapping of net neural activation (BB-TB) and motion data.
Mean error = 10.98° . RMSE= 15.97° .

5.3.4 Kalman Filter

Previously it was shown [79], [81], [83] that a model that uses a Kalman filter for error reduction could show 8.3–11.85% of error for an EMG-to-motion conversion. Therefore, a Kalman filter that directly maps neural activation to motion data was designed.

5.3.4.1 Kalman Filter Design

A Kalman filter (KF) [159] consists of two phases – signal estimation and correction, see Fig. 5.19. Each iteration goes through two steps: 1) the KF takes the motion X_{k-1} computed earlier and updates X'_k according to the information from a motion sensor U_{k-2} , 2) it then estimates the one-step-ahead signal X_k of the motion profile at the correction phase according to the noise Q_{KF} and R_{KF} .

The calculated muscle activity from the BB and TB muscles was added together to create the first input signal (X_k) to the KF. Motion data from the accelerometer were used as the second input signal (U_k). Estimation of motion X'_k relies on a previously corrected value of X_k and on the history of the signal U_k from the motion sensor. Two variables, P_k and G_k , are used in the process of correction. Both of them are functions of the noise. The process noise Q_{KF} and the measurement noise R_{KF} were defined for each individual during manual calibration of the KF. The goal of the calibration was to achieve an $RMSE \leq 2.0 \pm 0.1\%$ for a full FE movement that required the forearm to move from 0° to 130° . The output signal U'_k () from the KF is the estimated angular position profile (output frequency $f=1000$ Hz).

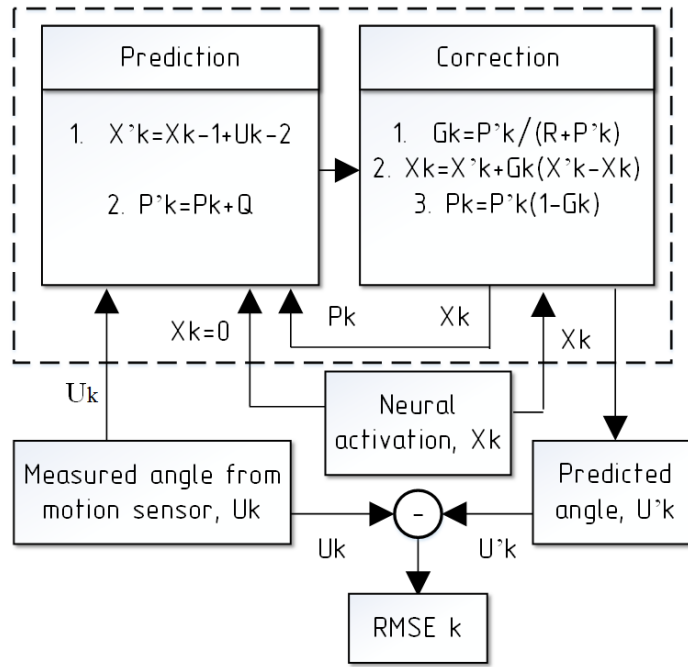


Fig. 5.19. Flowchart of data in Kalman filter,
where X_k is the sum of the neural activity from the BB and TB muscles, Q is the process noise, R is the measurement noise, P_k and G_k are function of the noise, U_k is the data from the motion sensor, \hat{U}_k is the estimated motion profile (equal to the X_k value at the correction phase), RMSE $_k$ is the error between the real motion profile and the estimated signal from the KF at each iteration.

5.3.4.2 Kalman Filter Application

Previous attempts at estimating motion using Kalman filters could not achieve errors lower than 8.3% [79], [81], [83]. Thus, such methods cannot be used in the BPI motion restoration trainings due to high possibility of overstretching weak muscles and reconstructed nerves. Alternatively, a method proposed in Section 5.3.3 combined with a customized Kalman filter from Section 5.3.4.1, may be a possible way to achieve high accuracy of EMG-to-motion conversion. Hence, below is described an example of the proposed speed estimation method, the goal of which is to achieve an error of position estimation of no more than 5° for each flexion–extension movement across all subjects and across different elbow ROMs, i.e., achieve at least 95% accuracy for the proposed EMG-to-motion estimation method.

The DSP starts from data filtering, as outlined in Section 5.3.1. The filtered EMG signal should be rectified (taking the absolute value of the EMG signal), see Fig. 5.20.

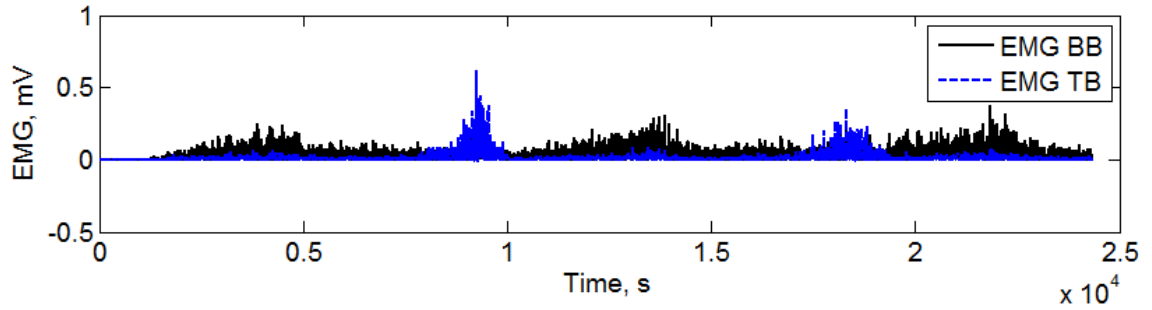


Fig. 5.20. Filtered and rectified EMG signal.

Then, the EMG signal should be individually normalized for each subject according to the prerecorded maximum and minimum EMG value from the BB and TB muscles, Fig. 5.21.

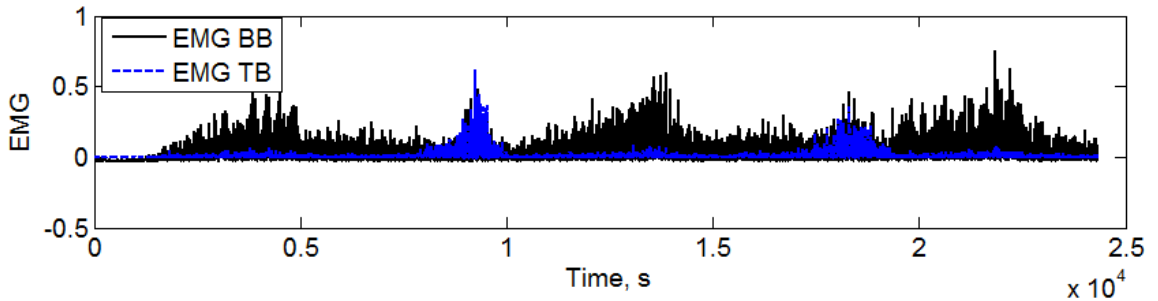


Fig. 5.21. Normalized EMG signal from BB and TB.
(max EMG from BB=0.5 mV, min EMG from BB=0.013 mV,
max EMG from TB=1 mV, min EMG from TB=0.00213 mV).

The normalized EMG signal $e(t)$ was used to calculate the neural activation [148], $u(t)$, as follows: $u(t) = \alpha_{\text{EMG}} \cdot e(t) - \beta_1 \cdot u(t-1) - \beta_2 \cdot u(t-2)$, where α_{EMG} , β_1_{EMG} and β_2_{EMG} are coefficients (the coefficients used were calculated following the method outlined in [148], as: $\alpha_{\text{EMG}}=0.0021$, $\beta_1_{\text{EMG}}=-1.78$ and $\beta_2_{\text{EMG}}=0.7821$). A preliminary result of mapping the neural activation to the motion profile shows a mean error of 0.65° and RMSE=0.8°, see Fig. 5.22.

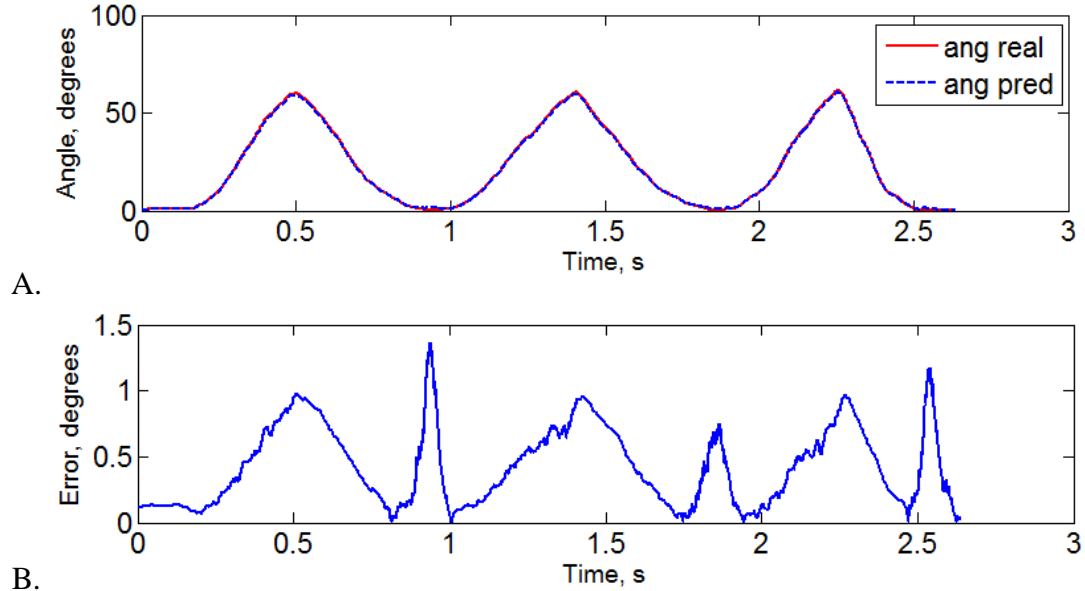


Fig. 5.22. Kalman Filter mapping of neural activation and motion data. Mean error = 0.32° . RMSE= 0.44° . Kalman filter gains: R=750, Q=0.1.

A. Real motion data vs. predicted motion. B. Error distribution.

Therefore, the proposed DSP technique has to be analyzed on a database of signals from healthy individuals in order to evaluate how accurate the method estimates forearm motion profile.

5.4 Conclusions

This chapter showed how a simple DSP technique can be used in motion trajectory and speed estimation. As outlined in Section 2.3.3, surface EMG recordings provide a safe noninvasive method of muscle activity quantification. Once the EMG data is converted into a digital form, digital filtering and mathematic processing allows mapping the resulting signal to a motion profile for trajectory/speed estimation. Hence, two methods for educational and assistive modes for BPI rehabilitation were proposed:

1. **Educational training.** RMS peaks of the EMG signal from the affected muscles can be used as an estimator of a moment when a forearm changes the direction of motion.
2. **Assistive training.** The difference of neural activation from the biceps and triceps can be mapped directly to the history of motion with the help of a customized Kalman filter. This allows estimating the speed profile of the forearm one step ahead.

The next chapter describes the prototype assessment under different rehabilitation scenarios that involved the mechatronic system, as well as the developed software and hardware of the control system.

CHAPTER 6

6 PROTOTYPE PERFORMANCE ASSESSMENT

The previous chapters have dealt with the design, development and construction of the wearable mechatronic elbow brace. For BPI rehabilitation, two modes of the system were proposed and described in Chapter 5. The following chapter focuses on evaluating the performance of the elbow brace under the two rehabilitation scenarios (educational mode and assistive mode), based on data collected from healthy volunteers.

6.1. Rehabilitation Modes Assessment

As mentioned in Chapter 5, motion practice and training repetition with appropriate feedback is necessary for successful sensorimotor reeducation. Thus, in order to provide BPI patients with an appropriate amount of training sessions, the control system of the developed elbow brace can be switched to the educational mode to be used at the stage when the patient's brain does not recognize signals from the new nerves, and to the assistive mode used at the stage when patients start to involve the affected arm in everyday activities. Therefore, an assessment of the brace performance under two rehabilitation scenarios was performed. The proposed methods presented in Section 5.3.2 and Section 5.3.3 of forearm direction/position estimation that corresponds to the educational/assistive mode were implemented in MATLAB and duplicated in C++ Visual Studio project, which communicates with the actuation system of the brace. In order to evaluate how the elbow brace responds to a control command during a simulated rehabilitation scenario, the proposed modes were evaluated for an ideal case (simulated in MATLAB) and then compared with the real world brace response to a control command, which involves the

same methods of the arm position/direction estimation (EPOS-based application). EMG and motion data that correspond to elbow flexion–extension movements were collected from healthy volunteers. The following section summarizes the methods of data collection and processing and the description of the setup used.

6.1.1. Data Collection

Thirty-five healthy volunteers that did not have any neural or musculoskeletal disorders associated with elbow, shoulder or neck were recruited for the trial. The study was reviewed and approved by the Western University Health Science Research Ethics Board. The study was conducted in the Wearable Biomechatronics Laboratory after each participant signed the Consent Form.

Prior the experiment, the following information was collected from each participant: age, dominant hand, gender, weight and height. According to geometrical and mass–inertial characteristics of the upper human limb in [82], the forearm and hand weight were calculated. The population of study included 35 participants with a mean age 25 ± 5 years old. 32 were right handed and 3 left handed. There were a total of 20 males and 15 females. The mean height of the participants was 174 ± 11 cm, their mean weight was 74.91 ± 17 kg, their mean forearm weight was 1.27 ± 0.25 kg, and their mean hand weight was 0.35 ± 0.08 kg.

Each participant was seated comfortably on a chair and asked to put his/her arm in an adjustable mechanical brace (Innovator X[®]) (see Fig. 2.3). The participant's arm was then secured to the linkage of the brace using straps. The brace restricts the movement of the limb to the sagittal plane when the upper limb is in the neutral position (upper arm against torso).

Two pairs of surface EMG electrodes were placed on the skin overlying the BB and TB muscles. A reference electrode was placed on the bony area (at the proximal head of ulna). The skin was prepared only in those areas where the EMG electrodes were placed. According to the SENIAM's (Surface EMG for a Non–Invasive Assessment of Muscles, 1999) recommendations for skin preparation, the skin was cleaned with alcohol pads. As the alcohol vaporized, EMG electrodes were placed parallel to the muscle fibers (2 cm apart), over the muscle belly, two thirds of the distance between the shoulder and the elbow, see Fig. 6.1. An accelerometer was placed on the inside of the forearm to track actual

motion profiles, 17 cm distal to the elbow joint (Fig. 1, distance between point A and point B).

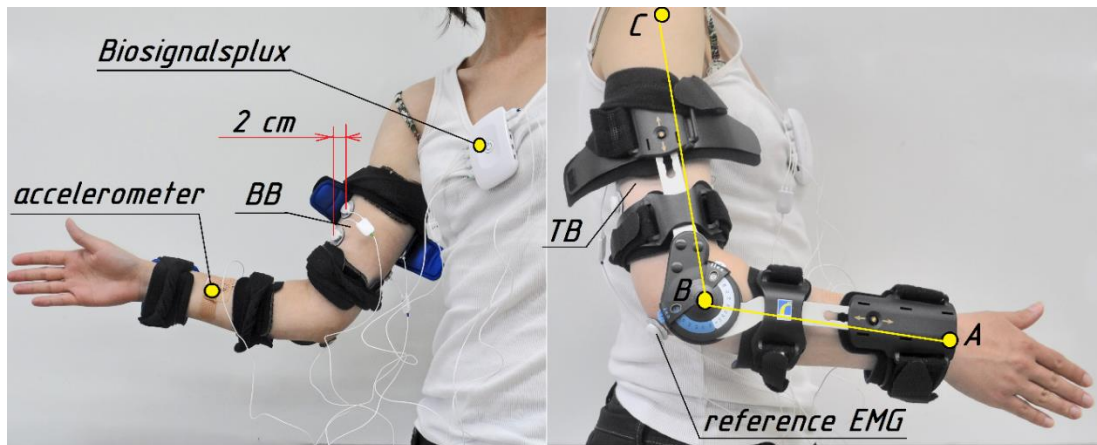


Fig. 6.1. Example of placement of the EMG sensing system and the mechanical brace.

Filtered data from the motion sensor were later compared with the estimated signal from the model. The root mean square error (RMSE) and the Pearson correlation coefficient (CC) between the estimated and the measured forearm motion profiles were used to estimate the accuracy and correlation between the model results and the observations. The correlation coefficients range from -1 to 1 where values close to 1 or -1 represent a high correlation.

Muscle activity and forearm acceleration data were tracked at a sampling rate of 1000 Hz with the help of a Wearable Body-Sensing Platform “Biosignalsplex” (Plux®). The sensed data were stored in a temporary file with the help of the “OpenSignals” software (Plux®).

Each subject performed six sets of FE movements. For each set of movements, a unique ROM was selected: 1) 0° – 45° , 2) 0° – 60° , 3) 0° – 90° , 4) 0° – 120° , 5) 45° – 105° and 6) 90° – 120° . Subjects were instructed to complete three elbow FE repetitions for each ROM. In order to eliminate the effects of muscle fatigue, subjects rested 2–5 minutes between each set. Stored data from the EMG electrodes and accelerometer were used as inputs to the MATLAB-based scripts that simulate the educational mode and assistive mode, and later as inputs to the EPOS-based control system for each mode at a time.

6.1.2. Setup Installation

The equipment used to assess brace performance in real time is shown in Fig. 6.2. The personal computer (HP ProBook 6560b with an Intel Core i5-2520M CPU at 2.50 GHz Processor, 8 GB RAM, and running Windows 7 Pro) was used for data acquisition and display. The control system of the device uses customized software developed in C++, two EPOS 24/5 Motion Controllers (Maxon Motors) and a sensing system (BioSignalPlus platform). The elbow brace was loaded with forearm (described in Section 4.2) that simulates naturally the distributed weight of a lower arm. An average weight of the lower arm across all participants equal to 1.65 kg was used for all tests.

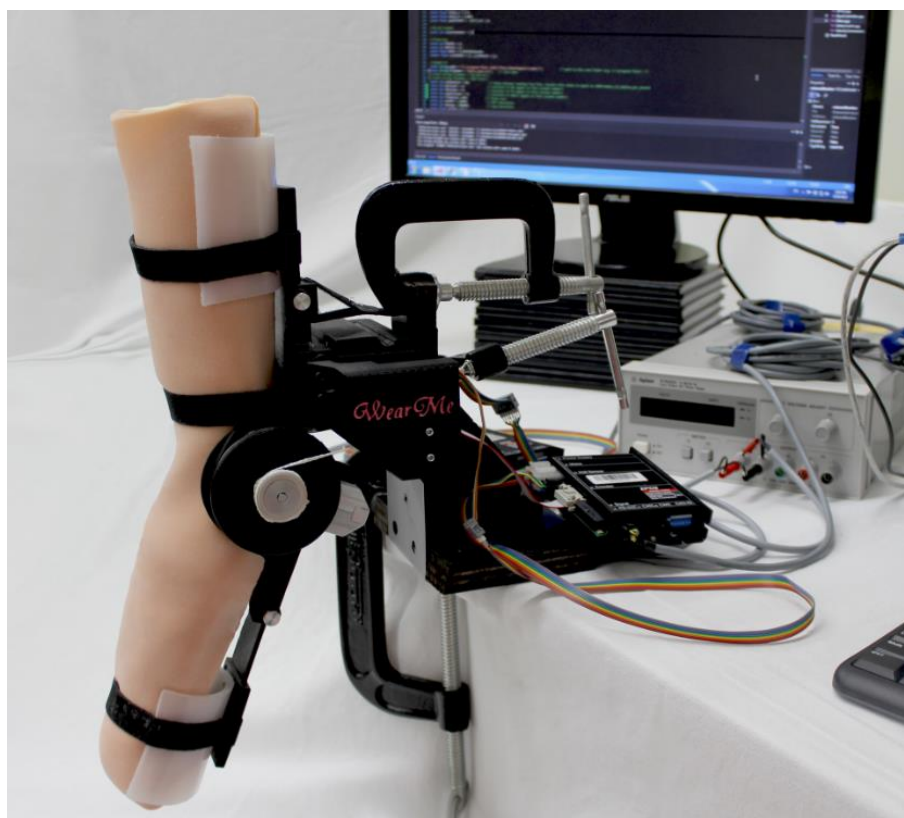


Fig. 6.2. Experimental setup.

Each component of the system is described below:

Sensing system The accelerometer and two pairs of EMG sensors of the BioSignalPlus system were used for data collection. Sensed data were stored in a temporary file, and then read by the C++ Visual Studio project or by the MATLAB script.

Software A MATLAB script was developed for both methods of simulation and assessment. Customized software was developed in C++ to duplicate the MATLAB script. The C++ Visual Studio project uses EPOS-driver

communication functions developed by a graduate research student. The detailed algorithms are presented in the following sections.

Speed Command The EPOS 24/5 motion controllers receive velocity commands from the Visual Studio project via RS232 and actuate the appropriate Maxon Planetary Gearhead (Part No. 143995, Maxon Motors) through the coupled Maxon EC-max 22 (Part No. 283840, Maxon Motors). Once the velocity command is issued to the EPOS 24/5, internal PID controllers track the desired motor velocity via the encoder. The final velocity of brace can be calculated as

$$n_{\text{brace}} = \frac{n_{\text{motor}}}{333 \cdot 3.14} \text{ °/s},$$

where 333 is the speed reduction ratio of Maxon Planetary Gearhead and 3.14 is the speed reduction ratio of the torque amplifier.

PID Controller The gains were derived by minimizing the absolute error between the set value (“target” black line) and the system response (“response” green line) for the speed mode of the EPOS controller, while the target response values of the system were tuned to a velocity step response of 2000 rpm with the following goals: maximum settling time of 25 ms and maximum presiding (i.e., dead) time of 5 ms. The computation of the PID parameters was done with the help of the Maxon software, which only allows the velocity step value, dead time and settling time to be varied. Based on the results of the tuning process, the gains of the controller were assigned as follows: P=402, I=56, D=0.

As mentioned earlier, the experimental setup was tested in two modes: the educational mode, which is described in Section 6.2 and the assistive mode, which is described in Section 6.3.

6.2. Educational Mode

To simulate the educational mode and test it on collected data, a MATLAB script and a Visual Studio project were developed to read and process the data according to the method outlined in Section 5.3. An example of the signal flow for the EPOS-based educational mode is shown in Fig. 6.4. Data acquisition, computational process and decision-making are done within one frame equal to 250 ms as recommended in [78]. After the 250 EMG data samples are read from the storage file, the RMS of the data is calculated for the window. Three conditions are checked within a frame. First, if the RMS EMG value is below a threshold (equal to the RMS of the EMG during a rest period), the U' value is the

same as for the previous frame (i.e. $U'_{k-1} = U'_{k-1}$). Otherwise, a second condition is checked. If the RMS EMG of the current frame is greater than the RMS EMG of previous frame (in order to calculate the slope of the U' signal), then a constant value, Δ , is added to the U' value. If the second condition is not satisfied, a constant value, Δ , is subtracted from the U' value. After the U' slope is updated, the system makes the decision of whether or not to change the direction of the motion based on the results from the last condition. If the U' value crosses the zero line (i.e., changes the sign from positive to negative or vice versa), the sign of the speed command sent to the motion controller is changed (i.e., the brace changes the direction of motion).

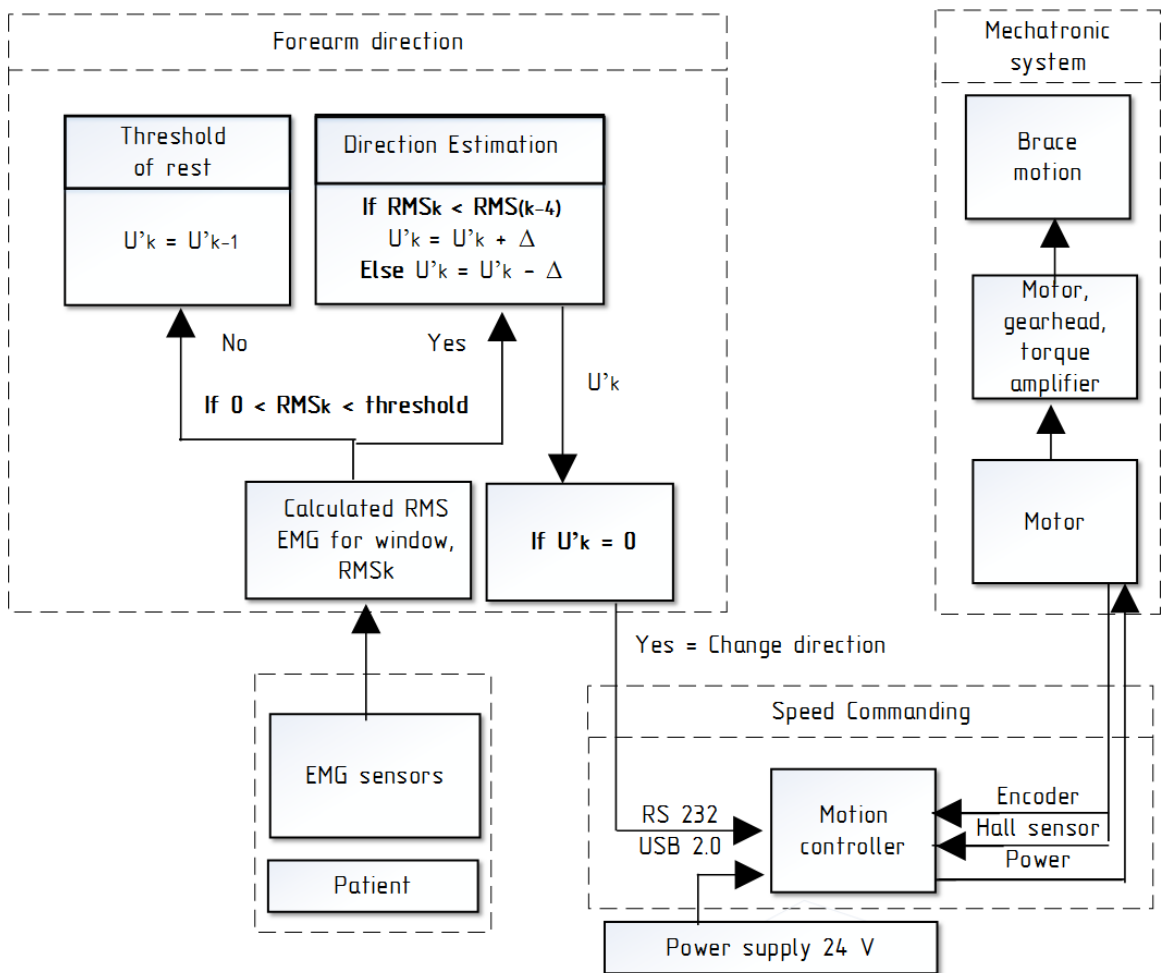


Fig. 6.4. Schematic representation of the signal flow for educational mode.

The results were analyzed based on the following criteria: if the estimated U' value crosses the zero line no later than time $time = t + window\ size$, where t is the moment when the real speed profile crosses the zero line, and $window\ size$ is a pre-set value of 250 ms, then the elbow brace direction needed to be changed and the system properly identified the change (True), otherwise, the system did not properly identify the change (False). The

overall mode performance was calculated as a percentage ratio of correctly estimated directions (True) to incorrect estimations (False).

6.2.1. Results

The mode was able to identify 86% of the forearm direction changes for the MATLAB-based application and 84% of the forearm direction changes for the EPOS-based application. The errors in detecting the direction of motion were a combination of the false negative and the false positive estimations of the forearm direction changes. An example of mode analysis is shown in Fig. 6.5. The first step (Fig. 6.5A) represents the results of EMG reading, filtering and calculation of the RMS of the EMG signals corresponding to the biceps and the triceps. The defined triceps RMS EMG is subtracted from the biceps RMS EMG in order to estimate the net RMS EMG signal (see Fig. 6.5B). Based on the net RMS EMG value, the method shown in Fig. 6.4 calculates the U' value for each frame (see Fig. 6.5C). Finally, the specific times at which the real speed and the estimated U' signal cross the zero line were compared, as shown in Table 5.1.

It was observed that the MATLAB-based educational mode estimates the change in trajectory 0.25–1.75 s before the actual motion performs the same change, while the EPOS-based mode predicts 0.25–0.75 s ahead. Such prediction ability, explained by the fact that the EMG signal peaks prior to the intended action [78], shows an advantage of this method. This prediction ability can be used to compensate for the delay that a mechatronic system may have due to a complex combination of hardware and software.

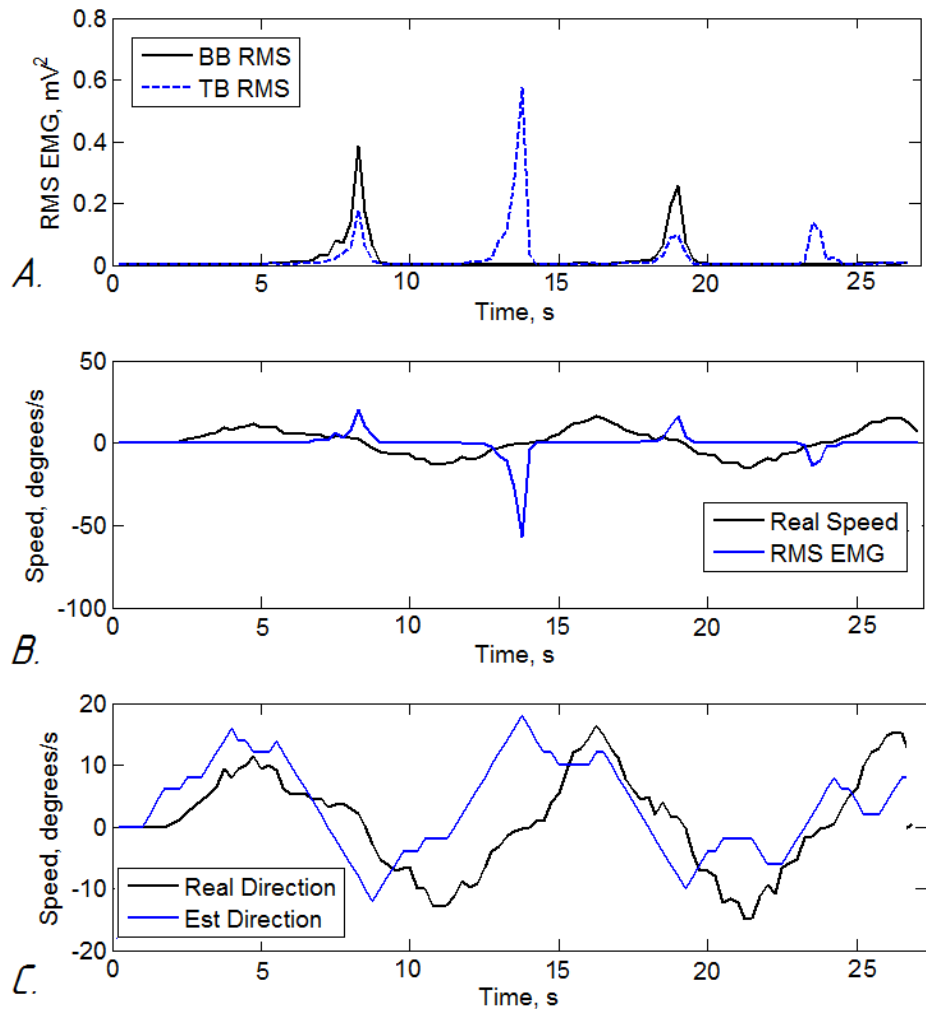


Fig. 6.5. Sample of data (ROM 0–90°) for the MATLAB-based forearm trajectory estimation. A) RMS EMG from BB (black) and TB (blue) muscles, B) Resulting RMS EMG (RMS EMG BB – RMS EMG TB) compared with the corresponding speed, C) Measured speed profile (black) compared with the estimated speed based on RMS EMG (blue).

Table 5.1. Sample performance of the education mode.

Moment when real speed crosses the zero line (s)	Moment when estimated U' signal crosses the zero line (s)	Detected change in direction, True/False
8.5	7.25	True
13.75	11.5	True
19.25	18	True
23.75	23.25	True

6.2.2. Additional interpretation of the results

The results of this experiment have shown that the proposed educational method can replicate BPI rehabilitation sessions with 84% accuracy for EPOS-based tests, see Fig. 6.6. Although, the therapist may perform the training with 92% accuracy [149] (see Fig. 6.6 *Reference case*), this experiment is limited to pre-recorded data. Contrary to the performed tests, real training sessions are based on the EMG signal from a patient that has direct visual feedback of the forearm position and, therefore, can self-correct the muscle contraction in order to amplify the EMG signal for better performance. Reichenbach, *et al.* [150] showed that the error of the hand positioning was reduced by about 10% when a constant visual feedback of the hand was provided. Thus, the results of the educational mode can be improved by testing on subjects that have constant visual feedback of the brace position (e.g., the system may achieve 92.4% of accuracy by applying the 10% increase rule to the current results, see Fig. 6.6 *Result with feedback case*).

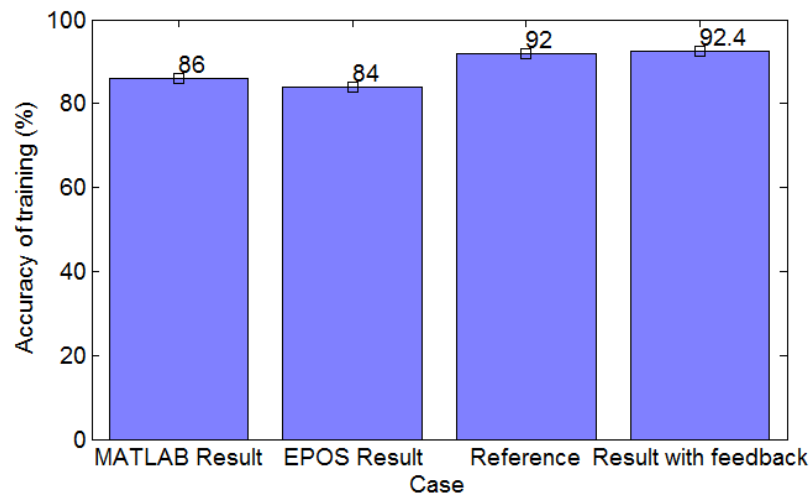


Fig. 6.6. Accuracy of training educational sessions for different cases.
MATLAB Result case is the measured accuracy of the educational mode simulated in MATLAB. **EPOS Result** case is the measured accuracy of the educational mode during elbow brace tests with the EPOS-based control system. **Reference** case is the reported accuracy of quantifying joint angle for physiotherapists. **Result with feedback** case shows a possible accuracy of training session when a patient has constant visual feedback.

6.3. Assistive Mode with PID Control

The proposed assistive mode was implemented and computed using MATLAB and later duplicated in Visual Studio, see Fig. 6.7. As described in Section 5.3.4, the proposed

method relies on the neural activation of the muscle X_k (calculated from the EMG signal) that is 1 frame behind, as well as on the angular position U_k (measured from the accelerometer) that is 2 frames behind the actual moment of estimation U'_k . The process of obtaining speed values in the Kalman filter is outlined in Section 5.3.4. The angular position based on the estimated speed was compared with the real angular data from the participant. The accuracy of position prediction and correlation coefficient across all data were calculated for both applications, as outlined in following sections.

In addition to the collected data (Section 6.1.1), each volunteer was asked to perform a maximal BB contraction. The EMG signal from the BB and the TB were recorded for 3 s of rest and 3 s of maximum contraction. The average EMG values during one full rest and one full contraction phase were used to identify the minimum and maximum values of the EMG signals for normalization purposes. The normalized EMG data (represented as a percentage) shows the strength of the signal from the muscles with respect to the maximum value for each subject. Hence, calculations of neural activations are unitless.

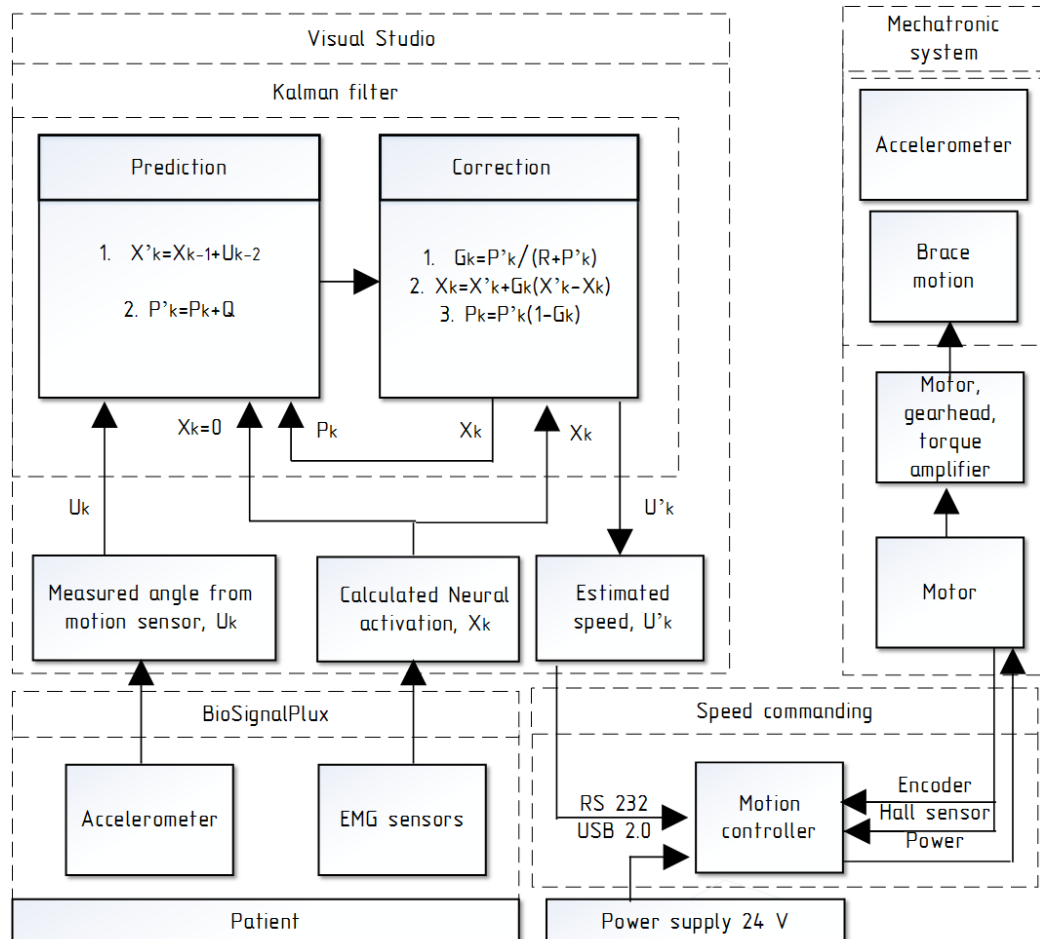


Fig. 6.7. Schematic representation of the signal flow for assistive mode.

6.3.1. Results

The error between the estimated motion in the MATLAB-based application and the real motion (1.4–2.6%), as well as the error between the estimated motion in the Visual Studio project (i.e., the command signal) and the real motion (1.74–3.51%) were within the required tolerance (0–4%), while the error between the brace positioning (as a response to a command speed) compared to the real motion was out of the acceptable range (4.78–8.29%). The assistive mode replicates the subjects' motion trajectory with high correlation ($CC=0.97\text{--}1.00$) for both applications. An example of a recorded EMG signal from the BB and TB muscles and their corresponding calculated neural activation calculated with the MATLAB script is presented in Fig. 6.8.A and Fig. 6.8.B, respectively. After the neural activity passes the Kalman filter, the forearm motion trajectory is estimated with an RMSE=1.67% (see Fig. 6.8.C) for the sample of data shown in Fig. 6.8.A. Despite the low error between the estimated motion (used as a command speed to the system) and the real motion, the error accumulates from the point at which the command speed is sent through the controller to the point at which the elbow brace responds to the command signal. As shown in Fig. 6.9, the final response of the system has an RMSE=6.58% (command speed vs. real speed) due to a quick change in speed direction. The same trend in error accumulating was found across all tests: from the stage when the command signal is estimated with an RMSE=1.74–3.51% to the stage when the elbow brace responds to the command signal with an RMSE=4.78–8.29%.

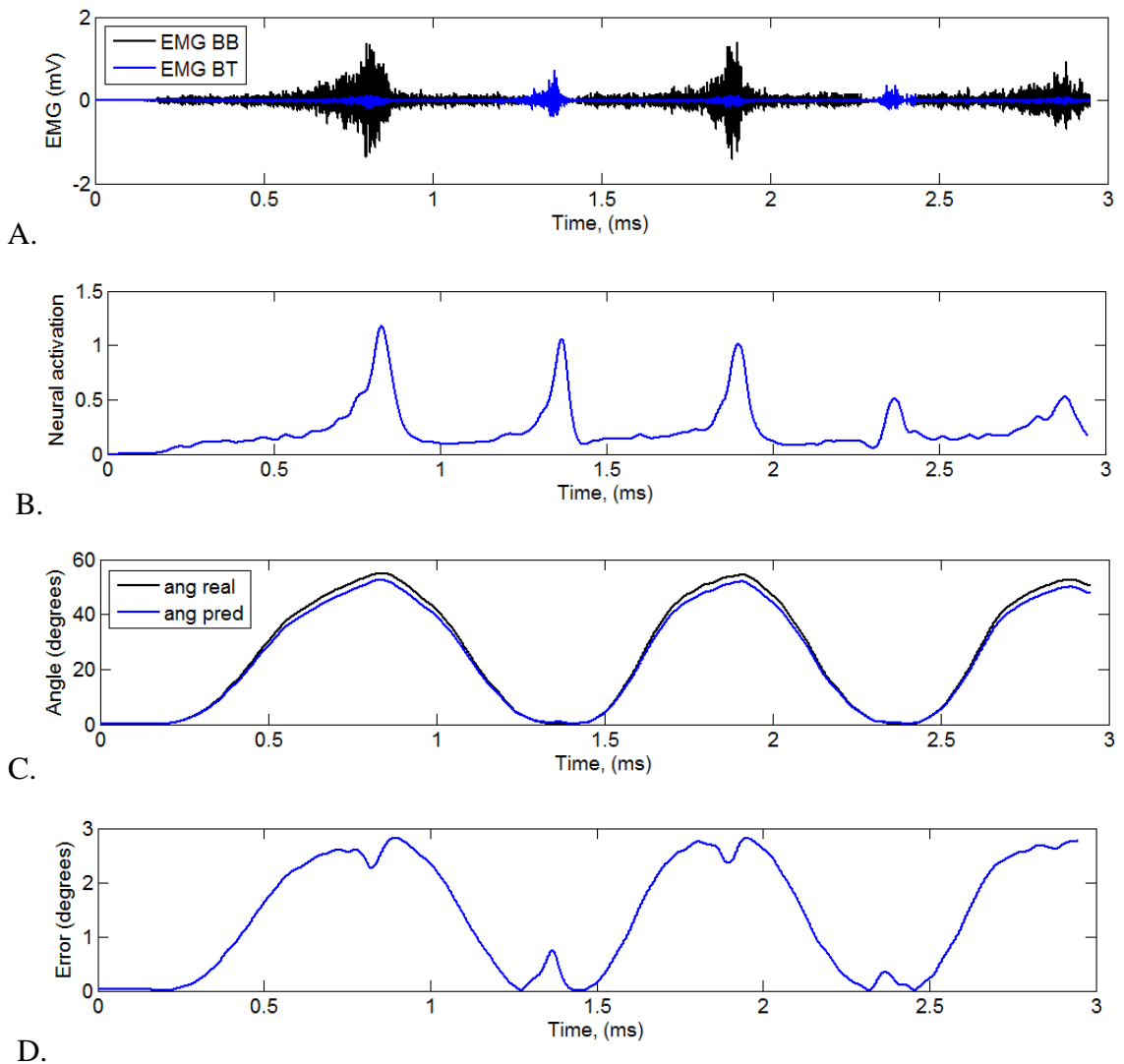


Fig. 6.8. Sample of data (ROM 0–60°) for the MATLAB-based application.
A) EMG signal from BB (black) and TB (blue) muscles, **B)** Resulting neural activation (sum of BB and TB neural activation), **C)** Measured motion profile (black solid line) compared with estimated motion from model (blue line). RMSE=1.67 %, CC=1, **D)** Error distribution (maximum error is 2.82°).

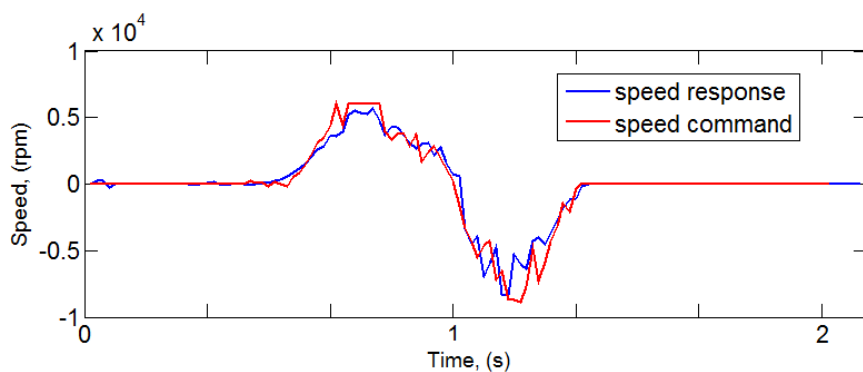


Fig. 6.9. Brace response to an estimated speed profile for a sample of data.

6.3.2. Discussion

The results for the EPOS-based mode assessment have shown that the system cannot reach the desired position by following a velocity profile. The same result was found by Karlsson [151], where he concluded that velocity control does not guarantee that the system will reach the set position under all conditions. Alternatively, the system performance can be improved by adding additional loops of control, such as: (1) switching speed/position control [153], (2) incremental position control [154] and (3) cascade control, which controls the velocity and the position simultaneously [151]. The downside of approach (1) is that the settling time of the system for each unit of command will be increased, while approach (2) does not control the velocity directly. To decrease the error between the desired and the actual brace dynamics, approach (3) was implemented in the assistive mode, as described in next section.

6.4. Assistive Mode with Cascade Control

In addition to the initial inner PID loop that controls the velocity (as shown in Fig. 6.7), an outer loop that estimates the position error (multiplied by a gain) for each frame was added, see Fig. 6.10, in order to improve the ability of the elbow brace to follow the desired trajectory. The PID loop makes sure that the desired motion profile is followed, while the outer position loop compensates for any mismatch of position that occurs. Thus, the cascade control [151] of the assistive mode treats the transmission of the system as a black box that has a nonlinear relation between the input speed and the output speed of the transmission.

The combination of the two feedback loops for the assistive mode of the brace position was implemented in C++ Visual Studio. Data from a motion sensor for the outer loop of the cascade control were acquired and stored with the help of the BioSignalPlux. The improved EPOS-based assistive mode was tested on the subject data collected as described in Section 6.1.1.

6.4.1. Results

The error between the brace positioning and the real motion (2.04–4.32%) was found to be within the required tolerance (0–4%) across all tests. Samples of data that show comparisons between the brace response to a command for the assistive mode with the PID

control and with the cascade control are shown in Fig. 6.11 and Fig. 6.12. For the PID control (Fig. 6.11A), the system follows the command speed with an RMSE=5.58% (brace speed vs. real speed). Finally, the brace positioning compared to the real positioning of a forearm (Fig. 6.11B) results in an RMSE of 6.11%. Although the command speed is estimated accurately, the system cannot follow the desired trajectory of the forearm motion with high precision (as described in [151]).

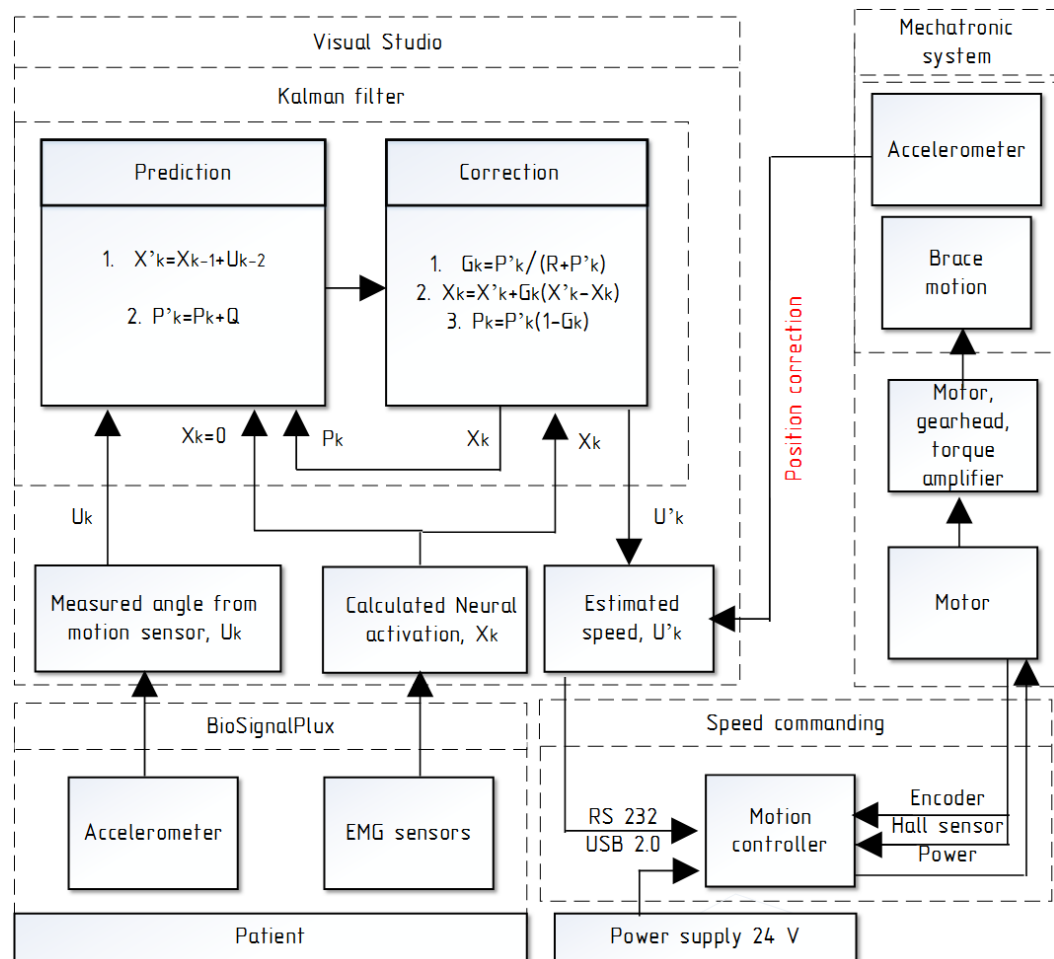


Fig. 6.10. Schematic representation of the improved signal flow for assistive mode.

For the cascade control, the command speed is constantly corrected by the outer control loop within the same frame where it was estimated and, thus, the brace speed is not expected to match the real speed profile (RMSE of 10.56% for the brace speed vs. the real speed), see Fig. 6.12A. By correcting the command signal, the resulting positioning of the brace follows the desired motion trajectory with an RMSE of 1.38%, see Fig. 6.12B. Results

show that by using cascade control, the error of the brace positioning can be decreased from 4.78–8.29% (the results of the brace response with PID control to a command signal) to 2.04–4.32% (the results of the brace response with cascade control to a command signal) without any hardware modifications, see Fig. 6.13.

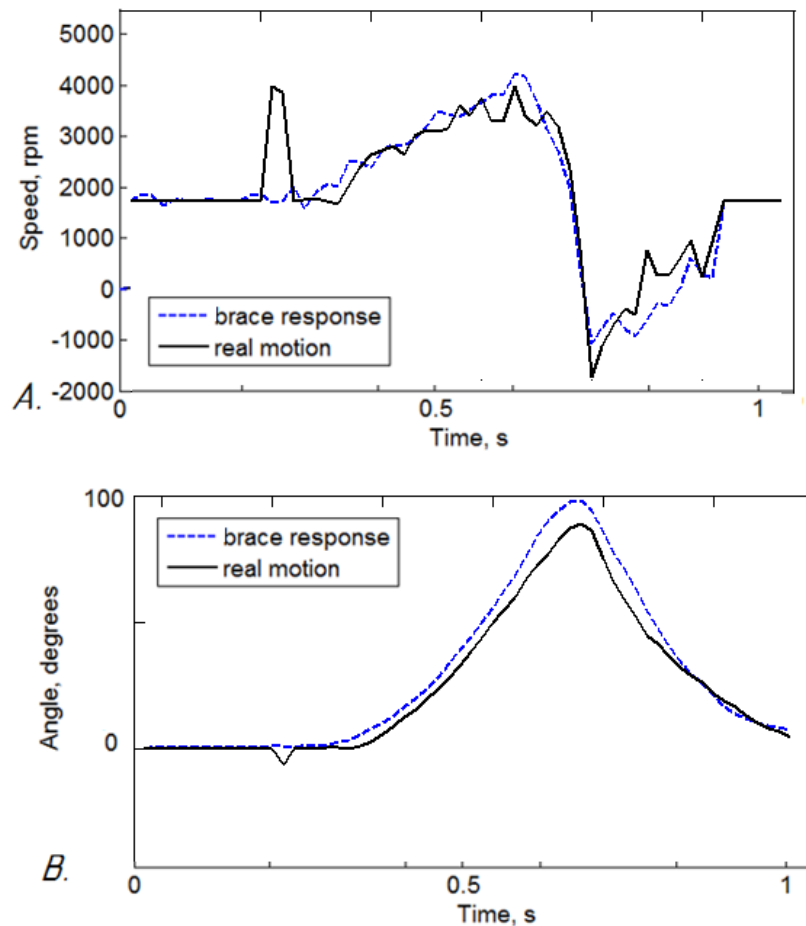


Fig. 6.11. Sample brace response to an estimated speed profile while the PID control was used. A. Speed comparison for the assistive mode (RMSE = 5.58%) between the real forearm motion and the brace response to the estimated motion. B. Position comparison for the assistive mode (RMSE = 6.11%) between the real forearm motion and the brace response to the estimated motion.

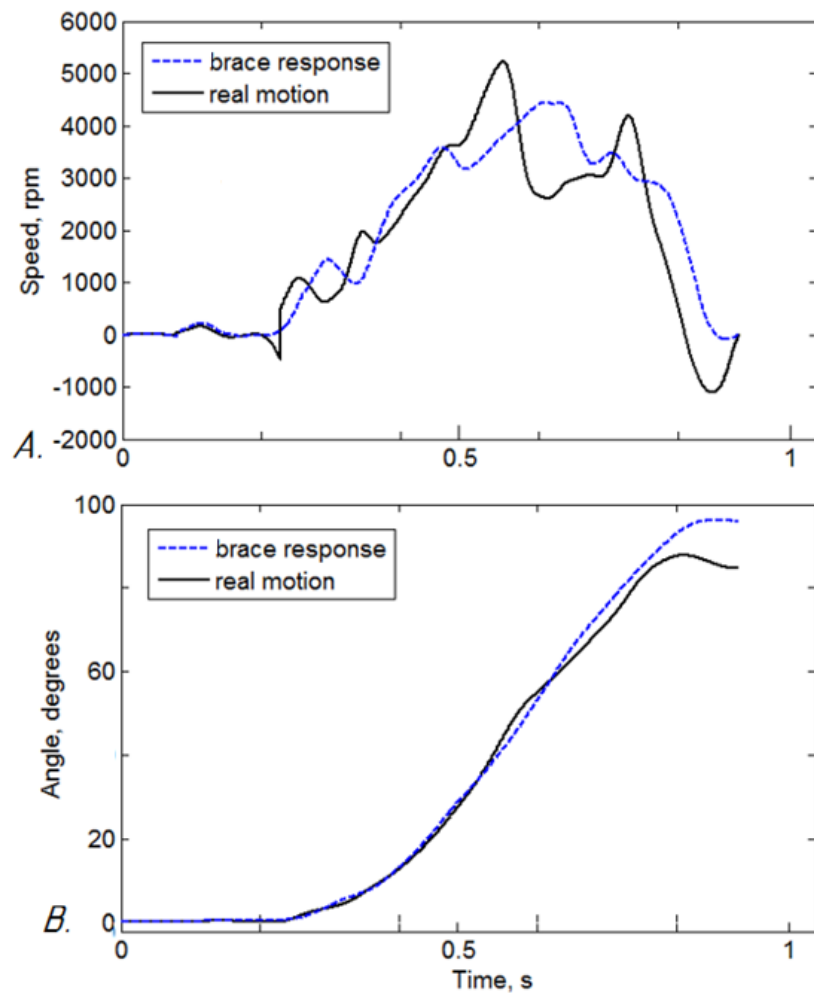


Fig. 6.12. Sample brace response to an estimated speed profile while the cascade control was used. A. Speed comparison for the assistive mode (RMSE = 10.56%) between the real forearm motion and the brace response to the estimated motion. B. Position comparison for the assistive mode (RMSE = 1.38%) between the real forearm motion and the brace response to the estimated motion.

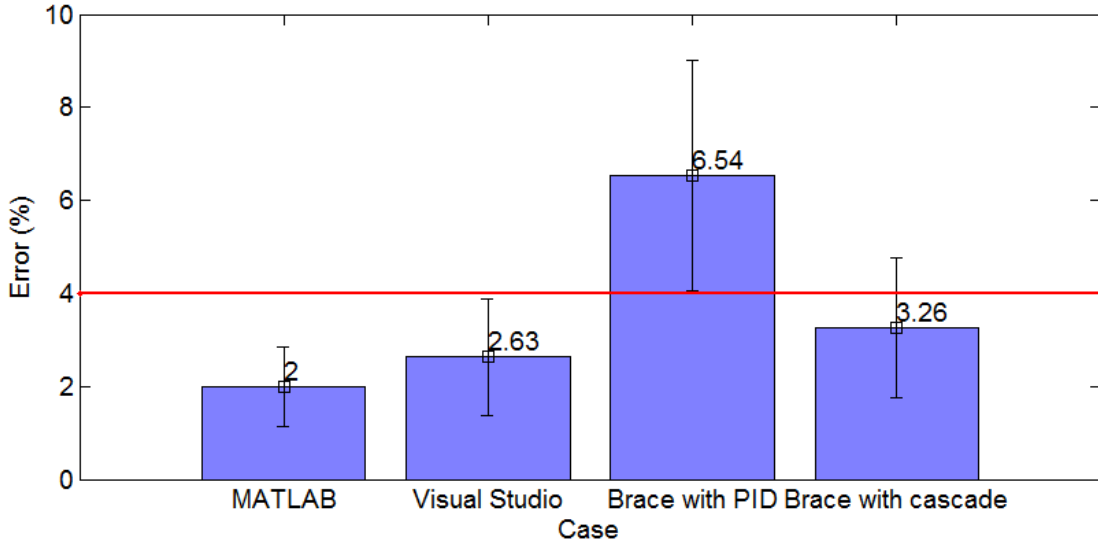


Fig. 6.13. Error accumulation at different stages of the assistive mode. MATLAB case is the calculated error in the MATALB script that simulates the estimation of the command speed. Visual Studio case is the calculated command speed in the control system of the elbow brace. Brace with PID refers to results of assistive mode assessment measured while the velocity of the actuators was controlled with the PID controller. Brace with cascade case shows the measured error of the brace positioning while the cascade control was used. The Red line represents the maximum acceptable error.

6.4.2. Discussion

Thus, the results of the experiments have validated that using EMG data from the biceps and triceps muscles provides better prediction accuracy than using only the biceps muscle data as in [81], and that a KF is a powerful tool for correcting the EMG-to-motion mapping technique (compared to the pure mapping strategy presented in [91]).

The accuracy requirements for the forearm positioning based on the literature review were set to be between 96.0 and 98.0%. However, during the training sessions with health care professionals, the joint position angle was quantified with 92% accuracy for angles greater than 100° and with 67% accuracy for angles less than 75° [149]. Thus, the achieved accuracy (97.4–98.6% for the MATLAB simulation and 95.68–97.96% for the real world EPOS-based tests across all subjects) of the proposed assistive mode was shown to be more accurate than manual limb positioning by the health care professionals [149] and than the previous efforts defined in the literature. The lower accuracy gathered for the elbow brace tests (4.32%) exceeds the upper bound by 0.32%. Nevertheless, the overall accuracy of the assistive mode provides a position error that lies within the acceptable range.

The variability of EMG signals caused by a vast amount of conditions and non-voluntary shoulder motions created a different error distribution for all subjects. Although no control was implemented for some subject-related parameters (posture, mental state and temperature), the model was able to make predictions with the desired accuracy.

6.5. Sources of Error and Limitations

The principal frequency of the EMG signal is concentrated in the 30–500 Hz range [134]. On the other hand, the main energy of the EMG signal is concentrated in the range of 0–500 Hz [171]. Thus, filtering of the EMG signal may cut down useful information that corresponds to the smallest force produced by the muscle and, therefore, decrease the accuracy of motion trajectory/speed estimation for small joint angles.

Using optimization techniques, a smaller accuracy error may have been attained when compared to using a manual model parameter calibration. However, optimization techniques are computationally expensive. In addition, optimized parameters can take longer to compute than the entire time devoted to the trials of one subject depending on which optimization technique is used. Lastly, EMG signals fluctuate naturally due to fatigue, temperature, environment and other factors. Therefore, the optimization would need to occur for every usage of the device that incorporates the proposed modes. The time constraints these factors place on parameter optimization are the reasons why manual calibration was chosen for the experiments.

6.6. Conclusions

A control system for the wearable mechatronic elbow brace was designed and tested. The control strategy consists of (1) the educational mode that moves the brace at a pre-set speed in the desired direction and (2) the assistive mode that estimates the desired speed of the forearm and moves the brace with respect to the desired position. Both modes were tested on the data collected from 35 healthy participants. The results of the brace movements were compared with the actual movements recorded from the participants.

The experiments have shown that the educational mode can achieve 86% of accuracy in trajectory estimation, while the brace control with a constant visual feedback may result in 95% accuracy (by considering the fact that the visual feedback increases limb positioning

accuracy by 10%). The assistive mode was tested with a PID controller and later with a cascade controller. The combined speed-position (cascade) control reduces the error between the desired motion and the brace movement by 3–4%. Therefore, the assistive mode with cascade control can achieve 2.04–4.32% error, which is within the required error tolerance (0–4%). The results of the tests demonstrate the potential to achieve robust device operation under different rehabilitation scenarios. Due to the limitations of the data, further assessment of the device with the help of data from the BPI patients is required to improve the control strategy.

CHAPTER 7

7 CONCLUSIONS AND FUTURE WORK

The work presented in this thesis was aimed at adapting robotic technology for home-based muscle training as part of the BPI postoperative rehabilitation process. A literature review was performed to identify whether the prior art in portable rehabilitation robotics for the upper limb could be applicable for maintaining muscle tropism after the nerves of the affected muscle are surgically repaired. It was found that there are currently no robotic prototypes or commercially available devices designed specifically for BPI patients that undergo a long-term postoperative process.

The wearable mechatronic elbow brace presented herein is an example of a device that can provide an automated 24/7 method of controlling muscle training outside of the clinical environment. A complex design of the device included the mechanical structure that maintains natural motions of an elbow and the control system that converts sensed EMG data to a profile of a desired movement. Based on the defined specifications, the prototype was built and tested in two modes, educational and assistive. Each mode was specifically designed to mimic the two types of training sessions with the therapist.

The experiments performed with the elbow brace have shown that EMG data can be successfully used for estimating the direction of the desired motion and moreover for estimating the speed profile of the intended movement. Although the assessment of the device was performed for the pre-recorded data from healthy participants, the device met the goals of the project.

7.1. Contributions

This work describes the design and control of a wearable elbow brace for BPI patients and outlines the application in which the device can be used during home-based muscle training. The specific contributions of this work are as follows:

1. A customized actuation system that can be adapted to each stage of the BPI rehabilitation process was developed. The drivers can be easily removed from the elbow brace by pulling a spring-loaded handle that decouples the transmission system from the output shafts of the gearheads, achieving the following goals:

- (a) To remove the transmission and actuation systems and use the device as a mechanical brace at the immobilization phase,
- (b) To use the decoupling handle as an emergency stopper,
- (c) To decrease the weight of the device in cases when the rehabilitation process requires active exercises only few times a day,
- (d) To replace/test the actuation system without reassembling the construction.

Other devices found in the literature practice stationary coupling of the actuation system to the device with limited or missing emergency decoupling.

2. A 2-DOF elbow motion model with active flexion–extension and passive carrying angle was used for the elbow brace design. In contrast to existing prototypes, the proposed device provides natural elbow motion and decreases alterations in joint anatomy and limitations of elbow motions.
3. The reliability of the device was increased by integrating mechanical stoppers into the system for limiting the ROM and by selecting critical components with rated life equal to the time of a full recovery. The results of the prototype assessment showed that the ability of this device to fix the forearm in a certain position is greater than that of commercially available static elbow braces.
4. Although, three types of torque transmission (chains, belts and cables) are commonly used in rehabilitation robotics, experiments have presented evidence towards the effectiveness of using cable driven transmissions for precise positioning of a forearm over other types.
5. Finally, a customized control system that consists of two modes was designed:
 - (1) The educational mode that moves the brace at a pre-set speed in the desired direction, and

-
- (2) The assistive mode that estimates the desired speed of the forearm and moves the brace with respect to the desired position.

The experiments have shown that the educational mode can achieve 86% of accuracy in trajectory estimation, while the brace control with a constant visual feedback may have up to 95% accuracy. The assistive mode was tested with PID control and later with cascade control. The combined speed–position (cascade) control allows an error reduction between the desired motion and the brace movement by 3–4%. Therefore, the assistive mode with cascade control achieved 2.04–4.32% error that is within the required error tolerance (0–4%). The results of the tests demonstrate the potential to achieve robust device operation under different rehabilitation scenarios.

7.2. Future Work

While the results of the work presented herein proved that the developed prototype of the wearable elbow brace can be used in a BPI rehabilitation program, further work is needed to improve the device appearance and functionality as presented below:

1. *Weight of the device.* Although the overweight of the prototype was compensated by the shoulder strap and detachable actuation system, further weight optimization of heavy components should be done. For example, the preferred mechanical design can be refined if use one motor with a spur gear splitter and one emergency decoupling button.
2. *Calibration process.* The current calibration process for the control modes was done manually, and, thus, requires further improvement. As the muscles become stronger, the system should be recalibrated properly daily or weekly. A possible improvement can result from the development of an automated method of control that determined whether the recalibration should take place. Additionally, the control system should be updated with a new automated method of calibration based on the calibration process that was performed manually.
3. *EMG data from BPI patients.* An in-depth study that analyzes how EMG signals from affected muscles in BPI patients differ from the EMG signal of healthy individuals, as well as how to quantify the progress of BPI rehabilitation should be done. Moreover, such research will increase the knowledge of EMG signals and how they can be used for rehabilitation goals.

4. *Clinician interface with the device.* A system that stores all movements through the entire day (24/7) and automatically uploads collected data to a database can become a powerful tool for clinicians, as a comprehensive analysis of progress may be done. For instance, an alert for the LNU phenomenon can be implemented in the analysis software. Moreover, by knowing exactly what training exercises were done and how the patient uses the affected arm during the day, the therapist can conclude what rehabilitation strategies work or which ones are more effective.
5. *User interface with the device.* A system that provides continuous visual/audio feedback and guidance to patients to improve quality of motion performance and adherence to instructions can increase the patient's motivation to perform all of the prescribed training exercises, as the healing process will be accelerated. Moreover, 24/7 access to a database that stores progress and therapist's comments is necessary to involve patients in the rehabilitation process. By having all of the changes tracked and summarized by a clinician, a patient can set personal goals for training exercises and constantly check whether he or she achieved the goal.
6. *Appearance.* Appropriate cover for the elbow brace has to be designed in order to meet aesthetical and cosmetic user requirements, e.g., Fig. 7.1. Moreover, the cover will isolate moving components and increase the user's safety by limiting access to the mechanical structure and the electrical components of the device.

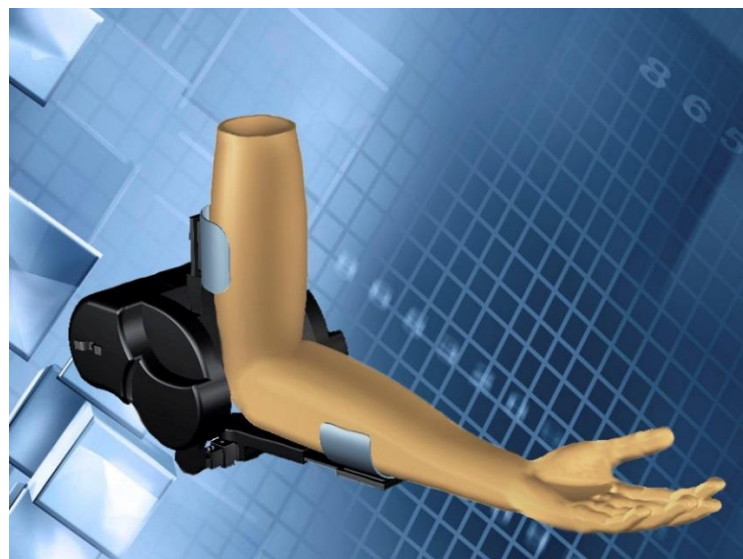


Fig. 7.1. Elbow brace housing.

A significant amount of work is still required in order to improve BPI robotic rehabilitation for home training, as discussed above. Future research will include how to create a self-tuning wearable elbow brace that a clinician can remotely adjust.

REFERENCES

- [1] Bhandari, M., 2013, "Orthopaedic Trauma Care: Finding the Evidence," <http://www.chairs-chaires.gc.ca/chairholders-titulaires/profile-eng.aspx?profileID=1598>
- [2] National Trauma Registry 2011 Report: Hospitalizations for Major Injury in Canada, 2008–2009 Data, Canadian Institution of Health Information, <http://www.cihi.ca>
- [3] Lai, S. M., Studenski, S., Duncan, P. W., and Perera, S., 2002, "Persisting Consequences of Stroke Measured by the Stroke Impact Scale," *Stroke*, **33**, pp. 1840–1844.
- [4] Noble, J., Munro, C.A., Prasad, V.S., and Midha, R., 1998, "Analysis of upper and lower extremity peripheral nerve injuries in a population of patients with multiple injuries," *J. Trauma*, **45**, pp. 116–122.
- [5] *Management of peripheral nerve problems*, G. E. Omer et al., eds., 2nd ed. Philadelphia: Saunders, c1998, ISBN: 978–0721642765.
- [6] Smania, N. et al., 2012, "Rehabilitation of brachial plexus injuries in adults and children," *Eur. J. Phys. Rehabil. Med.*, **48**(3), pp. 483–506.
- [7] Howard, A., Brooks, D., Brown, E., Gebregiorgis, A., and C. Yu-Ping, 2013, "Non-contact versus contact-based sensing methodologies for in-home upper arm robotic rehabilitation," *IEEE Int. Conf. Rehabilitation Robotics (ICORR)*, 24–26 June 2013, pp. 1–6.
- [8] Shena, J., and Wangb, Z.-W., 2014, "The level and influencing factors of quality of life in patients with brachial plexus injury," *Int. J. of Nursing Sciences*, **1**(2), pp. 171–175.
- [9] Van Dijk, J. G., Pondaag, W., and Malessy, M. J., 2001, "Obstetric lesions of the brachial plexus," *Muscle Nerve*, **24**(11), pp. 1451–1461.
- [10] *Treatment of elbow lesions: new aspects in diagnosis and surgical techniques*, A. Celli et al., eds., New York: Springer, c2008, ISBN: 978–8847005914.
- [11] Zampagni, M. L. et al., 2008, "Trend of the carrying angle during flexion–extension of the elbow joint: a pilot study," *Orthopedics*, **31**(1), p. 76.
- [12] *Biomechanics: Principles and Practices*. Peterson, D.R., Bronzino, J. D., eds., CRC Press, 2014, Chapter 2, ISBN-13: 978–1439870983.

- [13] *Treatment of Nerve Injury and Entrapment Neuropathy*. Y. Hirasawa, ed., Springer Science & Business Media, 2002, p.179, ISBN: 978–4431678830.
- [14] Wolff, A., 2007, “Hand rehabilitation,” Hand Clin., 2, pp. 1–262,
- [15] Elbow Immobilizer, Universal, <http://www.amazon.com/ALEX-Toys-Elbow-Immobilizer-Universal/dp/B004QJK8US>
- [16] Pil-O-Splint Adjustable Elbow Support,
http://www.amazon.com/Brown-Medical-A10113-Pil-O-Splint-Adjustable/dp/B0037IWZRS/ref=sr_1_3?s=hpc&ie=UTF8&qid=1437538780&sr=1-3&keywords=elbow+splint
- [17] MMAR Medical Group, Inc., 2015, “Upper extremity bracing : elbow bracing,” http://www.mmarmedical.com/Elbow_Arm_Shoulder_Braces_s/60.htm
- [18] Morrey, B. F., and Sanchez-Sotelo, J., 2009, “The Elbow and Its Disorders,” Elsevier Health Sciences, p.154.
- [19] Therapist Guidelines for the management of patients with an acute Brachial Plexus injury (pre and post-surgery). Royal National Orthopaedic Hospital, p. 3, <https://www.rnoh.nhs.uk/sites/default/files>
- [20] *Orthotics and Prosthetics in Rehabilitation*, M. M. Lusardi et al., eds., 2nd ed., 2007, p. 418, ISBN: 978–0323291347.
- [21] Duff, S.V., and Gordon, A.M., 2003, “Learning of grasp control in children with hemiplegic cerebral palsy,” Dev. Med. Child. Neurol., 45, pp. 746–757.
- [22] Shumway-Cook, A., et al., 2003, “Effect of balance training on recovery of stability in children with cerebral palsy,” Dev. Med. Child. Neurol., 45, pp. 591–602.
- [23] Radomski, M. V., and Latham, C. A. T., 2008, *Occupational Therapy for Physical Dysfunction*, Lippincott Williams & Wilkins, p. 423, ISBN: 978–0781763127.
- [24] Harris, P., 2015, “So, how much are we earning? The average Canadian salaries by industry and region,” <http://www.workopolis.com/content/advice/article/how-much-money-are-we-earning-the-average-canadian-wages-right-now/>
- [25] Lo, A. et al., 2010, “Robot-assisted therapy for long-term upper-limb impairment after stroke,” N. Eng. J. Med., 362, pp. 1772–1783.
- [26] Mehrholz, J., Platz, T., Kugler, J., and Pohl, M., 2008, “Electromechanical and robot-assisted arm training for improving arm function and activities of daily living after stroke,” Cochrane Database Syst. Rev., CD006876.
- [27] Mehrholz, J., Elsner, B., Werner, C., Kugler, J., and Pohl, M., 2013, “Electromechanical- assisted training for walking after stroke,” Cochrane Database Syst. Rev., CD006185.
- [28] Kwakkel, G., Kollen, B. and Lindeman, E., 2004, “Understanding the pattern of functional recovery after stroke: facts and theories,” Restor. Neurol. Neurosci., 22, pp. 281–299.

- [29] Timmermans, A. A., Seelen, H. A., Willmann, R.D., and Kingma, H., 2009, “Technology-assisted training of arm-hand skills in stroke: concepts on reacquisition of motor control and therapist guidelines for rehabilitation technology design,” *J. Neuroeng. Rehabil.*, **6**, pp. 1–18.
- [30] Volpe, B., Krebs, H., and Hogan, N., 2000, “A Novel Approach to Stroke Rehabilitation: Robot-Aided Sensorimotor Stimulation,” *Neurology*, **54**, pp. 1938–1944.
- [31] Lum, P. S., Burgar, C. G., Shor, P. C., Majmundar, M., and Van der Loos, M., 2002, “Robot-assisted movement training compared with conventional therapy techniques for the rehabilitation of upper-limb motor function after stroke,” *Arch. Phys. Med. Rehabil.*, **83**(7), pp. 952–959.
- [32] Volpe, B. T., Lynch, D., and Rykman-Berland, A., 2008, “Intensive sensorimotor arm training mediated by therapist or robot improves hemiparesis in patients with chronic stroke,” *Neurorehabil. Neural. Repair*, **22**(3), pp. 305–310.
- [33] Lo, C., Guarino, P. D., Richards, L. G., 2010, “Robot assisted therapy for long-term upper-limb impairment after stroke,” *N. Eng. J. Med.*, **362**(19), pp. 1772–1783.
- [34] Timmermans, A., Seelen, H., Willmann, R.D., and Kingma, H., 2009, “Technology-assisted training of arm-hand skills in stroke: concepts on reacquisition of motor control and therapist guidelines for rehabilitation technology design,” *J. NeuroEng. Rehabil.*, **6**(1), doi: 10.1186/1743-0003-6-1.
- [35] Lee, M. H., Son, J., Kim, J. Y., and Kim, Y. H., 2010, “Development and assessment of an EMG-based exoskeleton system,” *IFMBE Proc.*, **31**, pp. 648–650.
- [36] Lee, H., Lee, B., Kim, W., Gil, M., Han, J., and Han, C., 2012, “Human-robot cooperative control based on pHRI (Physical human-robot interaction) of exoskeleton robot for a human upper extremity,” *Int. J. Precis. Eng. Manuf.*, **13**(6), pp. 985–992.
- [37] Kim, K., Hong, K. J., Kim, N. G., and Kwon, T. K., 2011, “Assistance of the elbow flexion motion on the active elbow orthosis using muscular stiffness force feedback,” *J. Mech. Sci. Technol.*, **25**(12), pp. 3195–3203.
- [38] Pittaccio, S., Garavaglia, L., Viscuso, S., Beretta, E., and Strazzer, S., 2013, “Implementation, testing and pilot clinical evaluation of superelastic splints that decrease joint stiffness,” *Ann. Biomed. Eng.*, **41**(9), pp. 2003–2017.
- [39] Wu, T.M. and Chen, D.-Z., 2012, “Design and preliminary evaluation of an exoskeleton for upper limb resistance training,” *Front. Mech. Eng.*, **7**(2), pp. 188–198.
- [40] Gu, S., Wu, C. D., Yue, Y., Maple, C., Li, D. Y., and Liu, B. S., 2013, “Real-time compliance control of an assistive joint using QNX operating system,” *Int. J. Autom. Comput.*, **10**(6), pp. 506–514.
- [41] Ripel, T., Krejsa, J., and Hrbáček, J., 2014, “Patient Activity Measurement in Active Elbow Orthosis,” *Mechatronics*, pp. 817–824, doi: 10.1007/978-3-319-02294-9_103.

- [42] Schulz, S., Pylatiuk, C., Kargov, A., Gaiser, I., Schill, O., Reischl, M., Eck, U., and Rupp, R., 2009, "Design of a hybrid powered upper limb orthosis," *IFMBE Proc.*, 25, pp. 468–471.
- [43] Looned, R., Webb, J., Xiao, Z. G., and Menon, C., 2014, "Assisting drinking with an affordable BCI-controlled wearable robot and electrical stimulation: a preliminary investigation," *J. Neuroeng. Rehabil.*, 11, p. 51.
- [44] Mao, Y. and Agrawal, S. K., 2010, "Wearable cable-driven upper arm exoskeleton - Motion with transmitted joint force and moment minimization," *Proc. - IEEE Int. Conf. Robot. Autom.*, pp. 4334–4339.
- [45] Mao, Y. and Agrawal, S. K., 2011, "A cable driven upper arm exoskeleton for upper extremity rehabilitation," *Proc. - IEEE Int. Conf. Robot. Autom.*, pp. 4163–4168.
- [46] Song, Z. and Guo, S., 2011, "Development of a real-time upper limb's motion tracking exoskeleton device for active rehabilitation using an inertia sensor," *Proc. World Congr. Intell. Control Autom.*, pp. 1206–1211.
- [47] Wang, R.-J. and Huang, H.-P., 2012, "AVSER—active variable stiffness exoskeleton robot system: design and application for safe active-passive elbow rehabilitation," *Proc. of the 2012 IEEE/ASME Intl. Conf. on Adv Intelligent Mechatronics (AIM)*, pp. 220–225.
- [48] Vanderniepen, I., Van Ham, R., Van Damme, M., Versluys, R., and Lefever, D., 2009, "Orthopaedic rehabilitation: A powered elbow orthosis using compliant actuation," in *2009 IEEE International Conference on Rehabilitation Robotics, ICORR 2009*, pp. 172–177.
- [49] Martinez, F., Pujana-Arrese, A., Retolaza, I., Sacristan, I., Basurko, J., and Landaluze, J., 2009, "IKO: a five actuated DoF upper limb exoskeleton oriented to workplace assistance," *Appl. Bionics Biomech.*, 6(2), pp. 143–155.
- [50] Guo, S., Zhang, F., Wei, W., Guo, J., and Ge, W., 2013, "Development of force analysis-based exoskeleton for the upper limb rehabilitation system," *2013 ICME Int. Conf. Complex. Med. Eng. C*. 2013, pp. 285–289.
- [51] Schiele, A., Seiberth, H., Klär, P., and Hirzinger, G., 2010, "Mechatronics Characterization of a Novel High-Performance Ergonomic Exoskeleton for Space Robotics Telepresence X-Arm-2 Design Rationale Mechanical Sub-system Mechatronic Sub-systems," *i-SAIRAS 2010*, pp. 499–506.
- [52] Popov, D., Gaponov, I., and Ryu, J. H., 2013, "Bidirectional elbow exoskeleton based on twisted-string actuators," *IEEE Int. Conf. Intell. Robot. Syst.*, pp. 5853–5858.
- [53] Brauckmann, M., et al., 2013, "Soft Exo-Skeletal Arm for C4-C5 Trauma Induced Spinal cord Injuries," Biomedical Engineering Society Annual Meeting - BMES, Seattle, WA.

- [54] Vaca Benitez, L. M., Tabie, M., Will, N., Schmidt, S., Jordan, M., and Kirchner, E. A., 2013, "Exoskeleton technology in rehabilitation: Towards an EMG-based orthosis system for upper limb neuromotor rehabilitation," *J. Robot.*, vol. 2013, pp. 1–13.
- [55] Wiegand, R., Schmitz, B., Pylatiuk, C., and Schulz, S., 2011, "Mechanical Performance of Actuators in an Active Orthosis for the Upper Extremities," *J. Robot.*, vol. 2011, pp. 1–7.
- [56] Morizono, T., Komiya, T., and Higashi, M., 2009, "Study on a wearable ELbow joint capable of mechanical adjustment of stiffness," *Proc. - IEEE Int. Work. Robot Hum. Interact. Commun.*, pp. 552–557.
- [57] Ueda, J., Ming, D., Krishnamoorthy, V., Shinohara, M., and Ogasawara, T., 2010, "Individual muscle control using an exoskeleton robot for muscle function testing," *IEEE Trans. Neural Syst. Rehabil. Eng.*, **18**(4), pp. 339–350.
- [58] Hasegawa, Y., Watanabe, K., and Sankai, Y., 2010, "Performance evaluations of hand and forearm support system," *IEEE/RSJ 2010 Int. Conf. Intell. Robot. Syst. IROS 2010 - Conf. Proc.*, pp. 2645–2650.
- [59] Miranda, A. B. W., Yasutomi, A. Y., Souit, C., and Forner-Cordero, A., 2012, "Bioinspired mechanical design of an upper limb exoskeleton for rehabilitation and motor control assessment," *Proc. IEEE RAS EMBS Int. Conf. Biomed. Robot. Biomechatronics*, pp. 1776–1781.
- [60] Cempini, M., Giovacchini, F., Vitiello, N., Cortese, M., Moise, M., Posteraro, F., and Carrozza, M. C., 2013, "NEUROExos: A powered elbow orthosis for post-stroke early neurorehabilitation," *Proc. Annu. Int. Conf. IEEE Eng. Med. Biol. Soc. EMBS*, pp. 342–345.
- [61] Garrec, P., 2010, "Design of an anthropomorphic upper limb exoskeleton actuated by ball-screws and cables," *UPB Sci. Bull. Ser. D Mech. Eng.*, **72**, pp. 23–34.
- [62] Pehlivan, A. U., Celik, O., and O'Malley, M. K., 2011, "Mechanical design of a distal arm exoskeleton for stroke and spinal cord injury rehabilitation," *IEEE Int. Conf. Rehabil. Robot*, vol. 2011, p. 597–602.
- [63] Zhou, L., Bai, S., Andersen, M. S., and Rasmussen, J., 2012, "Design and Optimization of a Spring-loaded Cable-driven Robotic Exoskeleton," *25th Nord. Semin. Comput. Mech.*, pp. 205–208.
- [64] Tang, Z., Zhang, K., Sun, S., Gao, Z., Zhang, L., and Yang, Z., 2014, "An upper-limb power-assist exoskeleton using proportional myoelectric control," *Sensors (Basel)*, **14**(4), pp. 6677–6694.
- [65] Carignan, C., Tang, J., and Roderick, S., 2009, "Development of an exoskeleton haptic interface for virtual task training," *2009 IEEE/RSJ Int. Conf. Intell. Robot. Syst. IROS 2009*, pp. 3697–3702.
- [66] McBean, J. M., and Narendran, K., 2013, "Powered orthotic device and method of using same," U.S. Patent 8 585 620 B2.

- [67] Bleakley, S. M., 2013, "The effect of the MYOMO robotic orthosis on reach performance after stroke," Ph.D. dissertation, School of Health and Rehabil Sci, Univ. of Pittsburgh.
- [68] Fisher, B.E., and Sullivan, K.J., 2001, "Activity-dependent factors affecting poststroke functional outcomes," *Top Stroke Rehabil.*, **8**(3), pp.31–44.
- [69] Maclean, N., and Pound, P., 2000, "A critical review of the concept of patient motivation in the literature on physical rehabilitation," *Soc. Sci. Med.*, **50**(4), pp.495–506.
- [70] Maclean, N., Pound, P., Wolfe, C., and Rudd, A., 2000, "Qualitative analysis of stroke patients' motivation for rehabilitation," *Br. Med. J.*, **321**, pp.1051–1054.
- [71] Heedon, L., Wansoo, K., Jungsoo, H., and Changsoo, H., 2012, 'The technical trend of the exoskeleton robot system for human power assistance,' *Intern. J. Precis. Eng. and Manufacturing*, **13**, pp. 1491-1497.
- [72] Gopura, R.A.R.C., Kiguchi, K., and Li, Y., 2009, "SUEFUL-7: A 7DOF upper limb exoskeleton robot with muscle-model-oriented EMG-based control," *IEEE/RSJ International Conference on Intelligent Robots and Systems*, pp. 1126–1131, St. Louis, MO, USA.
- [73] Oberg, T., 1995. "Muscle Fatigue and Calibration of EMG Measurements," *J. Electromyogr. Kinesiol.*, **5**(4), pp. 239–243.
- [74] Perry, J.C., Rosen, J., and Burns, S., 2007, "Upper-Limb Powered Exoskeleton Design," *IEEE/ASME Transactions on Mechatronics*, **12**(4), pp. 408–417.
- [75] Cram, J. R., Kasman, G.S., and Holtz, J., 1998, "*Cram's Introduction to surface electromyography*," Gaithersburg Md.: Aspen Publishers, ISBN: 9780763732745.
- [76] Kiguchi, K., and Hayashi, Y., 2015, "EMG-Based Control of a Lower-Limb Power-Assist Robot," *Intelligent Assistive Robots*, Springer Tracts in Advanced Robotics, **106**, pp 371–383.
- [77] Freivalds, A., 2011," *Biomechanics of the upper limbs: mechanics, modeling, and musculoskeletal injuries*," 2nd ed. Boca Raton, Fla.: CRC Press, ISBN: 9781420091199.
- [78] Kamen, G., and Gabriel, D.A., 2010, "*Essentials of electromyography*," Champaign, IL: Human Kinetics, ISBN: 9781450408530.
- [79] Widjaja, F., Shee, C. Y., and Latt, W. T., 2008, "Kalman filtering of accelerometer and electromyography (EMG) data in pathological tremor sensing system," in Proc. *IEEE Int. Conf. Robot. Automat.*, Pasadena, CA,, pp. 3250–3255.
- [80] Chen, Y., Zhao, X., and Han, J., 2013, "Hierarchical projection regression for online estimation of elbow joint angle using EMG signals," *Neural Computing and Applications*, Springer-London, **23**, pp. 1129–1138.

- [81] Zhao, X.G., and Han, J.D., 2011, "A novel EMG-driven state space model for the estimation of continuous joint movements," in *IEEE Int. Conf. on Systems, Man, and Cybernetics, Anchorage*, pp. 2891–2897.
- [82] Geometrical and Mass-inertial Characteristics of the Upper Human Limb, <http://www.clbme.bas.bg/projects/motco/data/massinertial.html>
- [83] Zhang, Q., Hosoda, R., and Venture, G., 2013, "Human joint motion estimation for electromyography (EMG)-based dynamic motion control," in *Proc. Annu. Int. Conf. of IEEE Eng. in Medicine and Biology Society*, Osaka, pp. 21–24.
- [84] Mountjoy, K., 2008, "Use of a Hill-based muscle model in the fast orthogonal search method to estimate wrist force and upper arm physiological parameters," M.S. thesis, Depart. Electrical and Computer Eng., Queen's Univ., Kingston, Canada.
- [85] Youn W., and Kim, J., 2010, "Estimation of elbow flexion force during isometric muscle contraction from mechanomyography and electromyography," *Medical & Biological Engineering & Computing*, Springer-Verlag, 48, pp. 1149–1157.
- [86] Loconsole, C., Dettori, S., Frisoli, A., Avizzano, C. A., and Bergamasco, M., 2014, "An EMG-based approach for on-line predicted torque control in robotic-assisted rehabilitation," in *IEEE Haptics Symp.*, Houston, pp. 181–186.
- [87] Pau, J.W.L., Xie, S.S.Q., and Pullan, A.J., 2012, "Neuromuscular interfacing: establishing an EMG-Driven model for the human elbow joint," *IEEE Trans. Biomed. Eng.*, 59, pp. 2586–2593.
- [88] Wagner, H., Boström, K., and Rinke, B., 2011, "Predicting isometric force from muscular activation using a physiologically inspired model," *Biomechanics and Modeling in Mechanobiology*, Springer-Verlag, 10, pp. 955–961.
- [89] Kiguchi K., and Hayashi, Y., 2013, "Motion estimation based on EMG and EEG signals to control wearable robots," in *IEEE Int. Conf. Systems, Man, and Cybernetics, Manchester*, pp. 4213–4218.
- [90] Artermiadis P. K., and Kyriakopoulos, K. J., 2011, "Bio-inspired mechatronics and control interfaces," *Perception-Action Cycle*, Springer Series in Cognitive and Neural Systems, Springer New York, pp. 749–775,
- [91] Ullah K., and Jung-Hoon, K., 2009, "A mathematical model for mapping EMG signal to joint torque for the human elbow joint using nonlinear regression," in *Int. Conf. Autonomous Robots and Agents*, Wellington, pp. 103–108.
- [92] Burdea, G. C., ed., 1996, "*Force and touch feedback for virtual reality*," New York: Wiley, ISBN: 9780471021414.
- [93] Hill, A.V., 1950, "The series elastic component of muscle," *Proc. R. Soc. Lond. B. Biol. Science*, 141, pp.104–117.
- [94] McKee, P., and Morgan L., 1998, "*Orthotics in rehabilitation: splinting the hand and body*," Philadelphia, PA, pp. 51–68, ISBN: 9780803603516.

- [95] Hende, A., 2013, “*Anthropometry and Workspace Design*”, Comell University, lecture notes for course DEA 3250/6510.
- [96] Huston, R., 2008, “*Principles of Biomechanics*,” CRC Press, p. 442, ISBN: 9781420018400.
- [97] Pheasant, S., and Haslegrave, C. M., 2005, “*Bodyspace: Anthropometry, Ergonomics and the Design of Work*,” CRC Press, ISBN: 9780415285209.
- [98] Herman, I. P., 2007, “*Physics of the Human Body*,” Biological and Med. Physics, Biomed. Eng., Springer Science & Business Media, ISBN: 9783540296041.
- [99] Dubuisson, A. S., Kline, D. G., Amar, A. P., Gruen, J. P., Kliot, M., and Yamada, S., 2002, “Brachial plexus injury: a survey of 100 consecutive cases from a single service,” *Neurosurgery*, 51(3), pp. 673–683.
- [100] Doi, K., Muramatsu, K., and Hattori, Y., 2000, “Restoration of prehension with the double free muscle technique following complete avulsion of the brachial plexus. Indications and long-term results,” *J. of Bone and Joint Surgery*, 82(5), pp. 652–666.
- [101] McDowell, M.A., Fryar, C.D., and Ogden, C.L., 2009, “Anthropometric reference data for children and adults: United States, 1988–1994,” *National Center for Health Statistics. Vital Health Stat.*, 11(249).
- [102] Lymphedema—for health professionals (PDQ®), National Cancer Institute, <http://www.cancer.gov/cancertopics/pdq/supportivecare/lymphedema/healthprofessional/page1>
- [103] Pylatiuk, C., Schulz, S., Vaassen, H., and Reischl, M., 2008, “Preliminary evaluation for a functional support of the elbow and shoulder joint,” *Proc. of the 13th Conf. of the Intl. Functional Electrical Stimulation Society*, Freiburg, Germany, Sep. 21–25 2008, *Biomedical Technology*, 53, pp. 77–79.
- [104] Murray, I. A., and Johnson, G. R., 2004, “A study of the external forces and moments at the shoulder and elbow while performing everyday tasks,” *Clin. Biomech.*, Bristol, Avon, 19, no. 6, pp. 586–594.
- [105] Guenzkofer, F., F. Engstler, H. Bubb, and Bengler, K., 2011, “Isometric elbow flexion and extension joint torque measurements considering biomechanical aspects,” <http://www.researchgate.net/publication/228535401>.
- [106] Spires, M. C., Kelly, B. M., and Davis, A. J., 2013, “Prosthetic Restoration and Rehabilitation of the Upper and Lower Extremity,” Demos Medical Publishing, Dec 19, 2013, p. 382.
- [107] Murphy, D., 2013, “*Fundamentals of Amputation Care and Prosthetics*,” Demos Medical Publishing, p. 248, ISBN: 9781936287703.
- [108] DeLisa, J.A, 2005, “*Physical Medicine and Rehabilitation: Principles and Practice*,” Lippincott Williams & Wilkins Medical, p. 837, ISBN: 9780781741309.

- [109] Hammert, W. C., 2013, “*Peripheral Nerve Conditions: Using Evidence to Guide Treatment, An Issue of Hand Clinics,*” Elsevier Health Sciences, p.471, ISBN: 9780323242004.
- [110] Bonato, P., 2012, Interviewee, Interview with Dr. Poalo Bonato. 14 August 2012.
- [111] Minebea, “Ball Bearing Load Ratings and Life Calculations,”
<http://www.nmbtc.com/bearings/engineering/load-life/>
- [112] SDP/SI, “Elements of metric gear technology.”
http://www.google.ca/url?sa=t&rct=j&q=&esrc=s&source=web&cd=3&ved=0CCoQFjAC&url=http%3A%2Fwww.sdp-si.com%2FD805%2FD805_PDFS%2FTechnical%2F8050T017.pdf&ei=4ZvbVMjdGpTWapPfgegF&usg=AFQjCNHL-9_r6Ww2VViLR9GYuiAy03FW9g&sig2=viKGZqGaqlRvS7xYrp3ayA&bvm=bv.85761416,d.d2s&cad=rja
- [113] Gates Mectrol, “Timing Belt Theory,”
http://www.google.ca/url?sa=t&rct=j&q=&esrc=s&source=web&cd=1&ved=0CB0QFjAA&url=http%3A%2Fwww.gatesmectrol.com%2Fmectrol%2Fdownloads%2Fdownload_common.cfm%3Ffile%3DBelt_Theory06sm.pdf%26folder%3Dbrocure&ei=CJ7aVKiAMMeigwSU5IKgDQ&usg=AFQjCNH7uGki2sx5uzbW5XXWeNM_bvUfgkg&sig2=Om5B7J-ijbQBvtUJBgT9ag&bvm=bv.85761416,d.eXY&cad=rja
- [114] Renold Chain Selector, <http://www.renoldchainselector.com/ChainSelector>
- [115] Snow, E. R., 1994, “The load/Deflection behavior of Cable/Pulley Transmission Mechanism,” M.Sc. in Mechanical Engineering, Massachusetts Institute of technology.
- [116] *Handbook of Plastics Joining: A Practical Guide.* Cambridge University Press, Oct 23, 2008 - Technology & Engineering, ISBN: 9780080950402.
- [117] *Advanced Polymer Processing Operations.* Nicholas P. Cheremisinoff, eds., Univ. Press of Mississippi, Dec 31, 1998 - Technology & Engineering, ISBN: 9780080946627.
- [118] Johansen, J. D., Frosch, P. J., and Lepoittevin, J.-P., 2010, “Contact Dermatitis,” Springer Science & Business Media, Sep 29, 2010, p. 1252.
- [119] Kurowski, P., 2015, “Engineering Analysis with SOLIDWORKS Simulation,” SDC Publication, p.22, ISBN: 9781585036325.
- [120] Todd, R.O., and Woiciech, P., 2008, “*A.D.A.M. Student Atlas of Anatomy,*” Cambridge University Press, p.289, ISBN: 9780521887564.
- [121] Power Transmission Products Inc., *Spring loaded V-belt tensiometer,*
<http://www.carlislebelts.com>
- [122] *Industrial Maintenance,* M. Brumbach, J. Clade, eds., Cengage Learning, 2013, p. 135, ISBN: 9780766826953.

- [123]Carnegie Mellon University, 2008, "The Role and Implementation of Compliance in Legged Locomotion," ProQuest, p. 84.
- [124]*Mechanics of Materials*. J. M. Gere, B. J. Goodno, eds., pp. 1083–1087, ISBN: 9788170082156.
- [125]Schoen, D. C., 2000, "Adult Orthopaedic Nursing," Lippincott Williams & Wilkins, p.484, ISBN: 9780781718806.
- [126]Konczak, J., et al., 2015, "Impaired limb proprioception in adults with spasmodic dysphonia," *J Voice*, 2015 Feb 27, <http://www.ncbi.nlm.nih.gov/pubmed/25737471>.
- [127]Oblak, J., Cikajlo, I., and Matjacic, Z., 2010, "Universal Haptic Drive: A Robot for Arm and Wrist Rehabilitation," in *IEEE Transactions on Neural Systems and Rehabilitation Engineering*, <http://www.ncbi.nlm.nih.gov/pubmed/19846386>.
- [128]Cedar, S.H., 2012, "Biology for Health: Applying the Activities of Daily Living," Health & Fitness, p. 338, ISBN 9780230368088.
- [129]Hall, J. S., 2012, "Basic biomechanics," New York. NY: McGraw-Hill, ISBN: 9780073522760.
- [130]Holewijn, M., and Heus, R., 1992, "Effects of temperature on electromyogram and muscle function," *Eur. J. Appl. Physiol.*, 65, pp. 541–545.
- [131]*Routledge Handbook of Biomechanics and Human Movement Science*. Y. Hong, R. Bartlett, eds., Routledge, 2008, p. 420, ISBN: 9781134132348.
- [132]Anam, K., and Al-Jumaily, A.A., 2012, "Active Exoskeleton Control Systems: State of the Art," *Procedia Engineering*, 41, pp. 988–994.
- [133]Gottfried, B., 2006, "Spatial health systems," 1st Int. Conf. on Pervasive Comput. Techn. For Healthcare (PCTH 2006), Nov. 29-Dec.1, Innsbruck, Austria, pp. 7.
- [134]De Luca, C. J., 2002, "Surface Electromyography: Detection and Recording," Delsys Incorporated.
- [135]Bitzer, S., and Van der Smagt, P., "Learning emg control of a robotic hand: Towards active prostheses," *Proc. of the 2006 IEEE Int. Conf. on Robotics and Automation*, pp. 2819–2823.
- [136]Clancy, E. A., Bouchard, S., and Rancourt, D., 2001, "Estimation and application of EMG amplitude during dynamic contractions," *IEEE Eng. Med. Biol. Mag.*, **20**(6), pp. 47–54.
- [137]Clancy, E. A., Morin, E. L., and Merletti, R., 2002, "Sampling, noise-reduction and amplitude estimation issues in surface electromyography," *J. Electromyogr. Kinesiol*, 12, pp. 1–16.
- [138]Farina, D., Merletti, R., and Enoka, R. M., "The extraction of neural strategies from the surface EMG," *J. Appl Physiol.*, 96, pp. 1486–1495.
- [139]Reaz, M. B. I., and Hussain, M. S. F., "Techniques of EMG signal analysis: detection, processing, classification and applications," *Biol. Proced*, 8, pp.11–35.

- [140] Zardoshti-Kermani, M., Wheeler, B., Badie, K., and Hashemi, R., 1995, "EMG feature evaluation for movement control of upper extremity prostheses," *IEEE Trans, Rehabil, Eng.*, 3, pp.324–333.
- [141] Huxley, A.F., 1957, "Muscle structure and theories of contraction," *Prog Biophys Biophys Chem*, 7, pp. 255–318.
- [142] Hill, A.V., 1938, "The heat of shortening and the dynamic constants of muscle," *Proc R Soc Lond B*, 126, pp.136–195.
- [143] Hill, A.V., 1950 "The series elastic component of muscle," *Proc R Soc Lond B Biol Sci.*, pp.104–117.
- [144] Hayashibe, M., and Guiraud, D., 2013, "Voluntary EMG-to-force estimation with a multi-scale physiological muscle model," *BioMedical Engineering OnLine Journal*, 12:86, BioMed Central, pp.1–18.
- [145] Fleischer, C., and Hommel, G., 2008, "A Human-Exoskeleton Interface Utilizing Electromyography," *IEEE Trans. Robotics*, 24(4), pp.872–882.
- [146] Ding, Q., Zhao, X., Xiong, A., and Han, J., 2011, "A Novel Motion Estimate Method of Human Joint with EMG-Driven Model," *iCBBE 2011*.
- [147] *Basic orthopaedic biomechanics and mechano-biology*. V.C. Mow, R. Huiskes, eds., 3rd ed, Lippincott Williams and Wilkins, 2005, ISBN: 9780781739337.
- [148] Zajac, F.E., 1989, "Muscle and tendon: properties, models, scaling, and application to biomechanics and motor control," *Crit. Rev. Biomed. Eng.*, 17, pp. 359–411.
- [149] Banskota, B., et al., 2008, "Estimation of the accuracy of joint mobility assessment in a group of health professionals," *European Journal of Orthopaedic Surgery & Traumatology*, 18(301), pp. 287–289.
- [150] Reichenbach, A., et al, 2009, "Seeing the hand while reaching speeds up on-line responses to a sudden change in target position," *J Physiol.*, 587(Pt 19), pp. 4605–4616.
- [151] Karlsson, P., "Survey of methods of combining velocity profiles with position control, http://www.idt.mdh.se/kurser/ct3340/ht09/ADMINISTRATION/IRCSE09-submissions/ircse09_submission_22.pdf
- [152] Molony, D.C., Sparkes, J., and Noonan, J., 2004, "The orthopaedic angle on angles: the accuracy of health care professionals in assessing angular displacement," *Eur J Orthop Surg Traumatol*, 14, pp. 80–83.
- [153] Ryu, H.-M., and Sul, S.-K., 2002, "Position control for direct landing of elevator using time-based position pattern generation," *IEEE IAS Annual Meeting*, 1, pp. 644–649, October 2002.
- [154] Cho, J. U., and Jeon, J. W., 2005, "A motion-control chip to generate velocity profiles of desired characteristics," *ETRI Journal*, 27(5), pp. 563–568, October 2005.

- [155]Lloyd, D.G., and Besier, T. F., 2003, “An EMG-driven musculoskeletal model to estimate muscle forces and knee joint moments in vivo,” *J. Biomech.*, **36**, pp. 765–776.
- [156]Thelen, D.G., Schultz, A.B., Fassois, S.D., and Ashtonmiller, J.A., 1994, “Identification of dynamic myoelectric signal-to-force models during isometric lumbar muscle contractions,” *J. Biomech.*, **27**, pp. 907–919.
- [157]Bucanan, T.S., Lloyd, D.G., Manal, K., and Besier, T. F., 2005, “Estimation of muscle forces and joint moments using a forward-inverse dynamics model,” *Med. Sci. Sports Exerc.*, **37**(11), pp. 1911–1916.
- [158]*Gait analysis in the science of rehabilitation*. J. A. Delisa, C. K. Kerrigan, ed., 1998, ISBN: 9780756700218.
- [159]Chui, K., and Chen, G., 2009, “Kalman Filtering: With Real-Time Applications,” Springer Science & Business Media, p.229.
- [160]Grabiner, M.D., 1986, “Bioelectric characteristics of electromechanical delay preceding concentric contraction,” *Med. Sci. Sports Exerc.*, **18**, pp. 37–43.
- [161]Ives, J.C., Kroll, W.P., and Bultman, L.L., 1993, “Rapid movement kinematic and electromyographic control characteristics in males and females,” *Res. Q. Exerc. Sport*, **64**, pp. 274–283.
- [162]Zhou, S., 1996, “Acute effect of repeated maximal isometric contraction on electromechanical delay of knee extensor muscle,” *J. Electromyogr. Kines.*, **6**, pp.177–197.
- [163]Corcos, D.M., Gottlieb, G.L., Latash, M.L., Almedia, G.L., and Agarwal, G.C., 1992, “Electromechanical delay: An experimental artifact,” *J. Electromyogr. Kines.*, **2**, pp. 59–68.
- [164]Lourakis, M.I.A., 2005, “A brief description of the Levenberg-Marquardt algorithm implemented by levmar,” Technical Report, Institute of Computer Science, Foundation for Research and Technology, Hellas.
- [165]Knarr, B. A., 2009, “Design and analysis of a finite element model of the biceps brachii integrated with dynamic in vivo strain fields,” ProQuest LLC.
- [166]Cucca, Y.Y., McLay, S.V.B., Okamoto, T., Ecker, J., and McMenamin, P.G., 2010, “The biceps brachii muscle and its distal insertion: observations of surgical and evolutionary relevance,” *J Surgical and Radiologic Anatomy*, **32**(4), pp. 371–375.
- [167]Bahk, M.S., Burns, J.P., and Snyder, S.J., 2009, “Avoiding and managing complications of arthroscopic biceps tenodesis,” *J. Complications in Knee and Shoulder Surgery*, pp. 207–223.
- [168]Chang, Y.W., Su, F.C., Wu, H.W., and An, K.H., 1999, “Optimum length of muscle contraction,” *Clinical Biomechanics*, **14**(8), pp. 537–542.

-
- [169]Celli, A., Celli, L., and Morrey, B.F., 2008, “*Treatment of elbow lesions: new aspects in diagnosis and surgical techniques*,” Ed. Milano, ed., New York: Springer, c2008.
 - [170]Prodanovic, M., Malesevic, J., Filipovic, M., 2013, “Numerical simulation of the energy distribution in biological tissues during electrical stimulation,” Serbian J. of Electrical Eng., **10**(1), pp. 165–173, Feb. 2013.
 - [171]Lee, G., ed., “*Biomedical Engineering and Environmental Engineering*,” WIT Press, 2014, ISBN: 9781845648657.
 - [172]Grimaldi, G., and Manto, M., eds., “Mechanisms and emerging therapies in tremor disorders,” Springer, 2012, ISBN: 9781461440277.

Appendix A

Rated Life of Bearings

Prior the seven-step process of rated life calculation is done, the basic dynamic radial load rating of the bearing (C_r), ball diameter of the bearing (D_w), number of balls in the bearing (Z), speed of bearing operation in rpm (n), radial (R) and axial load (T) on the bearing should be determined. Below is a bearing specification used at the last iteration of bearing selection:

Table A.1. Bearing specification.

Basic dynamic radial load rating (C_r)	733 N
Ball diameter (D_w)	4.32 mm
Number of balls (Z)	10
Speed in rpm (n)	1142
Radial load (R)	40 N
Axial load (T)	28 N

1. Calculate the relative axial load:

$$\frac{T}{Z \cdot D_w^2} = \frac{30 \text{ N}}{9 \cdot 18.66 \text{ mm}^2} = 0.178 \frac{\text{N}}{\text{mm}^2}$$

2. Calculate e value to the relative axial load [111]:

$$e = 0.19 + \frac{0.178 - 0.172}{0.345 - 0.172} \cdot (0.22 - 0.19) = 0.191$$

3. Calculate the ratio of radial and axial load:

$$\frac{T}{R} = \frac{28 \text{ N}}{40 \text{ N}} = 0.7$$

4. Compare the load ratio and e value according the table in [111]:

$$\frac{T}{R} > e$$

5. Determine X and Y according tables in [111]:

$$X = 0.56$$

$$Y = 2.30 - \frac{0.178 - 0.172}{0.345 - 0.172} \cdot (2.30 - 1.99) = 2.19$$

6. Calculate dynamic equivalent load:

$$P_r = X \cdot R + Y \cdot T = 0.56 \cdot 40N + 2.19 \cdot 28N = 83 N$$

7. Calculate life hours:

$$L_{10} = \frac{10^6}{60 \cdot n} \cdot \left(\frac{C_r}{P_r} \right)^3 = \frac{10^6}{60 \cdot 1142 \text{ rpm}} \cdot \left(\frac{733 \text{ N}}{83 \text{ N}} \right)^3 = 14.59 \text{ rpm}^{-1} \cdot 689 \text{ N} = 10056 \text{ h}$$

Appendix B

Motor–Gearbox selection

This Appendix presents the summary of motor–gearbox selection according to actuation system specification in Section 3.3.4.

The best option for a single motor–gearbox combination that generates 3.6 Nm is Gearhead No. 2 and Motor No. 2, see Table B.3. The total weight of the most optimal motor–gearbox combination is 400g plus a 10 g Encoder, while the cost is \$417.00 per combination.

Table B.1. Gearhead selection for 3.6 Nm.

Part N	Max. continuous torque	Ratio and efficiency	Weight	US dollars	Required torque from Motor
(1) Planetary gearhead GPX 32 C Ø32 mm, 2-stage, 16:1–35:1	3.8 Nm	35:1 and 75%	180 g	184.00	0.145 Nm (145 mNm)
(2) Planetary gearhead GPX 32 LN Ø32 mm, 3-stage, 62:1–231:1	4 Nm	231:1 and 75%	230 g	207.00	0.023 Nm (23 mNm)

Table B.2. Motor selection for gearhead 3.6 Nm.

Part N	Continuous torque	Weight	Max. efficiency	US dollars
Motor for GH1				
(1) DCX 32 L Ø32 mm, Graphite Brushes, ball bearings	128 mNm	320 g	895 and 60V	264.00
Motor for GH2				
(2) DCX 26 L Ø 26mm, CLL precious metal brushes, sintered bearings	32.6 mNm	170 g	88% and 9V	210.00
(3) DCX 26 L Ø 26mm, CLL precious metal brushes, ball bearings	32.9 mNm	170 g	89% and 9V	223.00

Table B.3. Motor–gearhead selection chart for 3.6 Nm.

Gearhead No.	Motor No.	Weight	Cost, US dollars
1	1	180g +320g = 500g	\$184.00 + \$264.00 = \$448.00
2	2	230g +170g = 400g	\$207.00 + \$210.00 = \$417.00
2	3	230g +170g = 400g	\$207.00 + \$223.00 = \$430.00

An alternative option can be a stronger driver, e.g. a driver that can produce 17 Nm. The best option among single motor–gearbox combination that generates 17 Nm is Gearhead

No. 3 and Motor No. 6, see Table B.6. The total weight of the most optimal motor–gearbox combination is 350g plus a 10 g Encoder, while the cost is \$336.00.

Table B.4. Gearhead selection for 17 Nm.

Part N	Max. continuous torque	Ratio and efficiency	Weight	US dollars	Required torque from Motor
(1) Maxon Planetary Gearhead GP 32 C Ø32 mm, 1.0– 6.0 Nm, Ceramic Version 166	6 Nm	1093 : 1 and 60%	220 g	230.00	0.009 Nm (2 mNm)
(2) Maxon Planetary Gearhead GP 32 C Ø32 mm, 1.0– 6.0 Nm, Ceramic Version 166949	6 Nm	246 : 1 and 60%	220 g	213.00	0.041 Nm (41 mNm)
(3) Maxon Planetary Gearhead GP 32 C Ø32 mm, 1.0– 6.0 Nm, Ceramic Version 166979	6 Nm	6285 : 1 and 50%	250 g	250.00	0.002 Nm (2 mNm)

Table B.5. Motor selection for gearhead 17 Nm.

Part N	Continuous torque	Weight	Max. efficiency	Cost, US dollars
Motor for GH1				
(1) Maxon RE-max 29 Ø29 mm, Precious Metal Brushes CLL, 15 Watt, with terminal 226749	9.78 mNm	150 g	90 % and 9V	144.00
(2) Maxon RE-max 29 Ø29 mm, Precious Metal Brushes CLL, 9 Watt, with terminal 226767	9.81 mNm	160 g	89 % and 6V	145.00
Motor for GH2				
(3) Maxon EC-4pole 22 Ø22 mm, brushless, 90 Watt 323220	42.6 mNm	120 g	88% and 48V	516.00
(4) Maxon A-max 32 Ø32 mm, Graphite Brushes, 20 Watt, with cables 353237	43.1 mNm	240 g	80% and 9V	188.00
Motor for GH3				
(5) Maxon A-max 26 Ø26 mm, Precious Metal Brushes CLL, 7 Watt, with terminals 110181	4.45 mNm	110 g	84% and 4.5V	105.00
(6) Maxon A-max 26 Ø26 mm, Precious Metal Brushes CLL, 4 Watt, with terminals 110192	5.42 mNm	100 g	76% and 3.6V	86.00

Table B.6. Motor–gearhead selection chart.

Gearhead No.	Motor No.	Weight	Cost, US dollars
1	1	220 g+150 g =370 g	\$230+\$144=\$374.00
1	2	220 g+160 g =380 g	\$230+\$145=\$375.00
2	3	220 g+120 g =330 g	\$213+\$516=\$729.00
2	4	220 g+240 g =460 g	\$213+\$188=\$401.00
3	5	250 g+110 g =360 g	\$250+\$105=\$355.00
3	6	250 g+100 g =350 g	\$250+\$86=\$336.00

One more solution may be two motor–gearbox combinations that move each side of the device separately:

Table B.7. Dual option for gearhead 17 Nm.

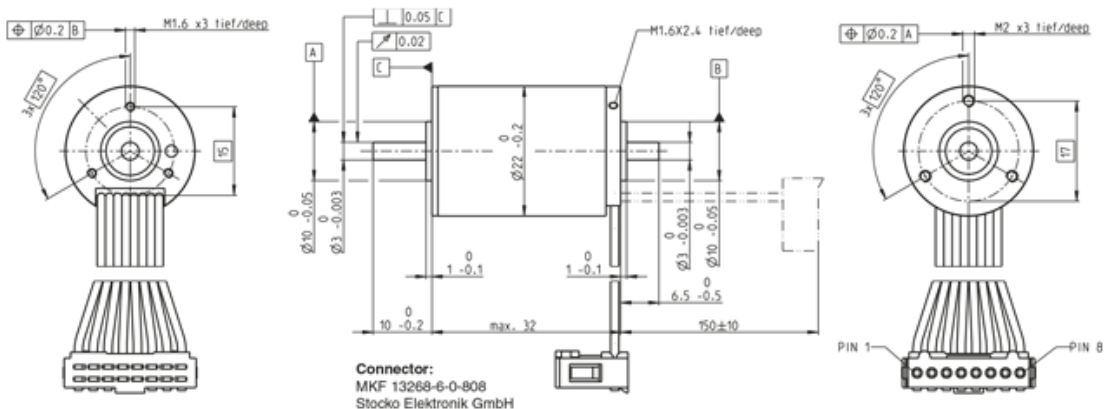
Part N	Max. continuous torque	Ratio and efficiency	Weight	Cost	Required torque from Motor
Maxon Planetary Gearhead GP 22 C Ø22 mm, 0.5–2.0 Nm 143995	1.8 Nm	333:1 and 49%	81 g	137.00	0.011 Nm (11 mNm)

Table B.8. Dual option for motor - gearhead 17 Nm.

Part N	Continuous torque	Weight	Max. efficiency	Cost
Maxon EC-max 22 Ø22 mm, brushless, 12 Watt, with Hall sensors 283840	10.8 mNm	83 g	65% and 24V	168.00

Appendix C

Motor Specification



Information: Drawings are not to scale.

Values at nominal voltage

Nominal voltage	24 V
No load speed	12100 rpm
No load current	77.3 mA
Nominal speed	8250 rpm
Nominal torque (max. continuous torque)	10.8 mNm
Nominal current (max. continuous current)	0.657 A
Stall torque	35.1 mNm
Stall current	1.94 A
Max. efficiency	65 %

Characteristics

Terminal resistance	12.4 Ω
Terminal inductance	0.488 mH
Torque constant	18.1 mNm/A
Speed constant	526 rpm/V
Speed / torque gradient	360 rpm/mNm

Mechanical time constant	8.47 ms
Rotor inertia	2.25 gcm ²

Thermal data

Thermal resistance housing-ambient	13.5 K/W
Thermal resistance winding-housing	1.72 K/W
Thermal time constant winding	1.84 s
Thermal time constant motor	567 s
Ambient temperature	-40...+100 °C
Max. winding temperature	+155 °C

Mechanical data

Bearing type	ball bearings
Max. speed	18000 rpm
Axial play	0 - 0.14 mm
Max. axial load (dynamic)	3.5 N
Max. force for press fits (static) (static, shaft supported)	53 N 1400 N
Max. radial load	16 N, 5 mm from flange

Other specifications

Number of pole pairs	1
Number of phases	3
Number of autoclave cycles	0

Product

Weight	83 g
--------	------

Appendix D

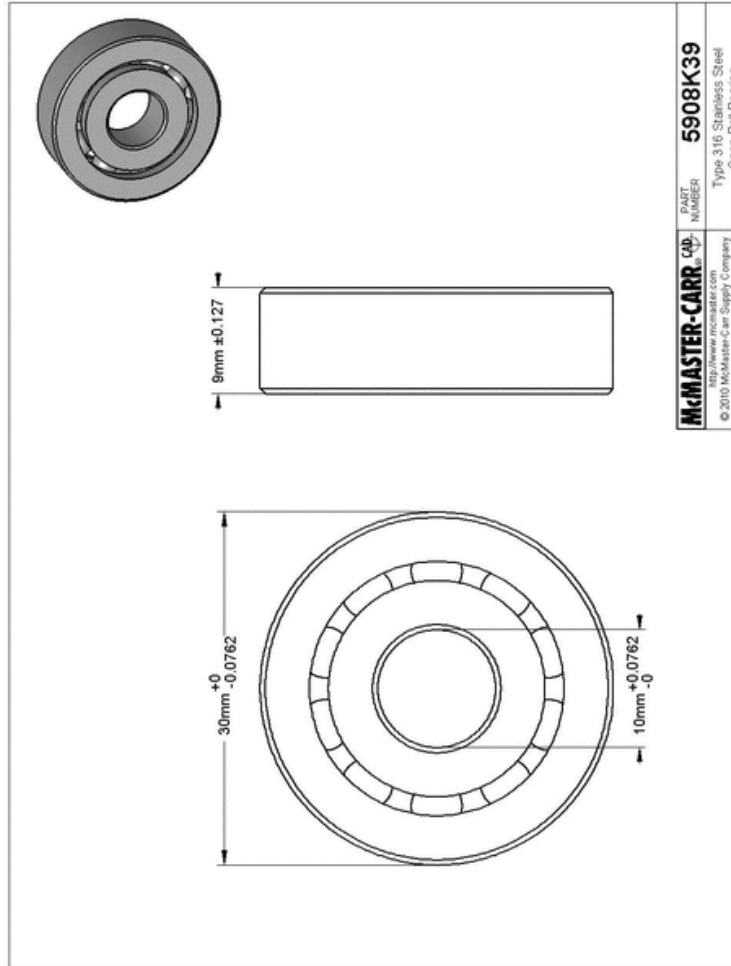
Bearing Specification

Stainless Steel Ball Bearing
for 10 mm Shaft Diameter, 30 mm OD, 9 mm Width



Each
In stock
\$28.93 Each
ADD TO ORDER

Bearing Type	Ball	Part Number	5908K39
Ball Bearing Style	Open	Manufacturer	McMaster-Carr
Bearing Material	Type 316 Stainless Steel	Product ID	5908K39
Ball Cage Material	Polymer	URL	McMaster-Carr Product Page
Temperature Range	-40° to 140° F	Notes	© 2010 McMaster-Carr Supply Company Information is from catalog or furnished by supplier.
For Shaft Diameter	10 mm		
For Shaft Diameter Tolerance	-0 mm to +0.0762 mm		
OD	30 mm		
OD Tolerance	-0.0762 mm to +0 mm		
Width	9 mm		
Width Tolerance	-0.127 mm to +0.127 mm		
Dynamic Load Capacity	165 lbs.		
Maximum rpm	1,142		
RoHS	Compliant		



The information in this 3-D model is provided for reference only. [Details](#)

Made of Type 316 stainless steel, these highly corrosion-resistant bearings are excellent for use in frequent washdown and caustic environments. All are open bearings, which means they run cool and are easy to lubricate. They have a polymer ball cage that withstands temperatures from -40° to 140° F.

Permissions and Approvals



Title: A wearable mechatronic brace for arm rehabilitation
Conference Proceedings: Biomedical Robotics and Biomechatronics (2014 5th IEEE RAS & EMBS International Conference on)
Author: Desplenter, T.; Kyrylova, A.; Stanbury, T.K.; Escoto, A.; Chinchalkar, S.; Trejos, A.L.
Publisher: IEEE
Date: 12-15 Aug. 2014
 Copyright © 2014, IEEE

LOGIN

If you're a copyright.com user, you can login to RightsLink using your copyright.com credentials. Already a RightsLink user or want to learn more?

Thesis / Dissertation Reuse

The IEEE does not require individuals working on a thesis to obtain a formal reuse license, however, you may print out this statement to be used as a permission grant:

Requirements to be followed when using any portion (e.g., figure, graph, table, or textual material) of an IEEE copyrighted paper in a thesis:

- 1) In the case of textual material (e.g., using short quotes or referring to the work within these papers) users must give full credit to the original source (author, paper, publication) followed by the IEEE copyright line © 2011 IEEE.
- 2) In the case of illustrations or tabular material, we require that the copyright line © [Year of original publication] IEEE appear prominently with each reprinted figure and/or table.
- 3) If a substantial portion of the original paper is to be used, and if you are not the senior author, also obtain the senior author's approval.

Requirements to be followed when using an entire IEEE copyrighted paper in a thesis:

- 1) The following IEEE copyright/ credit notice should be placed prominently in the references: © [year of original publication] IEEE. Reprinted, with permission, from [author names, paper title, IEEE publication title, and month/year of publication]
- 2) Only the accepted version of an IEEE copyrighted paper can be used when posting the paper or your thesis on-line.
- 3) In placing the thesis on the author's university website, please display the following message in a prominent place on the website: In reference to IEEE copyrighted material which is used with permission in this thesis, the IEEE does not endorse any of [university/educational entity's name goes here]'s products or services. Internal or personal use of this material is permitted. If interested in reprinting/republishing IEEE copyrighted material for advertising or promotional purposes or for creating new collective works for resale or redistribution, please go to http://www.ieee.org/publications_standards/publications/rights/rights_link.html to learn how to obtain a License from RightsLink.

If applicable, University Microfilms and/or ProQuest Library, or the Archives of Canada may supply single copies of the dissertation.

BACK

CLOSE WINDOW



**Western University Health Science Research Ethics Board
HSREB Delegated Initial Approval Notice**

Research Ethics

Principal Investigator: Dr. Ana Luisa Trejos
Department & Institution: Unknown, Western University

HSREB File Number: 105717
Study Title: EMG-driven Model for Motion Prediction
Sponsor: Natural Sciences and Engineering Research Council

HSREB Initial Approval Date: October 06, 2014
HSREB Expiry Date: December 31, 2016

Documents Approved and/or Received for Information:

Document Name	Comments	Version Date
Western University Protocol		2014/09/22
Data Collection Form/Case Report Form		2014/09/22
Letter of Information & Consent		2014/09/22
Instruments	List of Instruments	2014/09/22

The Western University Health Science Research Ethics Board (HSREB) has reviewed and approved the above named study, as of the HSREB Initial Approval Date noted above.

HSREB approval for this study remains valid until the HSREB Expiry Date noted above, conditional to timely submission and acceptance of HSREB Continuing Ethics Review. If an Updated Approval Notice is required prior to the HSREB Expiry Date, the Principal Investigator is responsible for completing and submitting an HSREB Updated Approval Form in a timely fashion.

The Western University HSREB operates in compliance with the Tri-Council Policy Statement Ethical Conduct for Research Involving Humans (TCPS2), the International Conference on Harmonization of Technical Requirements for Registration of Pharmaceuticals for Human Use Guideline for Good Clinical Practice Practices (ICH E6 R1), the Ontario Personal Health Information Protection Act (PHIPA, 2004), Part 4 of the Natural Health Product Regulations, Health Canada Medical Device Regulations and Part C, Division 5, of the Food and Drug Regulations of Health Canada.

Members of the HSREB who are named as Investigators in research studies do not participate in discussions related to, nor vote on such studies when they are presented to the REB.

The HSREB is registered with the U.S. Department of Health & Human Services under the IRB registration number IRB 00000940.



Letter of Information

Title: EMG-driven Model for Motion Prediction

Principal Investigator: Dr. Ana Luisa Trejos

You are being invited to participate in a research study directed by Dr. Ana Luisa Trejos to develop a model of how the human arm moves. At this initial visit, one of the collaborators working on this project will read through this consent form with you, describe the procedure in detail and answer any questions you may have. This study is being conducted by the following researchers:

Dr. Ana Luisa Trejos, Ph.D. (Principal Investigator)

Assistant Professor, Department of Electrical and Computer Engineering
The University of Western Ontario, London, Ontario, N6A 5B9

Associate Scientist, Canadian Surgical Technologies & Advanced Robotics (CSTAR)
Lawson Health Research Institute, 339 Windermere Road, London, Ontario, N6A 5A5

Shrikant Chinchalkar, (Co-Investigator)

Therapist, Schulich School of Medicine and Dentistry
Roth-McFarlane Hand and Upper Limb Centre
St. Joseph's Hospital, 268 Grosvenor Street, London, Ontario, N6A 4V2

Anastasila Kyrylova, M.E.Sc. (Coordinator)

Graduate Student, Biomedical Engineering Program
The University of Western Ontario, London, Ontario, N6A 5B9

Tyler Desplenter, B.Eng. (Coordinator)

Graduate Student, Department of Electrical and Computer Engineering
The University of Western Ontario, London, Ontario, N6A 5B9

Please Initial: _____

Version 1 (22-09-2014)

Page 1 of 4

The research institute of London Health Sciences Centre
and St. Joseph's Health Care, London.





Abelardo Escoto, M.E.Sc. (Coordinator)

Associate Researcher, Canadian Surgical Technologies & Advanced Robotics (CSTAR)
Lawson Health Research Institute, 339 Windermere Road, London, Ontario, N6A 5A5

Details of the Study:

The overall objective of this research is to develop a model that predicts a person's arm motion using muscle activity data so that it can be used to measure muscle activity in people that need support in lifting their forearm. We will test the proposed model in real-time to see if it can accurately predict motions from healthy subjects. To compare the performance of the model with real-world motions, a motion tracking system will collect data. Measured and predicted motions will be compared and analyzed. Results of the trials will provide valuable information for future improvements.

The experiments will be conducted at the Wearable Biomechatronics Laboratory in the after the Consent Form is signed by you and the Investigator. You will be asked to fill out a Trial Form with your personal information (age, gender, weight, height and hand dominance). After that, a research coordinator will measure some sections of your arm. Finally, you will be seated comfortably on a chair in front of a table and asked to put your arm in an adjustable brace. Your arm will then be secured to the brace using straps with padding on them. The brace limits the arm motion in one of your natural directions of motion.

The activity of the arm muscles will be recorded during the tasks by attaching small sensors to the skin overlying each muscle (biceps and triceps). The sensors do not obstruct normal movement and are not invasive. The skin where the sensors will be placed will be cleaned with alcohol. As the alcohol vaporizes, two circular electrodes will be placed on the biceps and two on the triceps.

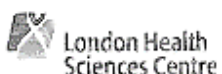
You will be asked to hold a 5 pound weight on your hand. You will be instructed to perform elbow flexion-extension tasks (biceps-curls) requiring you to move your lower arm through a specified range. You will perform 3 sets of 3 repetitions at 6 different ranges of motion (for a total of 54 repetitions), with breaks in between sets. The range of motion will be guided by the brace. We will measure arm motion and muscle activity while you perform these tasks. You will be given a few trial runs to learn to compensate for these loads in order to perform the task at

Please Initial: _____

Version 1 (22-09-2014)

Page 2 of 4

The research institute of London Health Sciences Centre
and St. Joseph's Health Care, London.





slow speeds (less than 5 s per motion). The total duration of the experiment is expected to be less than 2 hours.

Risks:

There is the potential for temporary muscle discomfort due to the tasks being performed. The mechanical brace will limit your motion in a single plane, which is one of your natural motion directions. The operation can be stopped immediately at any time if you wish. The loads for the trial are comparable to the weight of a text book.

NOTE: The participation in this study is voluntary. You may withdraw from the experiments at any time.

Benefits:

Although you may not benefit directly from this study, your participation may contribute to our basic knowledge of human mechanical dynamics, human muscle recruitment, and how to incorporate this knowledge into improving the treatment of musculoskeletal disorders.

Confidentiality:

All data will be stored in password protected personal computer (University of Western Ontario,). Hardcopies of any documents will be stored in locked cabinets in . The only documents containing your name will be the Consent Forms which will not be linked to any of the recorded data. Access to records and data is limited to authorized persons. Your anonymity will be protected at all times by using alphanumeric codes when analyzing your experimental data.

This project is supported by a Discovery Grant of the Natural Sciences and Engineering Research Council (NSERC) of Canada, by the Western Strategic Support for NSERC Success Grant and by the Academic Development Fund, Western University.

If you have any questions or concerns regarding participation in our study, please contact Dr. Ana Luisa Trejos at .

If you have any questions about the conduct of this study or your rights as a research subject you may contact Dr. David Hill, Scientific Director, Lawson Health Research Institute at . A copy of this information package is yours to keep for your personal records.

Please Initial: _____

Version 1 (22-09-2014)

Page 3 of 4

The research Institute of London Health Sciences Centre
and St. Joseph's Health Care, London.





CONSENT FORM

Title of Research: EMG-driven Model for Motion Prediction

Principal Investigator: Dr. Ana Luisa Trejos

Co-Investigators: Shrikant Chinchalkar

Collaborators: Anastasiia Kyrylova, Tyler Desplenter, Abelardo Escoto

For the Participant:

I have read and understand the above information describing this study. I have had the purposes, procedures and technical language of this study explained to me. I have been given sufficient time to consider the above information and to seek advice if I chose to do so. I have had the opportunity to ask questions which have been answered to my satisfaction. I am voluntarily signing this form. I will receive a copy of this consent form for my information.

If at any time I have further questions, problems or adverse events, I can contact Dr. Ana Luisa Trejos, the principal investigator of the project, at _____ or any of the investigators and collaborators on the project.

If I have any questions about your rights as a research participant or the conduct of this study, I may contact The Office of Research Ethics.

By signing this consent form, I am indicating that I agree to participate in this study.

**Name of Participant
(please print)**

Signature of Participant

Date

**Name of Person Obtaining
Informed Consent**

**Signature of Person Obtaining
Informed Consent**

Date

Please Initial: _____

Version 1 (22-09-2014)

Page 4 of 4

The research institute of London Health Sciences Centre
and St. Joseph's Health Care, London.





TRIAL FORM

Title of Research: EMG-driven Model for Motion Prediction

Principal Investigator: Dr. Ana Luisa Trejos

Co-Investigators: Shrikant Chinchalkar

Coordinators: Anastasiia Kyrylova, Tyler Desplenter, Abelardo Escoto

To be filled out by the Participant:

If you are not comfortable answering any of these questions, you do not have to respond.

Age: _____

Weight: _____ kg

Dominant hand: R L

Height: _____ cm

Gender: M F

To be measured and entered by the Coordinator:

Upper arm length: _____ mm

Upper arm circumference: _____ mm

Forearm length: _____ mm

Forearm circumference: _____ mm

Hand length: _____ mm

Hand circumference: _____ mm

Subject code: _____

Please Initial: _____

Version 1

Page 1 of 1

The research institute of London Health Sciences Centre
and St. Joseph's Health Care, London.



Curriculum Vitae

Name: Anastasiia Kyrylova

Post-secondary Education and Degrees: The National Technical University of Ukraine “Kyiv Polytechnic Institute” Kiev, Ukraine 2006–2010 B. Eng. with Honours

The National Technical University of Ukraine
“Kyiv Polytechnic Institute”
Kiev, Ukraine
2010–2012 M. Sc. Eng. with Honours

The University of Western Ontario
London, Ontario, Canada
2013–2015 M. Sc. Eng.

Related Work Experience: Teaching Assistant
The University of Western Ontario
2013–2015

Research Assistant
The University of Western Ontario
2013–2015

Relevant Publications:

A. Kyrylova, T. Desplenter, A. Escoto, S. Chinchalkar and A.L. Trejos, “Simplified EMG-driven model for active-assisted therapy,” IEEE/RSJ International Conference on Intelligent Robots and Systems, Workshop on Rehabilitation & Assistive Robotics, Chicago, Illinois, Sept. 14–18, 2014.

T. Desplenter, A. Kyrylova, T.K. Stanbury, A. Escoto, S. Chinchalkar, and A.L. Trejos, “A wearable mechatronic brace for arm rehabilitation,” IEEE RAS/EMBS International Conference on Biomedical Robotics and Biomechatronics (BioRob), Sao Paulo, Brazil, August 12–15, 2014, pp. 491–496.